AALBORG UNIVERSITY

DENMARK

Novel applications of constrast agents in structural biology of peptides and detergents

Franzmann, Magnus

Publication date:
2010

Document Version
Early version, also known as pre-print

[Link to publication from Aalborg University](#)

Preface

This thesis highlights the work done in the period from Marts 2007 to June 2010 by undersigned in order to obtain the Ph. D. degree. The work was done under The International Doctoral School of Technology and Science at the Faculty of Engineering and Science, Aalborg University, Denmark.

The thesis is divided into three parts. The first part describes the work with structural biology of antimicrobial peptides and detergents and how paramagnetic species can be used to study these. It furthermore gives an introduction to antimicrobial peptides, membrane and membrane mimicking systems and to nuclear magnetic resonance spectroscopy (NMR). Part two describes the work on the transmembrane part of the autotransporter adhesin involved in diffuse adherence (AIDA) and contains an introduction to outer membrane proteins and autotransporters. It furthermore contains an experimental section wherein materials and methods as well as results are presented. Part three contains four papers based on the thesis work with structural studies of peptides and all experimental data is presented in these papers. Two of these papers have been published in peer reviewed journals and one has been submitted to J Biomol NMR. Paper III summarizes the work carried out on the peptides maculatin and citropin and although it is not ready for publication in the current form it includes important observations relevant for the thesis. An elaborating discussion of the papers is found in part I.

This thesis does not include the published paper concerning the beta-sheet aggregation of kisspeptin-10 as the NMR part by which I contributed generally fall out of scope with the thesis. Likewise with the paper concerning the glycosylation on the extracellular domain of the Ag43 although this presents the modeling approach used to model AIDA.

The work of this thesis were carried out in the NMR laboratory at Department of Biotechnology, Chemistry and Environmental Engineering, Aalborg University under the co-supervision of Professor Daniel E. Otzen (Interdisciplinary Nanoscience Center, Department of Molecular Biology, University of Aarhus) and the supervision of Associate Professor Reinhard Wimmer. The Ph. D. study was funded by BioNET, a Danish research network for experimental and theoretical biophysics supported by the VILLUM KANN RASMUSSEN FOUNDATION.

I would like to acknowledge the following persons:

Reinhard Wimmer for excellent and dedicated supervision and for always providing invaluable help during my project.

Daniel E. Otzen for making this project possible and for always providing scientific inputs and inspiration.

Associated Professor Peter Fojan for help with the molecular dynamics simulations and peptide synthesis as well as letting me borrow the CD-spectrometer.

Kirstine Lykke Christensen for her work with maculatin and citropin.

Finn Lillelund Aachmann for his help with synthesizing the AIDA-β_1 plasmid and recording of AIDA-β_1 three dimensional spectra.

Thomas Boesen for help with the crystal screens.

The members of the biophysics groups at University of Aarhus for scientific discussions and for letting me borrow the laboratory equipment.

And last but not least, a great thanks to my friends, family and especially Stine Rudkjøbing Raklev for their love and support during my time as PhD student.

Aalborg University, June 9th 2010

Magnus Franzmann

Papers

Paper I **Quantitative use of paramagnetic relaxation enhancements for determining orientations and insertion depths of peptides in micelles.**
Franzmann M, Otzen D, Wimmer R
Chembiochem. 2009 Sep 21;10(14):2339-47.

Paper II **Divorcing folding from function: How acylation affects the membrane-perturbing properties of an antimicrobial peptide**
Vad B, Thomsen LA, Bertelsen K, Franzmann M, Pedersen JM, Nielsen SB, Vosegaard T, Valnickova Z, Skrydstrup T, Enghild JJ, Wimmer R, Nielsen NC, Otzen DE.
Biochim Biophys Acta. 2010 Apr;1804(4):806-20. Epub 2009 Dec 22.

Paper III **Structural studies of amphibian antimicrobial peptides in micelle and bicelles phospholipid**
Franzmann M, Christensen KL, Otzen DE, Wimmer R
Work in progress

Paper IV **Stereospecific assignment of protein NMR resonances using paramagnetic environment relaxation enhancements**
Franzmann M, Otzen DE, Wimmer R
Submitted to J Biomol NMR

Papers not included in the thesis

Beta-sheet aggregation of kisspeptin-10 is stimulated by heparin but inhibited by amphiphiles.
Nielsen SB, Franzmann M, Basaiawmoit RV, Wimmer R, Mikkelsen JD, Otzen DE.
Biopolymers. 2010 Mar 18. [Epub ahead of print]

Effect of glycosylation on the extracellular domain of the Ag43 bacterial autotransporter: enhanced stability and reduced cellular aggregation.
Knudsen SK, Stensballe A, Franzmann M, Westergaard UB, Otzen DE.
Biochem J. 2008 Jun 15;412(3):563-77.

Summary

Experimental methods for determining the insertion depth and the orientation of membrane embedded peptides and proteins are of great relevance for determining their biological functions. To the large and increasing numbers of identified straight α-helical antimicrobial peptides these methods are of great importance for elucidating their antimicrobial behavior as their orientation relative to the surface of bacterial membrane are one of the defining characteristic of their mode of action. To investigate how members of this group of peptides interact with membranes the model peptides novicidin, novispirin, acylated variants of novicidin, citropin and maculatin are used as model systems. These peptides are all derived from natural occurring animal peptides and they all form amphipathic α-helices in the presence of membranes and membrane mimicking environments like detergent micelles and lipid bicelles, which is typically used for studying peptide interactions with membranes.

By titrating dodecylphosphocholine (DPC) micelles with the contrast agent omniscan (Gd(DTPA-BMA)) the paramagnetic relaxation enhancement (PRE) values for all unambiguous proton signals were obtained. It was found that by correlating these PRE values with distances between the micelle center and DPC protons calculated using molecular dynamics simulations a PRE/distance correlation could be derived. Similar titration experiments were conducted on all the model peptides in micelle solutions and because PRE values of DPC and the peptides are comparable, it was possible to calculate the peptide protons distances to the micelles center from the DPC PRE/distance correlation. In DPC micelle solutions all of the studied peptides were located at the surface of the micelles with the hydrophilic part of the peptides clearly facing the solvent and the hydrophobic part buried at the hydrocarbon chains of the detergents. In anionic bicelles systems, which resemble the negatively charged bacterial membranes better than DPC micelles, it was based on qualitative analysis of residue specific PRE values shown that citropin is positioned parallel to the surface as expected from previous published results.

Maculatin was in contrast expected to be positioned perpendicular to the planner surface of membranes, however, stability issues with samples containing maculatin embedded in anionic bicelles prevented us from recording nuclear magnetic resonance (NMR) experiments that could substantiate this. Maculatin dissolved in zwitterionic bicelles did not exhibit the same stability issues and PRE values could therefore be recorded which showed that maculatin in these bicelles are located parallel to the surface. Combined with previously published data indicating a charge dependent membrane insertion of maculatin we speculate based on our stability observations and PRE measurements that maculatin is indeed positioned parallel to the bicelle surface in zwitterionic bicelles whereas it is positioned perpendicular to the bicelles surface in anionic bicelles causing bicelles degradation and subsequent precipitation.

NMR structure determination of proteins and peptides is mainly based on distances between protons derived from Nuclear Overhauser Effect (NOE) cross peak intensities. NOE cross peaks originating from two chemically nonequivalent, diastereotopic, protons can typically not be distinguished (stereospecific assigned). The distance is therefore calculated to a "pseudoatom"

located at the center between the protons that they represent and to prevent errors the distance is increased with a correction distance causing an inevitable loss of information. In this thesis a novel method of stereospecific assigning protons is presented. By titrating a model peptide, plectasin, with a free floating water soluble contrast agent, omniscan, information concerning the relative orientation of protons towards the solvent was obtained. From an ensemble of structures calculated without added stereo assignments we computer simulated a water shell surrounding the peptide wherein omniscan could be located and from this information regarding the orientation of proton pairs could be obtained. This information was correlated with the information from the titration experiments whereby the peaks could be stereospecific assigned. Recalculating the structure showed a significantly improved RMSD.

Finally, the transmembrane domain of the autotransporter protein adhesin involved in diffuse adherence (AIDA) was successfully refolded into different detergent micelles. Circular dichroism spectra revealed β-sheet secondary structure as expected based on previous publication. Heat modifiability test confirmed that the protein were correct folded, however, it was not possible to record NMR spectra with a resolution sufficient for recording three dimensional spectra usable for structural determination.

Resume

Bestemmelse af pertuberingsdybden og orientering af membran interagerende peptider og proteiner ved hjælp af eksperimentelle metoder er af stor betydning for en vurdering af deres biologiske funktioner.

For det stigende antal identificerede α-helix antimikrobielle peptider er disse metoder nødvendige for at kunne belyse deres antimikrobielle egenskaber, da peptidernes orientering i forhold til overfladen af bakterielle membraner er af afgørende betydning for deres virkemåde. Som modelsystemer til brug for undersøgelsen af, hvordan medlemmer af denne gruppe peptider interagere med membraner er anvendt peptiderne novicidin, novispirin, acylerede varianter af novicidin, citropin og maculatin. Alle disse peptider er afledt af naturligt forekommende animalske peptider og de danner alle amfipatiske α-helix strukturer i membraner og membran lignende miljøer såsom detergent miceller og lipid biceller, der ofte bruges som modeller til at studere peptiders interaktioner med membraner.

Paramagnetisk relaksation forstærknings (PRE) værdier for alle utvetydige proton signaler er målt ved at titrere dodecylphosphocholine (DPC) miceller med kontrastmidlet omniscan (Gd (DTPA-BMA)). Ved at sammenholde disse PRE værdier med afstande mellem micelle centrene og DPC protonerne, som er beregnet ved hjælp af computer simuleringer, har det været muligt at udlede en PRE/distance korrelation. Lignende omniscan titrerings eksperimenter er udført på alle modelpeptiderne i micelle opløsninger. Da PRE værdier for DPC og peptider er sammenlignelige er det muligt at beregne afstanden mellem peptidernes protoner og DPC micelle centre ud fra de målte PRE-værdier ud fra afstands korrelation fra DPC.

Det viste sig, at alle de undersøgte peptider er placeret ved overfladen af DPC micellerne med den hydrofile del af peptiderne stikkende ud fra micellerne og den hydrofobe del begravet ved DPC acylkæderne.

I anioniske bicelle systemer, som i højere grad ligner negativt ladede bakterielle membraner end DPC miceller er det, baseret på kvalitative analyser af PRE værdier, vist at citropin er placeret parallelt med overfladen som forventet ud fra tidligere offentliggjorte resultater.

Maculatin forventes i modsætning til citropin at være placeret vinkelret på den plane bicelle overflade, men problemer med stabiliteten af prøver indeholdende maculatin i anioniske bicelle opløsninger har forhindret optagelse af NMR spektre, der ville kunne dokumentere dette. Maculatin opløst i zwitterioniske bicelle opløsninger udviser imidlertid ikke samme stabilitets problemer og der kunne derfor måles PRE-værdier, som har vist, at maculatin i disse biceller ligger parallelt med overfladen. Sammenholdes stabilitet observationerne og målinger af PRE-værdier med tidligere offentliggjorte data, der viser en ladnings afhængig membran pertubering for maculatin, er maculatin formodentlig placeret parallelt med bicelle overfladen i zwitterionic biceller, hvorimod maculatin er placeret vinkelret på bicelles overflade i anioniske biceller, hvilket forårsager at bicellerne nedbrydes og efterfølgende udfælder.

Struktur bestemmelse af proteiner og peptider ved kernemagnetisk resonans (NMR) er hovedsagelig baseret på afstande mellem protoner beregnet ud fra nuklear overhauser effekt (NOE) krydstop intensiteter. Oprindelsen af NOE krydstoppe fra to kemisk forskellige, diastereotopiske protoner kan typisk ikke skelnes (stereospecifikt tilordnes). Afstanden er i stedet for beregnet til et "pseudoatom" placeret midt mellem de protoner de repræsenterer. Da afstanden er forøget med en korrektions afstand, vil dette uundgåeligt forårsage et tab af information. I denne afhandling præsenteres en ny metode til stereospecifikt at tilordne proton signaler. Ved titrering af et modelpeptid, plectasin, med et vandopløselige kontraststof, omniscan, fås oplysninger om den relative orientering af protoner imod den omsluttende opløsning. Fra et ensemble af strukturer beregnet uden stereospecifikke tilordninger er der computer simuleret en vand skal omkring peptidet hvori omniscan kan antage alle placeringer og ud fra dette er den relative orientering af proton par imod vandet bestemt. Herefter er disse orienteringsdata sammenholdt med data fra titreringens eksperimenterne, hvorved krydstoppene kunne stereospecifikt tilordnes. En gentagelse af struktur beregningen, men med de stereospecifike tilordninger, viste en væsentligt forbedret RMSD værdi i forhold til beregninger uden.

Det transmembrane domæne af autotransporter proteinet "adhesin involved in diffuse adherence" (AIDA), er succesfuldt blevet udtrykt og refoldet i forskellige detergent miceller. Cirkulære dichroism spektre viste β-foldeblad sekundær struktur, hvilket kunne forventes på baggrund af tidligere publikation. Varme modificerbarheds test har bekræftet, at proteinet var korrekt foldet, men det har ikke været muligt at optage NMR spektre med en tilstrækkelig høj opløsning, så de kunne anvendes til en strukturel bestemmelse af proteinet.

Abbreviations

Gd(DOTA)	gadolinium-tetraazacyclododecanetetraacetic acid
AIDA	adhesin involved in diffuse adherence
AMP	antimicrobial peptide
CD	circular dichroism
CL	cardiolipin
CMC	critical micelle concentration
COSY	correlation spectroscopy
DHPC	dihexanoyl-sn-glycero-3-phosphocholine
DMPC	1,2-dimyristoyl-sn-glycero-3-phosholine
DMPG	1,2-dimyristoyl-sn-glycero-3-phosphoglycerol
DOPE	discrete optimized potential energy
DPC	dodecylphosphocholine
DQF	double quantum filtered
DTT	dithiothretiol
FDA	food and drug administration
Gd(DTPA-BMA)	gadolinium−diethylenetriaminepentaacetic acid
GRAS	generally recognized as safe
GUV	giant unilamellar vesicles
HSQC	heteronuclear single quantum correlation
IPTG	isopropyl-β-D-thiogalactopyranoside
LPS	lipopolysaccharides
LUV	large unilamellar vesicles
MIC	minimal inhibition concentration
NMR	nuclear magnetic resonance
NOE	nuclear overhauser effect
NOESY	nuclear overhauser effect spectroscopy
OMP	outer membrane protein
oPOE	octyl polyoxyethylene
PAGE	polyacrylamide gel electrophoresis
PC	phosphatidylcholine
PE	phosphatidylethanolamine
PG	phosphatidylglycerol
PI	phosphatidyllinositol
PRE	paramagnetic relaxation enhancement
PS	phosphatidylserine
RDC	residual dipolar coupling
RF	radio frequency
SDS	sodium dodecyl sulfate
SPH	sphingomyelin
SUV	small unilamellar vesicles
TOCSY	total correlation spectroscopy
TROSY	transverse relaxation-optimized spectroscopy
UV	ultraviolet

Contents

Part I

Antimicrobial peptides

Bacterial resistance

The discovery of penicillin as an antibiotic agent by Alexander Flemming in 1928 provided for the first time humans with a tool to treat bacterial infections and thereby to survive a large number of life threatening diseases. It also provided the capability of performing surgery, organ transplantations and chemotherapy treatments without causing serious infectious complications and the introduction of antibiotics thereby revolutionized the entire medical sector. The industrial production of penicillin started in 1943 and the use of antibiotics quickly became widespread which between 1944 and 1972 lead to a dramatic increase of eight years to the average human lifespan what is unprecedented both before and after.[5] However, only four years after the mass production of penicillin started, the first studies of clinical bacterial resistance were reported[6] and since then the number of antibiotic resistant bacteria have been steadily increasing. According to the world health organization WHO up to 70% of hospital infections are resistant to all penicillins and cephalosporins (two types of commonly used antibiotics) and for many other infectious strains the percentage of resistant bacteria are close to 100%.[7] Even worse is the emergence of vancomycin resistant strains of *Enterococcus* bacteria in many hospitals around the world, as this antibiotic were thought to be the last line of defense against multiresistant bacteria. Because the pathogens are highly virulent and able to quickly adapt the resistance genes and thereby become resistant to newly developed antibiotics, the time period where the development costs can be returned are significantly reduced. The profits that can be made by the pharmaceutical companies are as a consequence also significantly reduced which is directly reflected in the number of new antibiotics that have been introduced to the marked in the last years. In the period between 1999 and 2008 there were only introduced nine new antibiotics[8] and there are no indications that this trend will change, causing leading scientist to proclaim that the antibiotic era is at an end.[9, 10]

There exist several different ways by which the microorganisms exhibit resistance to antibiotics. Penicillin and other β-lactam antibiotics targets a number of different bacterial enzymes which are necessary for the growth and maintenance of the peptidoglycan layer, and one of the most frequently observed resistance mechanism is an alteration of the penicillin binding sites on these enzymes, which prevents an interference.[11] Other well studied mechanisms are enzymatic drug modifications as are seen with β-lactamases like penicillinase[12] and overexpression of efflux pumps that actively pumps out the antibiotics before it causes damage to the bacteria.[13] Since the 1960s there have only been developed two new structural classes of antibiotics and because virtually all new antibiotics therefore are modifications of already existing products the resistance genes can easily adapt to the new antibiotics which is one of the main reasons that multidrug resistant bacteria are spreading out of control.[9] The need for new antibiotics is crucial in order to retain the ability to treat infectious diseases on a large scale. The rapidly

growing number of identified antimicrobial peptides (AMPs) constitute a group of very promising candidates for alternative treatment and might be part of a solution against multidrug resistant bacteria as will be discussed in details in the following sections.

Introduction to antimicrobial peptides

Antimicrobial peptides are a large group of structurally and sequentially very diverse antibiotics consisting of relatively short chains of amino acid polypeptides. These peptides play an evolutionary conserved role in the innate immune system (non-adaptive immunity) where they act on a broad range of microorganisms, typically with a low specificity. This enables a quick response to pathogens compared to the adaptive immune system as the AMPs do not require mobilization or expression of specialized cells which is highly beneficial at continuously exposed parts of animal's bodies such as the skin, the mouth and the intestine. AMPs have been shown to kill a wide range of bacteria including Gram-positive bacteria, Gram-negative bacteria and mycobacteria as well as some types of viruses, fungi and even cancer cells.[14] However, the specificity for these targets varies greatly within the different types of AMPs indicating that they act in various ways. Therefore most multicellular organisms secrete a mixture of different AMPs in order to protect them from the diverse threats.[15] Common for all AMPs are that they originate from larger precursors which experience post transcriptional modifications like proteolysis modifications, glycosidation, C-terminal amidation or isomerisation.[16] Furthermore, all known AMPs appear to fold into amphiphatic structures with separate clusters of charged and hydrophobic amino acids.[15]

Classes of antimicrobial peptides

The great diversity of peptide antibiotics makes it difficult to categorize them into defined groups, and as a consequence there have been various approaches in doing so. Mammal AMPs can be divided into two groups based on their evolutionary divergence where defensins differs from the large and structurally very diverse group of cathelicidins.[17, 18] The cathelicidin group has obtained its name from the 96 residue porcine peptide cathepsin L. inhibitor from which the molecules were first isolated[19] and they consist of a cathelin domain and a C-terminal AMP domain which will be described further. On a broader level the peptides are typically grouped by a combination of net charge, amino acid composition and the number of disulfide bridges that the peptides contain[14, 20]. On the following pages a short introduction to the different groups listed below:

1) Linear cationic α-helical peptides
2) Cationic peptides enriched for specific amino acids
3) Anionic and cationic peptides that contain cysteine and form disulphide bonds
4) Anionic peptides
5) Anionic and cationic peptide fragments of larger proteins

Linear cationic α-helical peptides

One of the largest and most well studied groups of AMPs is the group of small cationic peptides which are highly abundant and widespread in nature where they are found in all types of

organisms ranging from insects to higher mammals.[21] They act against most Gram-negative and Gram-positive bacteria but also some fungi and enveloped viruses. They are typically less than 40 residues long, do not contain any cystein residues that can form disulfide bridges and do not appear to form any secondary structure in aqueous solutions. However, in the presence of lipids, detergents or even some small organic compounds like alcohols[17, 22], they adapt a linear α-helical conformation which in several cases has a hinge or kink in the middle of the helix (see figure 2). The hydrophobic residues of the peptides are distributed in a manner so that they upon α-helix formation typically are located on one side of the peptides while the charged and hydrophilic residues are located on the other side, which makes them highly amphiphatic. This promotes an interaction with the lipid environment of the target cell membranes as the peptides thereby can be positioned between the lipid headgroups and their hydrophobic tails.

A great effort has been put into determining the mechanisms by which the AMPs target the bacteria without affecting the host cells. For the linear cationic α-helical peptides the main driving force is generally accepted to be the highly negatively charged surface of the prokaryotic membranes that contains a relative large amount of anionic phosphatidylglycerol (PG) compared to the more neutrally charged surfaces of eukaryotic membranes. Upon binding to the bacterial membrane the peptides disrupts the membranes by either forming pores or by destabilizing the membrane leading to a collapse of the lipid structure and consequently cell death. Three general models have been proposed to describe these interactions; the *barrel-stave model*[23], the *carpet model*[24] and the *toroidal pore model*[25]. In the *barrel-stave model* the peptides bind to the target membrane as either monomers or as oligomers before assembling on the membrane surface. Subsequently the peptides transverse the membrane by pore formation which lead to a breakdown of the electrochemical potential, pH gradient and osmotic regulation across the cell membrane and thereby causes the cell to die. As the typical bacterial membrane is approximately 30 Å thick, the peptides must be at least 20 residues long in order to span the entire width of the bilayer.[26] In the barrel-stave model the hydrophobic part of the peptides are bound to the lipid core of the membranes while the hydrophilic part of the peptides are bound to the lipid headgroups as well as the water within the pore and the water surrounding the membrane. As these peptides can interact with the hydrophobic core of the membrane it is assumed that the formation of the transmembrane pores are mainly driven by hydrophobic interactions and that they therefore bind to the lipids independent of their charge. A cartoon illustration of the barrel-stave model can be seen in figure 1C. In the *toroidal pore model* the peptides assemble on the membrane surface of the target cell until a critical concentration is reached as is also seen for the *barrel-stave* model. However, the peptides acting by the *toroidal pore model* do not bind to the hydrophobic tails of the membrane lipids but rather induces a bend from the outer surface of the membranes to the inner surface thereby forming pores. The lipid head groups continuously lines the hydrophobic core along with the AMPs which are placed in the interface between the charged head groups and the lipid tails. This can be seen in figure 1B. Because the peptides, acting by the *toroidal pore model,* mainly binds to this interface they are more sensitive to the lipid head group charge which causes them to be more specific towards the negatively charged bacteria surfaces. The *carpet model* is in many aspects similar to

the *toroidal pore model*. The peptides accumulate on surfaces of the bacteria covering the membrane like a carpet until a critical concentration is reached and the curvature of the membrane is disrupted in a detergent like manner displacing part of the membranes and thereby forming small lipid micelles as is illustrated in figure 1A. AMPs acting by the *carpet model* require a higher concentration of peptide compared to the *barrel-stave* and the *toroidal pore* models and in some cases the method has been shown to be peptide concentration dependent so that at low concentrations the peptides will form pores while at high peptide concentrations the peptides will break down the overall structure of the membrane.[24]
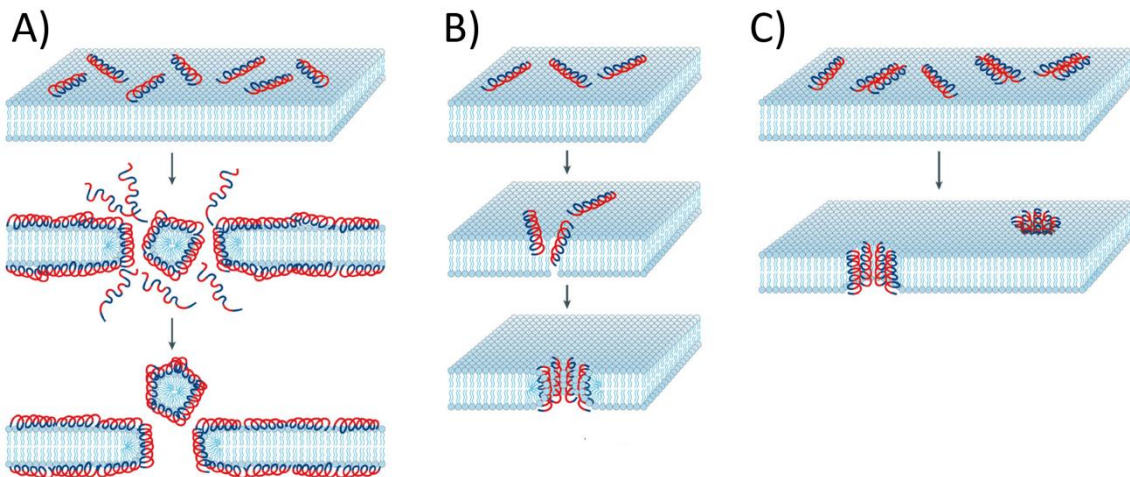
Figur 1 Schematic model of three general models of membrane disruption by α-helical cationic peptides. Hydrophobic regions of the peptides are colored red whereas hydrophilic regions are colored blue. (A) The carpet model where peptides cluster on the surface of the membrane in a detergent like manner which leads to a collapse of the membrane structure and subsequent micelle formation. (B) The toroidal model where the peptides bend the surface of the membrane to form pores that are lined by the peptides bound to the head groups of the lipids. (C) The barrel-stave model where peptides forms pores in the membrane by binding to the lipid tails with hydrophobic part of the peptides whereas the hydrophilic part of the peptides lines the water filled inner of the pores. Taken from [20]

Cationic peptides enriched for specific amino acids

Currently more than 80 cationic AMPs enriched for specific amino acids have been characterized. This is a relative small number compared to some of the other classes of AMPs according to the Antimicrobial Sequence Database.[27] The structural properties of the peptides are very diverse and vary from small α-helix to extended loops. The amino acids by which the peptides are enriched also vary and are highly dependent on the organisms from which they originate and can therefore be divided into subgroups. Some of the most well studied are the large group of Pro and Pro/Gly enriched peptides such as pyrrhoccoricin, apidaecin and drosocin that have been shown to primarily be active against Gram-negative bacteria. They are thought to kill bacteria by entering cells and inhibiting the molecular chaperone DnaK and not by perforating the membranes as it is seen for the small cationic α-helical peptides.[28] In humans a group of AMPs enriched for histidins, known as Histatins, has been isolated and show to target fungi with a high specificity compared to bacteria.[29] Furthermore are groups of Cys/Pro, Arg/Pro, Glu or Trp enriched peptides found in mammals where some of them show a very

broad specificity ranging from bacteria to enveloped viruses as it is seen for indolicidin which is a tryptophan enriched peptide.[27, 30]

Anionic and cationic peptides that contain cysteine and form disulphide bonds

The group of charged peptides that forms disulphide bonds was first recognized in 1956 by RC. Skarnes and coworkers where leukin from rabit leucocytes was isolated and later characterized.[31] The group was among the first peptides with antibiotic effect that were identified and has later become one of the most well studied groups with members from all classes of organisms ranging from animals, including humans, to plants and even fungi.[32, 33] The largest family within the group is the defensins which are small evolutionary conserved cysteine rich peptides with mainly β-sheet structures which are stabilized by three, or in rare cases four, disulfide bridges.[32, 34] There exist three subfamilies of defensins in vertebrates called α, β and θ where the latter is a distinct group of cyclic peptides that were identified by Tang et al. in 1999[35] The α- and β-defensins both consist of a triple-stranded β-sheet that are folded into a characteristic defensin β-sheet fold, but the pairing of the cysteins and the length of amino acids between the disulfide bonds varies between the two subfamilies. Clusters of positively charged amino acids are located in most of the α- and β-defensins but the distribution and predominance between either arginine or lysine varies greatly depending both on the organisms but also by which tissue they are secreted which makes it difficult to categorize the peptides based on these properties.[36]

The highest concentrations of defensins (>10 mg/ml) are found in tissues that are continuously exposed to microbial infections. α-defensins are mostly stored in granules which in leukocytes are fused to vacuoles containing the bacteria and thereby exposing the bacteria for a very high local concentration of peptide.[37] Likewise releases the paneth cells in the intestine granules containing high concentration of α-defensins into the small pits in the lumen of the gastrointestinal barrier.[38] In contrast are β-defensins in humans mainly secreted by epithelia of several organs, including skin.[39] The means of action against bacteria and other pathogens are less elucidated compared to the small cationic α-helix peptides described above, but it is widely accepted that they mainly act by disrupting the membranes of their target cells. Dye leakage experiments with vesicles clearly indicate that defensins forms pore in the bilayer and that the pores have a maximum width of 25 Å[40], however defensins have also been shown to interact with a wide variety of different components in the host cells and thereby trigger an immune response.[32] An example of this is the fungal defensin plectasin has been shown to interact with the bacterial cell-wall precursor Lipid II which causes an inhibition of cell-wall biosynthesis. [41] Furthermore have defensins been shown to induced a release of histamine through a rapid G protein-dependent response in rat peritoneal mast cells.[42]

Small peptides located in invertebrates like insects, plants and fungi that contain six or eight cysteins bonded by disulfide bridges are also called defensins despite that they have different structural properties compared to the vertebrate defensins, and despite that there are not found any evolutionary linkage between the two types of defensins. The structure of insect and

plant defensins contains typically an N-terminal α-helix that is linked to a C-terminal β-sheet segment through disulfide bonds going from cystein 1-4, 2-5 and 3-6.[32]

Besides the large family of defensins, the group of AMPs forming disulfide bridges is less defined although many of them form β-hairpin structures and are typically grouped by the number of disulfide bridges in the molecules.[15] The smallest of the single disulphide bridge AMPs can be represented by peptides like thanatin and brevinin whereas peptides with two disulphide bridges can be represented by the ~2 kDa hairpin structured peptides androctonin, protegrin 1 and tachyplesin which are found in both vertebrates and invertebrates.[43]

Anionic peptides

Very few anionic AMPs have been characterized compared to their cationic counterparts which is presumably because they are less abundant in nature due to their negative charge that prevents them from binding to the negatively charged bacterial membrane surfaces. The first anionic AMPs were reported in the early 1980s and have now been isolated from plants, invertebrates and vertebrates where they among other places have been found in the airway epithelial and in sweat glands from where the peptides are secreted into the sweat and transported to the epidermal surface.[44, 45] In most cases the anionic peptides appear to act by forming amphiphatic α-helices and subsequently interacting with and disrupting the membranes of the target cells despite having a net charge between -1 and -7 that presumably repels the negative membrane surface.[46] However, it has been suggested that these interactions may be facilitated by the formation of cationic salt bridges with the bacterial membranes although this has not been thoroughly investigated. Many of the anionic peptides require metal ions like zink as a cofactor in order to fold properly, but these are also likely to play a role in the formation of the mentioned salt bridges as well as neutralize some of the negative charges.[45]

Anionic and cationic peptide fragments of larger proteins

The sequential and structural properties of the protein fragments which exhibit an antibiotic effect overlap with many of the other groups of peptides and are therefore more difficult to distinguish. They are either produced by an enzymatic cleavage or by an autocatalytic reaction where a part of a larger protein without any related function obtains antimicrobial properties. For instance, a crude lysate of the bacterial strain *Helicobacter pylori* were searched for a cecropin motif but the search instead revealed that cleaved peptides from the N-terminus of the ribosomal protein RpL1 exhibits antimicrobial activity.[47] It has as a consequence been postulated that some of the Helicobacter pylori, which are located in the stomach and are resistant to the RpL1 derived peptides, undergo altruistic lysis that releases the AMPs into the gut and thereby suppresses faster growing bacteria.
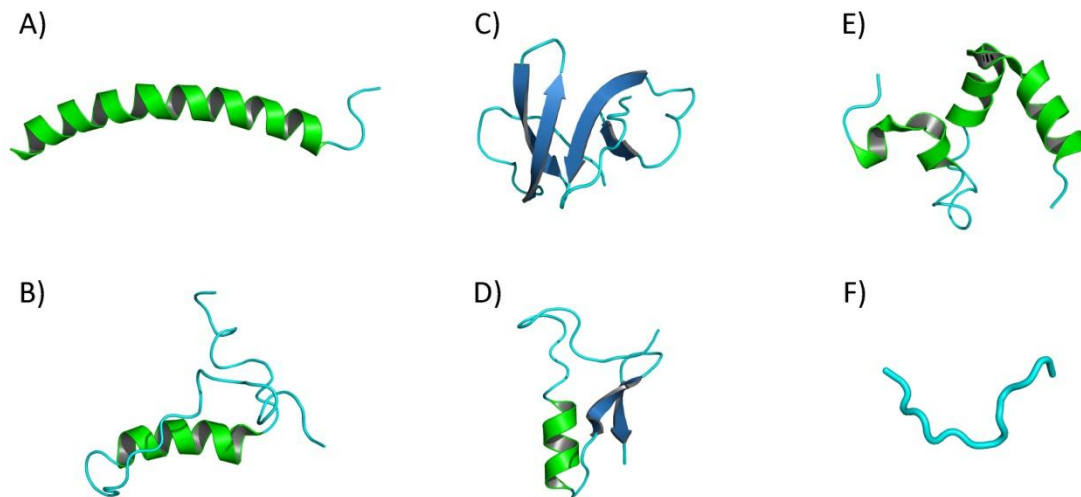
Figur 2. Representative structures of the different groups of AMPs. (A) Structure of the linear cationic α-helical human peptide LL-37 PDB code: 2K6O[48] (B) Structure of lactoferricin which is part of the larger protein lactoferrin PDB code: 1Z6V[49] (C) Structure of the human α-defensin-5 PDB code: 1ZMP[50] (D) Structure of insect defensin A PDB code: 1ICA[51] (E) Structure of anionic human AMP dermcidin-1L PDB code: 2KSG[52] (F) Structure of indolicidin which is high enriched for tryptophan PDB code: 1G89[53]

Bacterial AMP resistance

The selectivity for different types of bacteria and pathogens varies within the different groups of AMPs as described above. However, a number of common traits like positively charged membrane surface, low cholesterol content and distinctive electrochemical gradients appear to distinguish differences between the host cells and the bacteria. Although AMPs are naturally occurring and have existed alongside bacteria through evolution, bacterial resistance towards the peptides is not very widespread. This is likely caused by difficulties in changing the basic composition in the membranes without seriously affecting the viability of the bacteria. However, as will be described a number of instances have been reported where resistance against AMPs have been achieved through different mechanisms.

The bacteria *S. aureus* can become resistant to defensins and protegrins by a mutation in the mprF gene which leads to a lysine modification of PG in the bacterial membrane. The lyso-PG modifications causes a significant reduction of the negative charge of the membrane surface which consequently reduces the electrochemical attraction of primarily cationic AMPs to the membrane. The mutated bacteria were therefore able to survive larger peptide concentrations compared to the bacteria with more anionic membranes.[54] *S. aureus* has furthermore developed resistance towards some AMPs by reducing the transmembrane potential Δψ.[55] For some defensins this appears to be one of the major factors for the antimicrobial activity whereas other highly cationic defensins are less susceptible to changes in the Δψ. Other Gram negative bacterial strains have obtained resistance to cationic AMPs through a different mechanism where polyanionic sodium alginate which is highly similar to exopolysaccharides in the secretion of *P. auruginosa* have been shown to inhibit the AMPs.[56] The very negative charged alginate presumably interferes with the positive peptides before they reach the bacterial membrane and thereby prevents the AMPs from killing the bacteria. In Gram negative bacteria overexpression

of a group of genes regulates an aminoarabinose or 2-hydroxymyristate modification of lipid A which is one of the component of the bacterial membranes.[57] The modifications substitute a negative lipid A phosphate group with a free amino group and thereby changes the overall charge of the molecule and thereby the membrane hence reduces the AMPs affinity for the bacteria. Also *H. influenza* has been shown to reduce the membrane charge by incorporating a high content of phosphorylcholine bound to lipopolysaccharides (LPS).[58] As phosphorylcholine is rare in prokaryotic organisms but a major component in eucaryotic cell membranes the incorporation is presumably a method by which the bacteria further mimics the mammalian cells and thereby prevents getting targeted by the immune system and the AMPs. The phosphorylcholines importance for resistance is substantiated by its ability to decrease the susceptibility of different human AMPs expressed in the upper respiratory tract. [59]

As it is seen for prokaryotic resistance to conventional antibiotics some bacteria are capable of expressing proteases that degrade the molecules and thereby protects the bacteria. This is likewise the case for AMPs where some salmonella bacteria strains have been shown to express the endopeptidase PgtE which is highly similar to the outer membrane protease family OmpT and protease VII from *E. coli*.[60] These proteases cleave peptides at the center of paired basic residues or at the carboxy side of paired basic amino acid residues,[61] and because many AMPs are typically highly cationic they are therefore potential targets for these proteases. These proteases is however not effective against all AMPs as the tertiary structure of e.g. defensins, protegrin or CAMPs apparently provides steric hinderers from the proteases.[60]

Also efflux pumps are used by bacteria and fungi to obtain resistance against AMPs. This has been reported in several instances like the gonococcal MtrC-MtrD-MtrE efflux pump which not only protects the bacteria from antibiotics like penicillin but also from the human AMP LL-37.[62] Such efflux systems have furthermore been described in fungi where ABC type transporters have provided resistance to AMPs and other antifungal agents.[63]

The use of AMPs and especially the use of analogs of human peptides like LL-37 have raised a serious concern that bacteria would develop resistance to these peptides which through cross resistance could lead to bacterial strains that are immune to humans natural defenses.[64] The likelihood of this happening will of course increase if breakthroughs in development of these peptides as therapeutics, in farming and as food preservatives provide basis for a large scale production. Although only few reports of AMPs resistance have been reported as described above, they exist and must therefore be taken very seriously because the consequences could potentially be catastrophic.

AMPs as pharmaceuticals

Despite cases of resistance against AMPs which were described in the previous section, it is generally considered more difficult for the bacteria to develop resistance against AMPs compared to conventional antibiotics. Also, there appears to be none or very limited cross resistance between the different peptides. This is for instance seen with treatment against *P. aeruginosa* which causes the majority of infectious diseases in cystic fibrosis patients. By growing

bacteria in media with sub minimal inhibition concentration (MIC) of AMPs (less-than-lethal) it was with over 11 subcultures not possible to induce resistance to the AMP PG-1.[65] Similar results were shown for a number of different peptides where it through 30 subcultures only were possible to induce a 2-4 fold increase in MIC to the AMPs.[66] Comparable studies with the broad spectrum antibiotics norfloxacin and gentamicin have in contrast showed an up to 190 fold MIC increase.[65] Also attempts to induce resistance to the AMP pexiganan in both *E. coli* and *Staphylococcus* have been unsuccessful.[67] Because the microorganisms in most reported instances of AMP resistance are forced to change fundamental aspects of their membrane like reducing the overall charge, it appears that they weaken their natural defense against other factors. These include bile salts and some conventional antibiotics and this opens a door for combined treatment of infectious diseases with a cocktail of AMPs and conventional antibiotics.[68] Administered together this is likely to prevent or significantly reduce the occurrences of resistance and thereby to obtain more effective pharmaceuticals. This synergistic effect has been shown successful between colistin and rifampicilin in colistin resistant strains but until now there have not been any clinical trials of these different types of antibiotics used together.[68] Further encouraging results with AMPs are that they show great activity against a number of multidrug resistant bacterial strains like *S. aureus* and *P. auruginosa*, but also that they are capable of simultaneously act against a broad spectrum of pathogens in a very rapid manner.[66, 67]

According to public databases the number of identified and characterized AMPs are rapidly growing and there does not appear to be any slowdown in the increasing rate.[27] Despite that, only a very limited number of candidates have gone into clinical trials and in recent years and even fewer of these therapeutic candidates have been approved for pharmaceutical use. One of the potential drug candidates Pexiganan is a synthetic analog of magainin 2 derived from the african clawed frog *Xenopus laevis*. It showed great *in vitro* activity against 3,108 bacterial clinical isolates including Gram-positive and Gram-negative microbes, and at the same time it was not possible to induce resistance to it in different bacterial strains.[67] However, in 1999 the American Food and Drug Administration (FDA) rejected an application for the use of Pexiganan as a therapeutic antimicrobial agent for the treatment of foot ulcers. The rejection was based on Pexiganans disability to outperform already existing products with the same antibiotic abilities. Subsequently Pexiganan has reentered clinical trials under new ownership in order to get approval, but presently this work has been ongoing for more than 10 years. Also other promising drug candidates like Omiganan (an indolicidin), Iseganan (a protegrin) and Neuprex (a bactericidal increasing protein) have failed initial phase III clinical trials for treatment against their initially defined microbial targets. Like Pexiganan they have all reentered clinical trials with newly defined drug targets.[69]

There are currently only a handful of commercial available AMP drugs on the marked. Two of them are Polymyxin B and Colistin (Polymyxin E) which are cyclic lipodecapeptide antibiotics that act by binding to the LPS in the outer membrane of bacteria and thereby destabilize it. They were first discovered in 1962 and were subsequently marketed as a therapeutic against Gram

negative bacteria.[70] In the 1970s both Polymyxin B and colistin showed to be neurotoxic and consequently both drugs were abandoned for use as pharmaceuticals. However, in recent years the rapidly growing resistance to conventional antibiotics has deemed it necessary to reinstate Polymyxin B and Colistin as last resort drugs against extreme multidrug resistant bacteria. Although significant efforts have been invested in reducing the cytotoxicity of Polymyxins there has not been developed any 'second generation' drugs. In 2003 the FDA approved the anionic AMP Daptomycin for treatment of complicated wounds infected by multi resistant bacterial strains, otherwise no new peptides have been approved for antimicrobial treatment in the resent years.[71]

Despite the very limited commercial success with therapeutic AMPs so far there is still a great interest in developing new products from pharmaceutical companies due to the lack of alternatives and the continuously growing demand for new and effective broad spectrum antibiotics. Reasons for the lack of marketed products can be ascribed to various reasons although issues regarding toxicity and stability appear to be key obstacles to be addressed before a breakthrough can be achieved. Considerable efforts have been put into making AMPs less susceptible to protease degradation and one way of achieving this without losing the antibiotic effect could be conversion to D-enantiomers or peptoids.[72] Also, as mentioned above some peptide classes like defensins appear to be less affected by enzymatic degradation which may favor them with regards to some medical applications. Another way of reducing protease degradation is to make the peptides cyclic, which significantly increases their resistance and even in some cases increases their antimicrobial effect.[73] Cyclization can however have the very unfortunate effect that the peptides become more hemolytic compared to linear peptides which makes them unsuitable for pharmaceutical uses, however they might be interesting from other antibiotic perspectives.[73, 74] Many AMPs are hemolytic and especially peptides rich in tryptophan like omiganan and other indolicidins have this cytotoxic characteristic. Single amino acid mutations and introduction of arginine-trypthophan modules have been used in an effort to optimize the antimicrobial effect while reducing the cytotoxicity.[75, 76] Correlations between hemolytic effects and high hydrophobicity, high amphipathicity and high helicity have been shown using amino acids mutations. However, the amino acids compositions effect on hemolysis and cytotoxicity in general still remains to be further elucidated so that AMPs can be designed.

The high costs of producing AMPs compared to conventional antibiotics can be a limiting factor for therapeutic use of AMPs and alternatives to chemical synthesis are clearly needed. In 2005 the Danish medical company Novozymes reported that they successfully expressed a fungal defensin AMP in a fungi expression system which is one way of reducing the cost of production, although this is not generally applicable for AMPs.[33] Another problem to overcome is the sensitivity to physiological salt concentration, divalent cations and mucins which are found in many of the target areas of the AMPs.[77] Although it is possible to modify existing AMPs to tolerate higher salt concentrations most peptides requires altering of fundamental properties like charge and hydrophobicity which is likely to influence the overall activity of the peptides. In

some cases it might be necessary to rethink the field of application of the AMPs and use them in areas with lower salt concentrations.[56]

Other applications of AMPs

Besides from the most obvious use of AMPs as therapeutics in the medical sector other industries are also using AMPs as antibiotics. The food industry has been using the bacteriocin AMP Nisin since it was first introduced in 1953 and was the first AMP to get the FDA notification Generally Recognized as Safe (GRAS).[78] Later a number of similar bacteriocins with increasing potential like lacticin 3147 have been marketed.[79] Nisin is a polycyclic 34 amino acid cationic peptide which has hydrophobic characteristics and contains a number of lanthionines and methyllanthionines. It is stabilized through a number of thioether linkages which are likely to increase its resistance against high temperature and low pH. It is fermented by lactic *streptococci* and is mainly used in dairy products where it acts against Gram-positive bacteria.[80] AMPs are also used as a disinfecting agent within the area of personal care where e.g. a synthetic cecropin is used to kill bacteria in contact lens solutions.[81] Although the industrial use of AMPs are still very limited compared to other antimicrobials a brief look through the public European patent database (ep.espacenet.com) reveals numerous patents granted for use in as different areas as cosmetics, hygiene products, sterilization products and feed products. It therefore seems probable that we within the coming years will see a much wider use of AMPs in household and industrial products.

Biological membranes and membrane mimicking systems

Phospholipids

Phospholipids are a group of lipids and are some of the main components in all cellular membranes. The phospholipids are composed of four components: fatty acids, a phosphate group, an alcohol and a backbone which can consist of different molecular compositions and defines the type of the phospholipid (see figure 3). In biological systems the most abundant phospholipids have a glycerol backbone and are known as glycerophospholipids. Another biological relevant type contains a sphingosine backbone (sphingomyelin) which is only present in animal cell membranes and especially in the myelin sheath which surrounds nerve cell axons.[82] The phospholipid alcohol is covalently bound to the phosphate group and depending on the molecule the lipids obtain a number of different properties which are reflected in the several different variations of phospholipids that is seen in nature. In glycerophospholipids, the carboxyl group of each fatty acid is esterified to the hydroxyl groups on carbon-1 and carbon-2 of the glycerol backbone, and the phosphate group is attached to carbon-3 by an ester link (see figure 3).
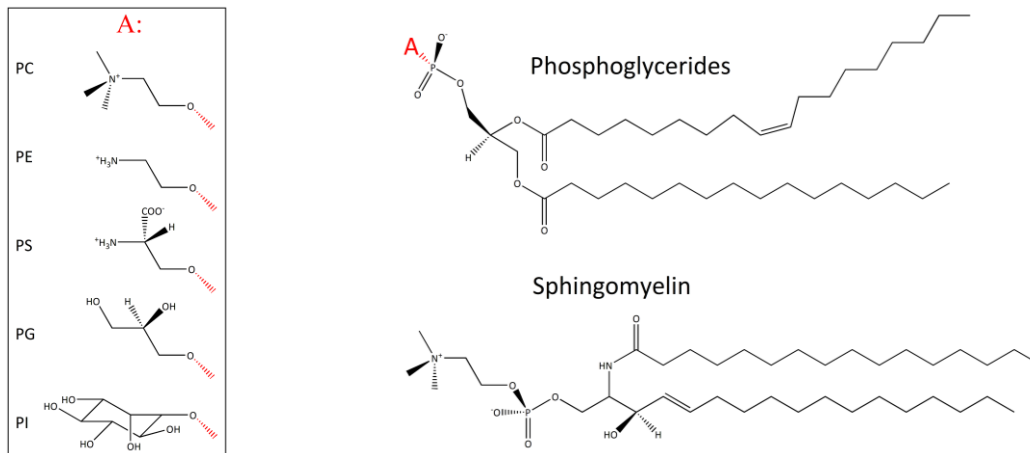
Figur 3. Chemical structures of phospholipids. The phosphate is esterified at the position "A" by a compound bearing a hydroxyl group with some of the most abundant in the box.

Mammalian cell membrane

The basis for all living cells is their ability to compartmentalize and thereby to build and uphold the specialized environments that are necessary for the chemical processes within the cells. The cell wall which is also known as the plasma membrane was in 1972 described by Singer and Nicholson as a 'fluid mosaic' describing the plasma membrane of mammalian cells as a liquid surface wherein the membrane associated components like membrane proteins move around freely (see figure 4).[83] Later models have however described the membrane as more mosaic than fluid but the basic principles remains.[2] In mammalian cells the plasma membrane is typically 30 Å thick and consists mainly of various phospholipids that combined with cholesterol constitute approximately 50 % of the molecules.[84] The lipids are arranged in a bilayer with the hydrophilic head groups of the molecules facing the inner and outer perimeter of the membrane and the hydrophobic tails of the lipids facing each other thereby constituting the center of the bilayer (see figure 4). The major structural lipids in eukaryotic plasma membranes are sphingomyelin (SPH), phosphatidylcholine (PC), phosphatidyllinositol (PI), phosphatidylserine (PS), phosphatidylethanolamine (PE) and cardiolipin (CL). The composition of these lipids varies among the different organelles but the main constituent in all the membrane types (mitochondrial, endoplamatic reticulum, plasmamembrane, lysosomal membrane etc.) are PC followed by PE which are both zwitterionic molecules. This gives a relative neutrally charged membrane surface of the eukaryotic cells compared to the negatively charged prokaryotic surfaces which will be described in the next section.

Bacterial cell membrane

The plasma membrane of prokaryotes is like the eukaryotic cell membrane mainly composed of phospholipids and membrane proteins that enable the cells to uphold a differentiated chemical environment within the cells. Based on the physical properties of their cell membranes, bacteria can be divided into two groups known as Gram positive and Gram negative bacteria (see figure 5). Gram positive bacteria distinguish themselves from Gram negative bacteria and eukaryotic

cells by having a thick (20-40 nm) peptidoglycan layer surrounding the cell wall which provides a physical barrier that stabilizes and protects the bacteria from the environment.[85] This petidoglycan layer provides the basis for binding of a number of polymers including teichoic and teichuronic acids and is furthermore stainable with gram staining (crystal-violet dye) giving name to the group of bacteria.[86] The method of gram staining were published by the Danish doctor Hans Christian Gram in 1884 as a technique for distinguishing bacteria with similar clinical symptoms but has later developed into the property that defines the overall characteristic of bacterial groups.[4] Gram negative bacteria are characteristic in that they have two lipid membranes enclosing the cytoplasmic in contrast to both Gram positive bacteria and eukaryotic cells. The two membranes are termed the outer- and inner-membrane and encompass the periplasmic space wherein a peptidoglycan layer much thinner (1-7 nm) than seen for Gram positive bacteria is placed.[85] A further distinguishing feature in Gram negative bacteria is the presence of a layer of LPS which covers the outer membrane of the bacteria.[87] The LPS layer is easily recognized by animal immune systems and will typically induce a strong immune response when introduced to these.[88] The enzymes responsible for the growth and maintenance of the LPS layer are furthermore the target for a number of different antibiotics like penicillin as mentioned in the *Bacterial resistance* section.
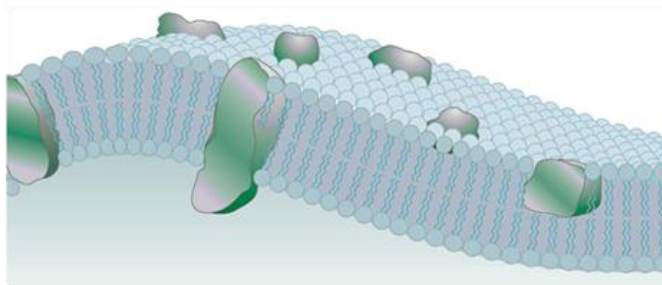
Phospholipids	Plasma membrane
SPH	16.0
PC	39.3
PI	7.7
PS	9.0
PE	23.3
CL	1
Cholesterol/Phospholipid (mol/mol)	0.4

Figure 4. Lipid composition of plasma membrane from rat liver sph (sphingomyelin), pc (phosphatidylcholine), pi (phosphatidyllinositol), ps (phosphatidylserine), pe (phosphatidylethanolamine), cl(cardiolipin) (adapted from [2])

The phospholipid composition of bacterial membranes differs from that of eukaryotic membranes and is generally more anionic. In *E. coli* which is a Gram negative bacteria strain, the most abundant phospholipid is PE, which constitutes 70-80% of the total phospholipid (both membranes), whereas PG (15-20%), PS (~1%), and CL (<5%), a diphosphatidylglycerol, are found in smaller amounts.[89] The phospholipid composition of the outer membrane is slightly enriched in PE compared to the inner membrane.[90] Gram positive bacteria typically have a considerably higher concentration of PG as is seen for B. megaterium with the majority of its phospholipids being PG (48%) compared to PE (35%), CL (11%) and glucosaminyl PG (6%).[91] The relatively high concentration of PG in prokaryote cell membranes compared to in eukaryotic cells is the main reason for the bacterial membrane being more negatively charged.
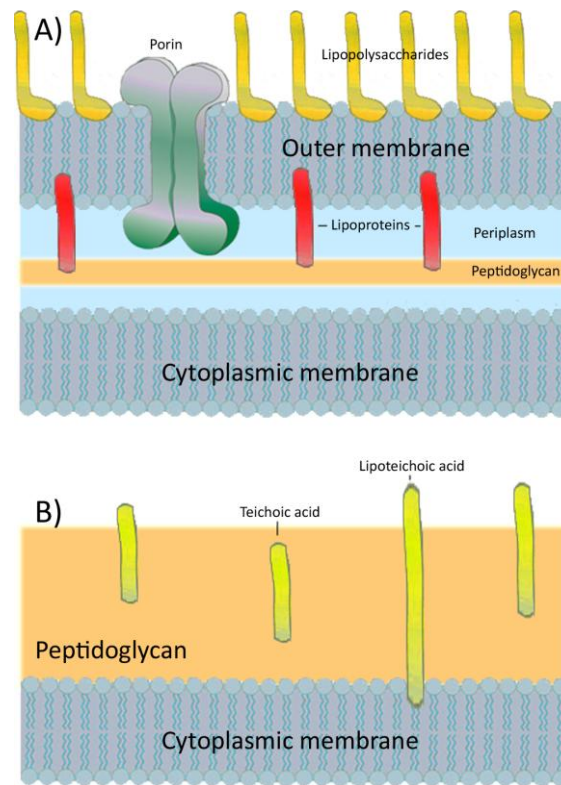
Figur 5. Schematic representation of Gram negative (A) and Gram positive (B) bacterial membrane. The Gram negative membrane is composed of an outer and inner membrane separated by the periplasm wherein a small peptidoglycan is located. The Gram positive membrane consists of a single bilayer encapsuled by a thick peptidoglycan layer. Inspired by [2] and [4].

Membrane mimicking systems

Detergents

Detergents are amphipathic molecules that are typically comprised of a hydrophobic portion, usually a long alkyl chain called the tail, attached to a hydrophilic functional group called the head group. They belong to a class of surface active agents (surfactants) that reduces the surface tension in hydrophobic/hydrophilic mixtures like oil/water by adsorbing to the interface.[92] The ability to detach lipids from surfaces has made detergent widely used in cleaning products but they are also extremely useful in protein science where they are used in a variety of applications like polyacrylamide gel electrophoresis (PAGE), membrane mimicking, membrane permeabilization, membrane dissolution, inclusion body solubilization, crystallization and many more. They are typically grouped by the overall charge of their head groups thus given four groups: anionic, cationic, zwitterionic and non-ionic. The structures of some commonly used detergents are shown in figure 6.

Micelles

Despite the detergents ability to solubilize in aqueous solutions at low concentrations the hydrophobic nature of the detergent tails are very energetically unfavorable for the molecules when they are dissolved in aqueous solutions. When increasing the detergent concentrations the molecules will driven by the hydrophobic effect start to self assemble and form non-covalent clusters in solution. The point at which the assembly commences occurs over a narrow

concentration range and is termed the critical micelle concentration (cmc). When increasing the concentration above the cmc all added detergent will go into micelles however the monomeric concentration of detergent will remain equal to the cmc.[93] The cmc varies depending on the detergent and can relatively easy be determined using a number of different methods like surface tension measurements light scattering or dye experiments[94], although the latter method might have the unfortunate effect that the addition of dye slightly alters the cmc. When micelles are formed they are capable of absorbing more detergents as well as solubilizing hydrophobic and amphipathic molecules like proteins and lipids and thereby make mixed micelles. Initially the detergents will form spherical micelles, whose sizes depend on the properties of the used detergent, but when increasing the concentration more complex shapes like ellipsoidal, rod-like and doughnut shaped detergent aggregates will start to form.[95] Consequently the dynamical properties of the micelles will change as the tumbling rate of the micelles diminishes when transforming into larger aggregates.

sodium dodecyl sulfate (SDS)

dodecylphosphocholine (DPC)

cetyltrimethylammoniumbromide (CTAB)

1,2-dimyristoyl-sn-glycero-3-phospho-(1'-rac-glycerol)(DMPG)

n-dodecyl-β-D-maltoside (DDM)

1,2-dihexanoyl-sn-glycero-3-phosphocholine (DHPC)
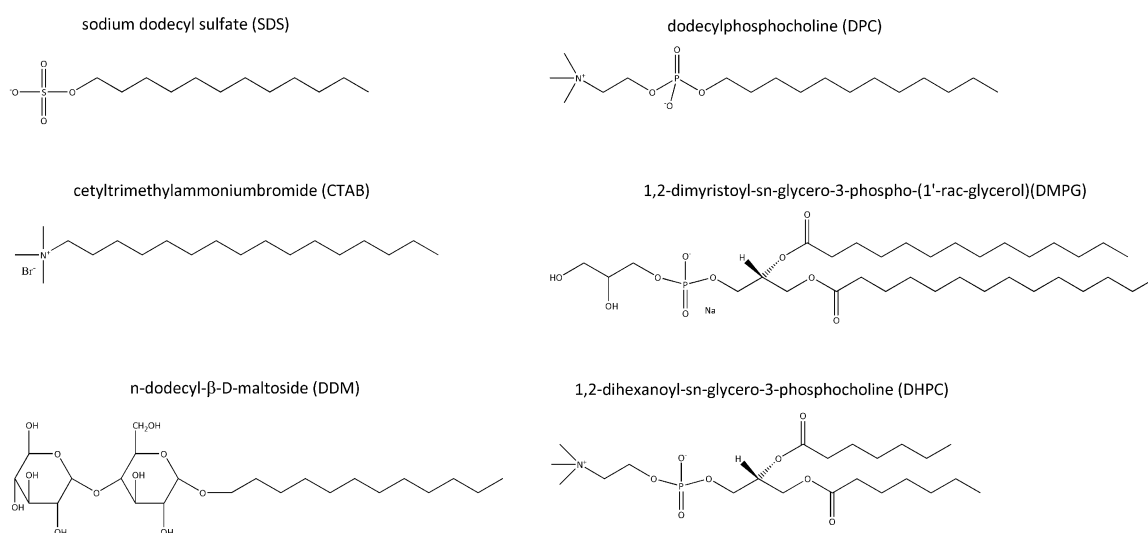
Figur 6. Chemical structures of some common detergents obtained from Sigma Aldrich homepage

Bicelles

Bicelles are non-covalently bound lipid aggregates consisting of a mixture of relative long chain lipids and either shorter chained lipids or short chain detergents.[96, 97] When mixed properly the long chain lipids in theory form soluble disc shaped planar bilayers where the hydrophobic lipid tails are shielded from the water by a rim of short chained lipids (see figure 7) thus stabilizing the macromolecular structure. The size of the bicelles is determined by the ratio of the long chain/short chain lipids (q) and the total phospholipid concentration (c_L), however, they are typically mixed so the diameter is approximately a few hundred angstroms and the width is approximately 40 Å. Bicelles were initially described by Sanders and Prestegard for studying membrane associated biomolecules using solid state NMR[97, 98] but have later been adapted for studies of proteins and peptides in solution. Due to the diamagnetic properties of the lipids commonly used for making bicelles they spontaneously align with the lipid long axis

perpendicular to external magnetic fields greater than 1 T.[97] This property causes an incomplete averaging of anisotropic magnetic interactions which makes it possible to measure the relative orientation of parts of proteins and peptides as the residual dipolar couplings (RDCs) are dependent on the orientation against the external field and are no longer averaged out by isotropic tumbling.[99]
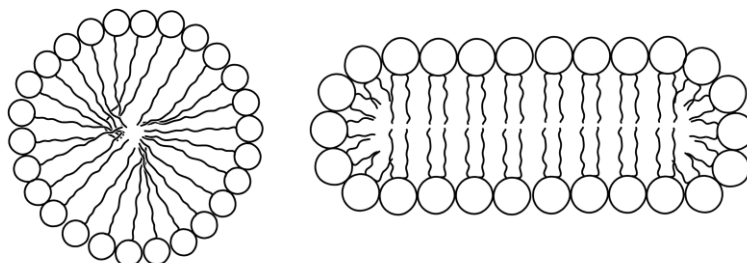
Figur 7. Both micelles (left) and bicelles (right) are largely monodisperse and noncompartmentalized macromolecular structures consistent of either detergents, lipids or a mixtures of these.

Besides a widespread use in alignment media bicelles are also used as membrane mimicking systems because they provide a more native like lipid environment compared to micelles due to the more planar shape of the bilayers.[100] Furthermore, some of the micelle detergents affect the structure of membrane proteins whereas the much lower bicelle detergent concentration does not affect the protein structures to the same extent. Like with micelles it is easier to obtain homogeneous lipids/detergents in bicelles compared to lipid vesicles which combined with their smaller sizes makes them much more suitable for NMR studies.[101]

Liposomes

Liposomes are self-closed structures of lipid bilayers with an aqueous phase on both sides of the bilayer which are typically spherical and of varying sizes. Phospholipid liposomes were first described in the 1960s as multilamellar vesicles structures with several concentric bilayers with water filled gaps in between.[102] Because the lipid composition can be varied and thereby vary the thickness, charge and several other factors of the liposomes, it is possible to create liposomes which highly resemble the properties of biological membranes. Many different types of liposomes have been described and liposomes have been extensively used as membrane mimicking model systems and more recently also as drug delivery systems.[103] The most commonly used liposomes are unilamellar which as the name implies only contain a single bilayer encompassing its aqueous inside. They are typically grouped according to the diameter of the vesicles and named either small unilamellar vesicles (SUV), large unilamellar vesicles (LUV) or giant unilamellar vesicles (GUV). SUV refers to liposomes less than 100 nm but typically around 40 nm which can easily be formed by sonicating larger multilamellar vesicles.[104] LUVs ranges in size from 200- 800 nm and can be prepared by pressing lipids through e.g. 200 nm pores which gives relative uniform sized liposomes.[105] GUV size ranges from 5 – 200 µm and can be prepared using various methods depending on the desired size. Because the size of these liposomes is comparable with the size of many cells, many studies of membrane properties have been using GUVs.[106] This is further enhanced by the ability to study these liposomes using light

microscope whereby a number of morphological changes like budding, healing, endocytosis and other cytomimetic processes can be observed.[107] As liposomes can be prepared with different aqueous solutions in and out, it is furthermore possible to measure even small disruptions of membrane by measuring dye leakage from liposomes where the encapsulate phase contains dye.[108]

Nuclear Magnetic Resonance

Introduction

NMR is a very powerful technique for studying structural and dynamical properties of peptides and proteins, and it is currently the only method by which these can be studied in solution at atomic resolution. In the following a short introduction to the basic principles of NMR will be given.

All atomic nuclei and electrons have an intrinsic property called spin which generates a magnetic field. The fields have an angular momentum associated with them and the values for these are according to the Schrödinger equation +½ or -½ (also denoted α and β respectively) for the most commonly studied nuclei (^{1}H, ^{13}C, ^{15}N and ^{31}P). When the nuclei are placed in a strong magnetic field (B_0) the angular momentum axis coincides with the field direction of the magnetic moments which causes a energy difference between the α and β states. α has a z-component aligned with the external field and is therefore in a lower energy state than β which opposes the external field. This causes a population bias toward the lower energy states according to the Boltzmann distribution, and the energy difference (ΔE) between the two spin states is defined as:

$$\Delta E = h\nu = \frac{h\gamma B_0}{2\pi}$$
(1)

where h is Planck's constant, ν is the frequency and γ is the gyromagnetic ratio. Because the energy of a photon is E=hν it is possible to change the spin angular momentum by applying a radio wave with the same energy as ΔE to the nuclei whereby the α and β states will resonate and the two populations equalize.[109]

Modern NMR spectrometers can excite all nuclei in the range of interest at the same time by applying a radio frequency (RF)-pulse to the sample, which tilts the magnetization vector away from the equilibrium position along the external magnetic field. The excited magnetization oscillates in the xy-plane about the z-axis creating an observable RF, and it is the frequency of this signal that is recorded as it returns to its equilibrium. This decay is known as free induction decay (FID) and is converted into a frequency spectrum using the Fourier transformation.[110]Due to a shielding effect by local nuclei and electrons for each nucleus, variations in the parts per million (ppm) scale occur in the magnetic field, and thereby in the frequencies. As a consequence do different structural environments give rise to different frequencies from each nucleus which can be observed in the NMR spectra. These variations are referred to as chemical

shifts and the ppm unit is adapted due to its independence of the external field strength, which is very practical when spectra from spectrometers with different field strengths are to be compared.

The magnetic field of neighboring non-equivalent nuclei affects each other by either *through bond* or *through space* couplings. Through bond connectivities (called scalar couplings or J-couplings) arises through the transfer of magnetization between two nuclei mediated by the electrons participating in the bonds. They originate from either dipole interactions or Fermi contact interactions in cases where the electron occupies the s-orbital, and can be between either identical atom types (homonuclear) or different atom types (heteronuclear). The coupling constants are independent of the external magnetic field strength and the magnitude of them is typically dependent on the number of bonds separating the nuclei and the molecular geometry. They are denoted depending on the number on the number of bonds (e.g. ^1J, ^2J, ^3J), and in protein samples couplings between nuclei separated by more than three bonds are rarely visible. To ease the interpretation of spectra the multiple peaks per nuclei originating from the J-couplings are often merged into one by a decoupling pulse which refocuses the coupling.

Local magnetic fields generated by nuclei affect one another through space without any contributions from the electron clouds which is known as dipolar coupling. However, in solution state NMR the tumbling of the molecules is isotropic and very fast on the NMR timescale which causes the time averaged dipolar coupling to become zero.

Relaxation

As mentioned above the magnetization of the nuclear spin (M) will return to its Boltzmann equilibrium position along the B_0 axis (z-axis) after perturbation. This time dependent decay is caused by energy transfer between the nuclear spin and its surroundings given by the equation:

$$M_z(t) = M_0 - [M_0 - M_z(0)]e^{-R_1 t} \tag{2}$$

where R_1 is the *longitudinal* relaxation rate and $M_z(0)$ is z-axis magnetization at time = 0.[111] It is possible for the observable xy-magnetization to disappear without returning to the equilibrium along the z-axis. This is caused by the loss of phase coherence, meaning that the signals will be distributed equally in the xy-plane and thereby cancels out. The time dependency of this *transverse* relaxation is determined by the R_2 rate constant and caused by interactions with neighboring spins in the sample, and is like longitudinal relaxation given by a first order equation:

$$M_{xy}(t) = M_{xy}(0)e^{-R_2 t} \tag{3}$$

where $M_{xy}(0)$ is either magnetization along the x- or along the y-axis at time = 0 and R_2 is the *transverse* relaxation rate.[111] There are several mechanisms by which the nuclear spins are interacting with the surrounding nuclei and electrons and both intra- and inter-molecular

processes can lead to relaxation processes. The overall relaxation properties of nuclei can be defined as a combined contribution of several mechanisms:

$$R(observed)=R(DD)+R(SR)+R(CSA)+R(SC)+R(Q)+R(e) \tag{4}$$

where R(DD) is the contribution from dipole-dipole interactions, R(SR) from spin rotation, R(CSA) from chemical shift anisotropy, R(SC) from scalar couplings, R(Q) from quadrupole interactions and R(e) from couplings with unpaired electrons.

Dipolar relaxation

For a two spin system there exists four energy levels with a total of 12 transitions (see figure 8).
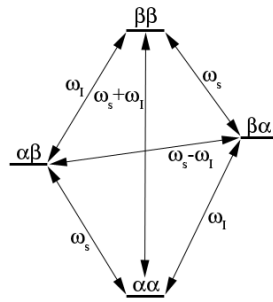
Figure 8. Energy levels of a two spins system consisting of I and S spin and transitions between them. Transitions involving a single spin flip require the energy at Larmor frequencies ω_I or ω_S. Transitions can also occur through double- and zero-quantum transitions. All transitions also exist with opposite signs.

In systems without any paramagnetic spices or quadruple nuclei present the dominant relaxation mechanism for energy exchange for spin ½ nuclei is DD interactions. The DD relaxation is made up of two overall contributions called auto relaxation and cross relaxation which for two unlike spins I and S is given by the Solomon equations[112]:

$$\frac{dI_z}{dt}=-\rho_I(I_z-I_z^0)-\sigma_I(S_z-S_z^0) \tag{5}$$

$$\frac{dS_z}{dt}=-\rho_S(S_z-S_z^0)-\sigma_S(I_z-I_z^0) \tag{6}$$

where ρ_I and ρ_S are the auto relaxation rates and σ_I and σ_S cross relaxations rates. When the proteins reorientate in the solution, the nuclei experience different local fields, and the relaxation rates are therefore dependent of the protein tumbling rates.[112] The auto relaxation rates (R_1 and R_2) in a two spin systems (I and S) where we assume a fixed distance between the spins are given by[111]:

$$R_1^I=\left(\frac{\mu_0}{4\pi}\right)^2\frac{\hbar^2\gamma_I^2\gamma_S^2S(S+1)}{r_{IS}^6}\left\{\tfrac{1}{4}J(\omega_I-\omega_S)+\tfrac{3}{4}J(\omega_I)+\tfrac{3}{2}J(\omega_I+\omega_S)\right\} \tag{7}$$

$$R_2^I=\left(\frac{\mu_0}{4\pi}\right)^2\frac{\hbar^2\gamma_I^2\gamma_S^2S(S+1)}{r_{IS}^6}\left\{\tfrac{1}{4}J(0)+\tfrac{1}{8}J(\omega_I-\omega_S)+\tfrac{3}{8}J(\omega_I)+\tfrac{3}{4}J(\omega_S)+\tfrac{3}{4}J(\omega_I+\omega_S)\right\} \tag{8}$$

where J(ω) is the spectral density functions, μ_0 is the permittivity of free space, . ω_I and ω_S is the larmor frequencies of the spins and r_{IS} is the distance between the spins. For an isotropic rotational diffusion of a rigid rotor or spherical top the spectral density functions are given by:

$$J(\omega) = \frac{2}{5} \frac{\tau_c}{(1+\omega^2 \tau_c^2)} \qquad (9)$$

where τ_c is the correlation time which is the time for the molecule to rotate by one radian and therefore are dependent on molecular size, solvent viscosity and temperature. ω is the larmor frequencies. A rule of thumb is that τ_c is in the order of picoseconds for small molecules and in the order of nano seconds for larger biological macromolecules in aqueous solutions. In all protein and peptide samples $\omega\tau_c \gg 1$ which causes very low R_1 rates compared to R_2 rates and as a consequence transverse relaxation is the dominating relaxation mechanism when studying biological molecules.

The dipolar interactions between nuclei causes a transfer of spin polarization from one spin population to another via cross relaxation which causes the Nuclear Overhauser effect (NOE). RF pulses with frequency ω_S will equalize the αα and βα populations as well as the ββ and αβ populations (see figure 8). These levels will equalize through cross relaxation where ($\omega_I + \omega_S$) will populate level αα by transferring magnetization from ββ originating from βα and likewise will level ($\omega_I - \omega_S$) transfer magnetization to level βα via level αβ. The dipolar cross relaxation rate is given by:

$$R^I = \left(\frac{\mu_0}{4\pi}\right)^2 \frac{\hbar^2 \gamma_I^2 \gamma_S^2 S(S+1)}{r_{IS}^6} \left\{ -\frac{1}{4} J(\omega_I - \omega_S) + \frac{3}{2} J(\omega_I + \omega_S) \right\} \qquad (10)$$

Because of the distance dependency of NOEs they can provide information regarding nuclei which are in close proximity of each other (typically only observable on distances less than 5 Å) and this information is of prime interest for structural studies of proteins as these nuclei may be far apart in the polypeptide chain.[113]

Scalar and Quadrupole relaxation

The scalar relaxation occur when nuclei interact through chemical bonds (J-couplings) and the spin I can feel the neighboring spin S in two forms. *Scalar relaxation of the first kind* can occur when values of J_{IS} is changing due to reorientation of atoms in accordance with the Karplus relationship. *Scalar relaxation of the second kind* is for spin I dependent on the rapid relaxation of spin S which could be a result of chemical exchange where nuclei I and S is shifting between a bound and unbound state which can be seen for exchangeable protons like NH or could be cause by a binding to a quadrupolar nucleus.[111] The latter nuclei has a spin >½ and is characterized by a non-spherical distribution of electrical charges and it possesses an electric magnetic moment. The quadrupolar couplings are typically in the MHz range which consequently causes the nuclei to relax very quickly and the presence of quadrupolar nuclei will therefore typically dominate the overall relaxation rate if they are present.

CSA relaxation and spin rotation relaxation

Chemical shifts are defined by the magnetic shielding from the external field and chemical shift variations within molecules are caused by their different structural environments. These local fields are anisotropic and because of molecular motions the components of the local fields reorientates with respect to the axis of the external field which is a cause of relaxation.[111] The maximum CSA of a nucleus is determined by its maximum chemical shift range and CSA relaxation is consequently predominant for nuclei with large chemical shift ranges like ^{31}P, ^{13}C and ^{15}N whereas CSA relaxation of protons are much less pronounced. After dipolar relaxation is CSA relaxation the second largest contributor to the overall relaxation properties of nuclei with large chemical shift ranges when quadrupolar and paramagnetic species are not present.[111]

Spin rotation relaxation has the largest impact in small symmetric molecules and can therefore be neglected when considering larger biological molecules. Spin rotation interactions originate from rotating electronic charge distributions like methyl groups which generates a magnetic field which is proportional to the magnitude of the rotational angular momentum. By means that will not be elaborated here the generated magnetic field contributes to spin relaxation of neighboring nuclei.
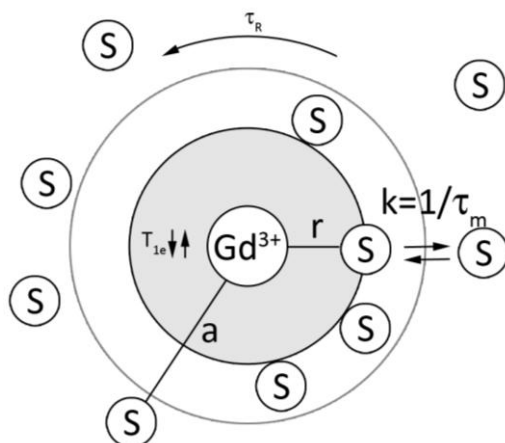
Paramagnetic Relaxation

Paramagnetic species are characterized by having unpaired electrons which generate local magnetic field and is typically seen in free radicals or transition metal complexes. The relaxation mechanisms for paramagnetic relaxation are the same as for other relaxation mechanisms like nuclear dipolar relaxation and scalar relaxation except that the interaction is between a nucleus and an electron. The reason the other relaxation rates and R(e) are separated in eq. 4 is that although the mechanisms are the same the impact on neighboring spins is considerable different. Considering eq. 7 and 8 it is seen that the relaxation rates are dependent on both the gyromagnetic moment of the spins I and S and dependent on the spin angular momentum e.g. ½ for protons. Because the gyromagnetic ratio of electrons is much higher compared to that of nuclei ($1.760 * 10^{11}$ $s^{-1}T^{-1}$ compared to $2.6752 * 10^{8}$ $s^{-1}T^{-1}$) the relaxation rates in the presence of paramagnetic species are significantly increased which is known as paramagnetic relaxation enhancement (PRE). Furthermore does many widely used paramagnetic species like Gd^{3+}, Mn^{2+} and Ni^{2+} have a spin angular moment different than ½ ($\frac{7}{2}$, $\frac{5}{2}$ and 1 respectively) which also increases the relaxation rates.

The initial way of describing paramagnetic relaxation was formulated by Solomon, Bloembergen and Morgan in the 1950s and 1960s. Solomon first described the paramagnetic relaxation as a pure dipolar relaxation[112] and later J-couplings (scalar relaxation) and relaxation properties for higher spin numbers were added to the equations in collaboration with Bloembergen and Morgan.[114] The Solmon-Bloembergen-Morgen equations make a number of assumptions like assuming a fixed distance between spin I and spin S which limits the theory.

For describing the relaxation properties of non fixated paramagnetic species like contrast agents it is necessary to divide the overall paramagnetic relaxation rate into three separate

contributions namely inner sphere, outer sphere and second sphere relaxation. Inner sphere represents the relaxation contribution for the nuclei directly bound to the paramagnetic species whereas outer sphere represents the relaxation occurring due to dipolar interaction between nuclei and electrons with unrestricted relative molecular motions, typically occurring with solubilized paramagnetic agent (see figure 9).

Figur 9. Schematic representation of the three relaxation spheres surrounding paramagnetic Gd wherein relaxation of the spin S is defined by inner sphere (gray circle), second sphere (white circle) and outer sphere relaxation (area outside the circles) occurs. Inspired by[1]

Inner sphere relaxation is typically the most important contribution to the overall paramagnetic relaxation rate and the predominant amount of data recorded on soluble Gd^{3+} chelates have been analyzed using inner sphere theory (Solmon-Bloembergen-Morgen theory).[115] The longitudinal relaxation rates are given by:

$$R_1 = \frac{2}{15}\left(\frac{\mu_0}{4\pi}\right)\frac{\gamma_H^2 \left(g_J \mu_B\right)^2 J(J+1)}{r^6}\left(\frac{3\tau_c}{1+\omega_H^2\tau_c^2}\frac{7\tau_c}{1+\omega_S^2\tau_c^2}\right)+\frac{2}{3}J(J+1)\left(\frac{A}{\hbar}\right)^2\left(\frac{\tau_e}{1+\omega_S^2\tau_c^2}\right) \quad (11)$$

$$\frac{1}{\tau_c} = \frac{1}{T_{1e}} + \frac{1}{\tau_M} + \frac{1}{\tau_R} \quad (12)$$

$$\frac{1}{\tau_e} = \frac{1}{T_{1e}} + \frac{1}{\tau_M} \quad (13)$$

where J is the electronic spin, r is the distance between the electron and ^1H spin, g_J is the Lande factor, μ_B is the Bohr magneton, τ_R is the complex correlation time, $A/\hbar$ is the electron nuclear hyperfine coupling constant, T_{1e} is the electron relaxation and τ_M is the lifetime of the intermolecular adduct. It should be noted that the first part of the equation originates from dipolar relaxation whereas the latter part originates from scalar couplings.

Outer sphere relaxation account for approximately 40 % of the relaxation of monoaquo Gd^{3+} complexes and originates from dipolar modulations when spins diffuse within proximity of each other. The longitudinal relaxation is described as[1]:

$$R_{1p}^{OS} = C^{OS}\left(\frac{1}{aD}\right)\left[7J(\omega_S) + 3J(\omega_I)\right] \tag{14}$$

$$J(\omega) = \text{Re}\left[\frac{1 + \frac{1}{4}\left(i\omega\tau_d + \frac{\tau_d}{T_{1e}}\right)^{\frac{1}{2}}}{1 + \left(i\omega\tau_d + \frac{\tau_d}{T_{1e}}\right)^{\frac{1}{2}} + \frac{4}{9}\left(i\omega\tau_d + \frac{\tau_d}{T_{1e}}\right)^{\frac{1}{2}} + \frac{1}{9}\left(i\omega\tau_d + \frac{\tau_d}{T_{1e}}\right)^{\frac{1}{2}}}\right] \tag{15}$$

$$j = 1, 2$$

$$\tau_d = \frac{a^2}{D} \tag{16}$$

where C^{OS} is a constant ($5.8 * 10^{-13}$ s^{-2}M^{-1}) and the non-Lorentzian spectral density function contain the dependence on τ_S. At the magnetic fields of interest it depends primarily on the distance of closest approach a (see figure 9), related to the molecular dimension and charge distribution of the complex, and on the relative diffusion coefficient of solute and solvent D.

To fully describe the paramagnetic relaxation mechanisms the second sphere relaxation mechanism has been introduced. This relaxation mechanism contributes to the overall relaxation mechanism when the spin S is fixated at the paramagnetic electron for longer time than the diffusional correlation time τ_d which is seen when chelated paramagnetic complexes is non-covalently bound to the nuclei through hydrogen bindings. The relaxation rate theory of second sphere relaxation are identical to that of inner sphere relaxation if the lifetime of the interactions is long compared to the time required for the affected nuclei and the chelated paramagnetic agent to diffuse past each other.[115] Because there is not covalent bonds between the spins the rate constant equations differ in that there is no relaxation through scalar couplings:

$$R_1 = \frac{2}{15}\left(\frac{\mu_0}{4\pi}\right)\frac{\gamma_H^2\left(g_J\mu_B\right)^2 J(J+1)}{r^6}\left(\frac{3\tau_c}{1 + \omega_H^2\tau_c^2} \frac{7\tau_c}{1 + \omega_S^2\tau_c^2}\right) \tag{17}$$

Structural determination of proteins and peptides

Homonuclear spectra

As the name implies does homonuclear spectra transfer magnetization between nuclei of the same kind which almost exclusively is protons. Homonuclear spectra provided the basis for the first structural determination of proteins and peptides using NMR and are still widely used for this purpose. Three of the most common types of spectra will briefly be discussed in the following and the content of this section is based on the textbooks by Wüthrich et al.[110] and Cavanagh et al.[111]

Correlation spectroscopy (COSY) spectra is the simplest form of two dimensional NMR spectra with only two RF pulses separated by an evolution time wherein magnetization is transferred from one nuclei to a neighboring homolog nuclei through scalar bonds. It is possible to observe correlations through three bonds and the information provided can play a very important role for resonance assignments of small chemical molecules, peptides and even small proteins. Because the diagonal and cross peaks differ in phase by 90° it is not possible to phase the signals so that both are simultaneously absorptive which can cause problems with spectral overlap due to broad signals. However, by applying an extra RF pulse at the end of the pulse scheme it is possible to only select double quantum coherences whereby all peaks in the spectra have the same phase. Double quantum filtered (DQF) COSY spectra are consequently by far the most widely used type of COSY spectra.

Total Correlation spectroscopy (TOCSY) transfers magnetization through scalar couplings. Isotropic mixing transfers magnetization between coupled spins which typically are separated by up to five bonds although in polypeptides it is only possible to seen connections within the amino acids of the spin. All peaks in TOCSY spectra are absorptive and in-phase in both dimensions in contrast to DQF-COSY spectra which give dispersive signals. The TOCSY spectra are extremely important for successful resonance assignment in non-isotope labeled polypeptides and is often used together with DQF-COSY spectra for initial identification of spin-systems.

Nuclear Overhauser Effect spectroscopy (NOESY) spectra transfers magnetization through space via cross relaxation as described in the section *dipolar relaxation*. Because dipolar couplings are dependent on the inverse sixth power of the distance between the two spins it is possible to obtain information regarding which spins is within approximately 5Å of each other in space but not necessarily close to each other in the amino acid sequence of the polypeptide. This information is of the utmost importance when determining the secondary and especially the tertiary structure of proteins and peptides.

Heteronuclear spectra

For large proteins (typically >10 kDa) the amount of signals will in 2D homonuclear spectra typically reach a level where spectral overlap is inevitable which makes it impossible to assign all signals and consequently determine the structure. To overcome this problem it is possible to record heteronuclear spectra wherein magnetization is transferred between different types of nuclei, typically protons and nitrogen or carbon. These types of spectra increases the obtainable amount of information, makes it possible to add extra dimensions e.g. 3D, 4D and through advanced pulse sequences makes it possible to selectively record spectra with different types of couplings which all aides the process of assigning the signals. Because both the predominant isotopes of nitrogen and carbon are not spin ½ it is necessary to isotope label the proteins with the appropriate isotopes depending on the spectra one wants to record (^{13}C and ^{15}N in the case of carbon and nitrogen). Because the natural abundance of ^{13}C is 1.1% it is however possible to record spectra on samples that are not enriched with the isotope although it takes considerable longer time.

Heteronuclear single quantum correlation (HSQC) spectra transfers magnetization from protons to typically ^{15}N or ^{13}C through scalar couplings and after an evolution time the magnetization is transferred back to the protons and a FID is recorded. HSQC spectra are widely used because they provide a great dispersion of the signals and because of the simplicity of the spectra due to the relative low amount of signals (one pr. amide group in ^{1}H,^{15}N-HSQC spectra of proteins).

Structure determination strategies

Although different approaches for structural determination of proteins and peptides exist, the general strategy were first developed by Kurt Wüthrich and coworkers[110]. For proteins and peptides the first step is the recording of correlation spectra from which sets of signals belonging to the same amino acids can be defined and the type of spin systems can be identified. Secondly the signals are assigned to specific residues in the predetermined primary sequence based on through space connections obtained from the NOESY spectra aided by knowledge about the spin systems obtained from the correlation spectra. Following the resonance assignment the remaining NOEs are assigned providing information about interresidual connections and atoms within close proximity of each other. NOEs are subsequently integrated and the volumes are converted into distance restraints which are used as input for structure calculation programs. Additional input can be obtained from chemical shift values as these contain information regarding the torsion angles in the backbone of proteins.[116] Also RDCs and psedo constact shifts can be used as restraints in structure calculations however these will not be discussed further in this thesis. The first set of calculated structures is used to evaluate the NOE assignments based on a error function defined by the structure calculation programs which typically is based on the calculated structures fulfillments of factors like torsion angles and steric overlap.[117] After cleanup of the NOEs a final set of structures are calculated and typically the 20 structures fulfilling the target function the best are selected and energy minimized.

Pseudoatoms

It is not possible from normal homo- or heteronuclear spectra to distinguish between chemically nonequivalent, diastereotopic proton signals bound to the same nucleus as it is seen for different carbon-hydride groups in amino acid side chains. Consequently is it not possible to stereospecific assign the signals hence use them for structure calculations even though they can provide important information for the structure calculations. To overcome this problem pseudo atoms have been introduced which are hypothetical atoms with no mass placed at the center between the non assignable protons.[118] When volumes of the integrated NOEs are converted to distances the distance is then calculated to the pseudo atoms instead of the protons. However, because the distance to the protons is only rarely the same as to the pseudo atoms it is necessary to correct the calculated distance with the maximum distance between the pseudo atom and the protons which is the largest possible error. Although this prevents violations in the structure calculation it also introduces an unwanted uncertainty as the introduced error in most cases is much lower than the pseudo atom correction accounts for.

It is therefore desirable to stereo specifically assign as many protons as possible which can be done using various computational and experimental methods. For some amino acid types (valine and leucine) it is possible to stereospecific assign the protons by using fractional ^{13}C labeling combined with knowledge of the biosynthetical pathways.[119] Other labeling schemes rely on selectively deuterating glycine and leucine protons whereby stereospecific assignment can be made.[120] A completely different approach is to analyze the local conformation around methylene groups which can be done either manually[121] or systematically using grid searches in combination with preliminary structures[122] Furthermore, C,H and H,H dipolar couplings can be used for determining the stereospecificity of CH_2 groups provided that additional structural information is known.[123] Software programs which have been developed by Peter Güntert and coworker are additional methods of determining the stereospecific assignments of amino acid sidechain protons which relies on scalar couplings in combination with NOEs (HABAS) or diastereotopic substituents based on distance restraints and calculated structures (GLOMSA).[124, 125]

Discussion of papers

Paper I, II and III

This section elaborates on Paper I (Quantitative Use of Paramagnetic Relaxation Enhancements for Determining Orientations and Insertion Depths of Peptides in Micelles), Paper II (Divorcing folding from function: How acylation affects the membrane-perturbing properties of an antimicrobial peptide) and Paper III (Structural studies of amphibian antimicrobial peptides in micelle and bicelles phospholipid environments), which describes the results of the thesis work performed on peptides interaction with membrane mimicking detergents and lipids using solution NMR. The overall purpose of this study was to investigate how peptides and especially peptides with antimicrobial properties interact with membranes, and to achieve this we used the peptides novicidin, novispirin, acylated variants of novicidin, citropin and maculatin as model systems. Common for the peptides we used is that they all originate from naturally occurring AMPs where they act as first line of defense against microbes in epithelia of their respective host organisms. They are furthermore all members of the group of *linear cationic α-helical peptide* described previously hence the structural properties of the peptides are very similar. Their net charge at physiological conditions ranges from +2 and +3 for maculatin to +6 for novispirin, novicidin and they all have an amphipathic nature when structured.

Novispirin, novicidin and acyl-novicidin are all derivatives of ovispirin which again is derived from the larger AMP SMAP-29 from sheep. Ovispirin has the very unfortunate property that it is highly cytotoxic to human epithelial cells and hemolytic for human erythrocytes which clearly limits its use as therapeutic in humans.[126] In a pursuit to reduce these characteristics, single amino acid mutations were carried out by Sawai et al. and the result of this work showed a promising reduction of hemolytic behavior without compromising the AMP effect of the peptide in the derived group called novispirins.[75] The efficiency of novispirin has been significantly improved through point mutations where the mutation of Gly18 to Phe18 has decreased the MIC against the gram positive bacteria *L. monocytogenes* and *S. aureus* from 0.125–128 µg/ml to 0.031–32 µg/ml.[127] This novispirin derivative is known as novicidin and it retains the relative low hemolytic effect as observed from novispirins.

In paper I we used the two model peptides novicidin and novispirin for studying interactions between members of the *linear cationic α-helical peptide* group and model mimicking dodecylphosphocholine (DPC) micelles. DPC titration experiments with the peptides using far ultraviolet (UV) circular dichroism (CD) were recorded prior to the recording of the NMR spectra (figure 10). These spectra revealed in agreement with previous studies[128] that neither of the peptides exhibited any secondary structure in buffer solutions or with DPC concentrations below cmc (1.1 mM). At DPC concentrations just exceeding cmc value the circular dichroism (CD) signals at 208 and 222 nm shifted towards negative values for both the novicidin and novispirin samples, clearly indicative of α-helix formation. NOESY spectra of the peptides in pure buffer solution showed very sharp signals for all amino acids which are typically seen for peptides with high flexibility (low τ_c values), often seen in unstructured proteins and peptides. Furthermore

were water exchange peaks seen for all H^N peaks reflecting the exposure of the amide protons toward the solvent. Upon addition of DPC the lines broadened and new cross peaks characteristic of α-helix occurred (e.g. *i, i+3*) whereas exchange peaks for a number of amino acids disappeared, all clear signs of micelle binding. The proton signals of both novispirin and novicidin dissolved in DPC micelles were manually assigned with the aid of standard sets of homo/hetero nuclear spectra, and the subsequently calculated structures revealed as expected two highly identical α-helices spanning the entire length of the peptides (see paper I, fig 2). Likewise the structure of c16-novicidin was determined in DPC micelle solutions from which it was seen that the N-terminal attached acyl chain(s) does not affect the structure of novicidin (see paper II, fig 8). Although the structures of novicidin, novispirin and acyl-novicidin were almost identical the antimicrobial effects of novicidin are considerable higher than that of novispirin as mentioned above.
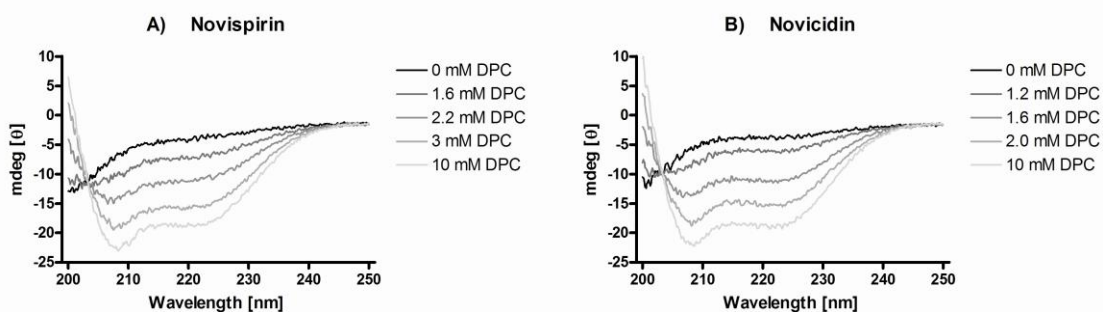

Figure 10. Far-UV CD spectra of Novispirin and Novicidin in the presence of varying amounts of DPC. From the local minima induced at 208 and 222 nm it is clear that DPC induces α-helix formation in both peptides.

So far no one has been able to formulate the optimal characteristic for AMPs with respect to high antimicrobial activity and low cytotoxic effect – perhaps because they in some aspects contradict each other. However, the activity of the peptides are most likely made up of five different factors; charge, conformation, amphipathicity, hydrophobicity and polar angle (see figure 11)[3]
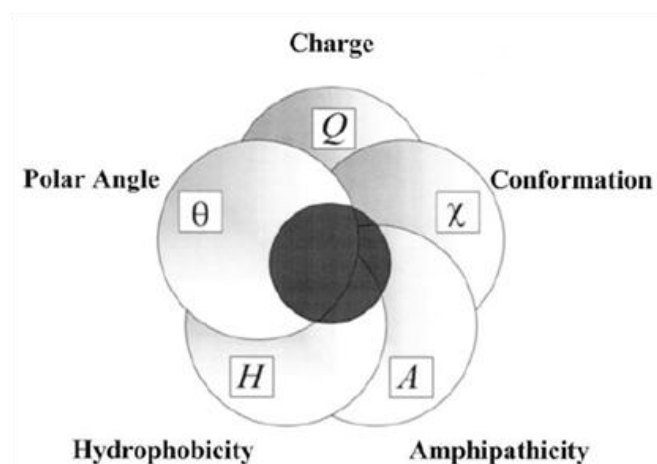

Figur 11. Interrelationship between relevant factors influencing the activity of AMPs. Adapted from[3]

It has been suggested that the helicity of peptides plays a major role in the activity of the group of linear cationic α-helical peptides[20, 129] however it is clear from our structural determination of novispirin, novicidin and acyl-novicidin that the difference in AMP activity between these peptides is not caused by this factor. Exchanging a Gly to a Phe does not affect the charge of peptides and it is therefore in our case not this factor affecting the activity either. The remaining three factors are in the case of novispirin and novicidin overlapping as the mutation to the more hydrophobic Phe increases the hydrophobicity, changes the polar angle and makes the amphipathicity more pronounced. Pathak et al. suggest that increased amphipathicity has a larger positive impact on the AMP activity than the hydrophobicity.[130] As calcein release studies from GUV's upon exposure to novicidin and acyl variant show (paper II, fig 3), increasing the hydrophobicity by attaching an acyl groups to the peptide actually deteriorates the activity of the peptides. This effect appears to be more pronounced with the longer and more hydrophobic c16 acyl chain than the c12 and especially the less hydrophobic c8 chain (paper II, fig 3). This is in contrast to previously published studies of acylated peptides which have shown that the aggressiveness of AMPs is correlated with the length of the attached carbon chain[131] and that the chain length correlates with the membrane permeabilizing ability so that the activity is increased by the added hydrophobicity.[132] By titrating micelle embedded novicidin and acyl novicidin with the paramagnetic probe gadolinium–diethylenetriaminepentaacetic acid (Gd(DTPA-BMA)) it was possible to qualitative asses that the acylated and more hydrophobic peptide variant was deeper inserted into the micelles than the wild type (paper II, fig 8). However, the acylation of novicidin increases the concentrations needed for vesicle disruption, and furthermore leads to a decreased preference for zwitterionic vesicles compared to partially anionic vesicles (see paper II, fig 3). There is no obvious explanation for this reduced membrane disrupting abilities, however it can be speculated that the acylated novicidin variants help retaining the overall composition of the membrane (paper II). The polar angle is a measurement of the relative proportion of polar versus nonpolar facets of an AMP conformed to an amphipathic α-helix. A smaller polar angle, and therefore a greater hydrophobic surface, is associate with an increased capacity to permeabilize membranes.[3] However, as both novispirin and novicidin have an α-helical amphipathic structure and therefore do not have any large sequentially combined hydrophobic areas, the introduction of a single hydrophobic amino acid does not change the over polar angle noticeable and this cannot account for the MIC difference between novispirin and novicidin either.

For a better understanding of the peptides interaction with the model membranes we sought to develop a method by which we could obtain high resolution data without costly isotope labeling of the peptides which would allow for recording of RDCs (paper I). Prior to our work a method for estimating peptide orientation and immersion depth based on titrating micelle bound peptides with chelated paramagnetic Gd^{3+} was developed by Zangger and co-workers.[133] They expanded the use of Gd(DTPA-BMA), which were first used by Ottinger et al.[134] for studying proteins, to be used for obtaining PRE values of micelles embedded peptides. However, their method did only encompass perfectly straight helices and because the tilt angle and orientation

were fitted to the combined PRE values the method was vulnerable to PRE value errors from single amino acids.

We adapted the use of Gd(DTPA-BMA) for measuring PRE values of micelle bound peptides from Respondek et al.[133] but our method differs to theirs in all other aspects. By determining the distances between the center of a micelle and the peptide atoms we were able to retrieve information concerning both the insertion depth and the relative orientation based on independent calculation for each atom. However to get to this point we first had to calculate a correlation function between PRE values and distances (within the micelles)(paper I, fig 1). DPC micelles were titrated with Gd(DTPA-BMA) and all unambiguous signals were assigned and PRE values measured. Distances between the micelle center and the assigned DPC atoms were averaged from an ensemble of MD simulated micelles and plotted as a function of the PRE values from which we could fit the distance to a r^{-3} dependent curve(paper I, fig 1). With the calibration curve in hand we could, based on the assumption that the calibration curve were transferrable between DPC and peptides atoms, calculate distances between micelle centers and peptides atoms (paper I, fig 4 and paper III, fig 4). Subsequently, we applied the calculated distances between the peptide atoms and the center of the micelles as low weighted distance restraints to the structure calculation program CYANA[117] along with the previously NOE and torsion angle derived constraints and recalculated the structures of novispirin, novicidin, citropin and maculatin. The outcome contained not only the high resolution structures but also data regarding the exact placement of the peptides in the micelles (paper I, fig 5 and paper III fig 5). Direct comparison of novispirin and novicidin showed that the C-terminal part of novicidin was buried deeper in the micelles compared to that of novispirin, and because the C-terminal end of novicidin is more hydrophobic compared to novispirin due to the Gly to Phe substitution, the result is highly probable. It was furthermore seen that novicidin was rotated slightly around the helix axis compared to novispirin. The effect of this from a biological perspective (if any) is however not clear.

The two amphibian AMPs maculatin and citropin did like novispirin and novicidin only fold in the presence of amphipathic molecules and their structure was consequently solved in DPC solutions revealing two α-helices. They were chosen as model systems because of the results from Ambroggio et al. that by using differently sized fluorophores elegantly showed that maculatin formed pores in GUVs whereas citropin destroys the overall structure of the bilayers through the AMP carpet mechanism.[135] We therefore speculated that we based on differences in PRE curves obtained from titration with Gd(DTPA-BMA) and a polylysine dendrimeric form of 24 gadolinium-tetraazacyclododecanetetraacetic acid complexes (24Gd(DOTA)) in micelles and bicelles would be able to distinguish between peptides acting by pore formation and peptides acting by the carpet mechanism. Because the Gd(DTPA-BMA) titration of maculatin and citropin were conducted using the same DPC concentration and buffer conditions as in paper I the PRE/distance calibration curve was directly transferrable (paper III). The calculated distances between the micelle centers and citropin and maculatin atoms revealed that both peptides were placed at the surface of the micelles in the zwitterionic buffer/detergent interface (paper III, fig

5). Since the geometry and size of micelles are completely different than bilayers it is not surprising to find maculatin near the surface of the micelles. We therefore wanted to conduct Gd(DTPA-BMA) titration experiments with the peptides dissolved in bicelles hoping that the more planner lipid bilayer would enhance the formation of membrane penetrating pores in the case of maculatin (paper III, fig 2) . The PRE curves of citropin were as expected highly comparable with almost identical maximal values in DPC micelles and anionic DMPG/DMPC/DHPC bicelles. Much to our regret we were not able to record any titration curves with maculatin dissolved in anionic bicelles due to low stability. We therefore conducted the titration experiments in zwitterionic DMPC/DHPC bicelles which did not exhibit the same signs of instability. The maximum PRE values for maculatin in DMPC/DHPC bicelles showed a great resemblance with the PRE values in DPC micelles when titrated with Gd(DTPA-BMA) implying that the peptide is positioned at the surface of the bicelles. The PRE values of maculatin in DMPC/DHPC bicelles titrated with 24Gd(DOTA) were much more ambiguous and left much room for speculations. However, when comparing the maximal PRE values with the values from the micelle titration similarities are seen which suggests that the peptides is located at the surface of the bicelles as well. Previous publications have reported different lipid binding properties of maculatin depending on the charge of the lipids where maculatin appears to be located near the surface of zwitterionic bilayers and more deeply buried in anionic bilayers.[136] Due to the stability differences between zwitterionic and anionic bicelles when maculatin is present it is clear that the peptide interacts differently with the two types of bicelles as they without maculatin present do not show any signs of instability. It furthermore seems perfectly logical that maculatin destroys the overall composition of bacteria-like membranes due to its very nature as an AMP. Therefore, to study peptides inserted perpendicular to the surface of the membrane on a timescale suitable for NMR studies it is crucial to find a peptide without any membrane disrupting properties.

As seen from eq. 17 the transverse dipolar relaxation rate hence the PRE value depends on the rotation of the interacting nuclei/electrons (τ_c), and consequently can PRE values not be uncritically compared between nuclei with different correlation times. When PRE is plotted as a function of τ_R (paper III, fig 3) it reaches its maximum at ~0.3 ns with lower relaxation rates for both faster and slower correlation times. Because the correlation times for DPC and the peptides are slower and faster than 0.3 ns respectively the relaxation rates are by coincidence very similar (63 s^{-1} for DPC compared to 62, 66 and 73 s^{-1} maculatin in bicelles, maculatin in micelles and citropin in micelles, respectively) despite the large deviation in τ_R (see figure 3). Furthermore, because the calculated distances are dependent on the inverse third power of the relaxation rates the differences become negligible whereby the PRE values between DPC and the peptides can be directly compared. It is therefore in our case valid to use the PRE values obtained from DPC to produce a distance to PRE correlation curve usable for calculating distances between the solution (the paramagnetic agents) and micelle embedded peptides.

Paper IV

This section elaborates on Paper IV (Stereospecific assignment of protein NMR resonances using paramagnetic environment relaxation enhancements), which describes the results of the thesis work regarding stereospecific assignment of protons in peptides and proteins.

Only very few techniques can provide high resolution structural information of proteins and peptides. This limited group consists of X-ray crystallography, computational chemistry and NMR spectroscopy. Where X-ray crystallography has played a dominating role in structural determination of proteins and protein complexes, problems with crystallizing small peptides have made this technique inadequate for this type of studies. Although various methods like attachment to fusion proteins have made peptide crystallization possible it remains a troublesome way of determining peptide structures.[137] Computational studies of peptides are becoming more and more widespread and the ever growing available computer resources combined with increasingly sophisticated software makes these calculations valuable. However, simulation studies will always only be as good as the input and the results will presumably always suffer from a certain amount of mistrust caused by the lack of experimental evidence.

Since the first structure determination techniques using NMR spectroscopy was pioneered by Wüthrich and coworkers in the 1980s one of the main assets of NMR has been the capability to study small proteins and peptides in solution.[113] Isotope labeling of proteins and advanced pulse schemes like TROSY have over the years significantly extended the size limit of proteins which are amenable to NMR solution structure analysis.[113] However, the predominant part of the structures determined by NMR are still peptides and small proteins.

The overall purpose of our study was to make it possible to improve the resolution of calculated structures within the limits of the existing structural determination approaches. As a model peptide we chose a 40 amino acid residue defensin named plectasin whose structure has previously been published.[33] We assigned all ambiguous proton and carbon cross peaks from COSY, TOCSY, NOESY and ^{1}H,^{13}C-HSQC spectra based on the published resonances[33] and subsequently calculated the structure based on distance restraints obtained from NOEs and torsion angle constraints obtained from chemical shifts. The calculated structures of the peptide did highly resemble the previously published structure as expected (paper IV, fig 1).

We then recorded an inversion recovery ^{1}H,^{13}C-HSQC spectra from which we could determine the T_1 relaxation times of all ambiguous cross peaks. However due to spectral overlap in the low ppm range the number of proton signals with measurable relaxation times were primarily H^α and H^β side chain atoms which typically have relative higher ppm values compared to H^γ and H^δ. As the T_1 relaxation times can be obtained from a multitude of different types of spectra, problems with spectral overlap could to some degree be overcomed by recording different types of spectra. We titrated the protein sample with the chelated paramagnetic agent Gd(DTPA-BMA)[134] and recorded a inversion recovery spectrum and measured the T_1 relaxation times for each titration point. Because the increased relaxation rate induced by Gd^{3+} are dependent on the inverse third power of the distance to the affected atoms we could compare PRE values of

the peaks originating from stereo pairs relative to each other (paper IV, tab 1). The nuclei with the relative highest values must necessarily be closest to the solvent containing the paramagnetic agent as the dynamical properties of the protons are the same because they are bound to the same carbon. However it is not possible to compare the PRE values between the stereopairs as the dynamics in side chains and throughout the peptides can vary and PREs as elaborated above varies with τ_c.

To use the relaxation rate information in the structure calculations we had to correlate the data with the initially calculated structure ensemble. Unless stereo specific assignments are given to CYANA in the input file the program will base its calculation on distances to pseudoatoms placed between stereo proton pairs. We assumed that Gd(DTPA-BMA) could take the same positions as water surrounding the peptide except from a 5.9 Å shell where steric hindrance of the chelate prevented the Gd^{3+} to enter. This is an assumption previously described by Zangger and coworkers.[138] By computer simulating water around the calculated ensemble of peptide structures we obtained information about which of the protons were placed relative closest to the solvent hence the paramagnetic agents. As the 20 calculated structures deviated slightly and the relative orientation of the protons therefore deviated in some instances we only selected stereo pairs with consensus in 90% or more of the structures. It was then straight forward to correlate the peaks with the largest change in relaxation rate with the protons closest to the solvent and provide this information as stereospecific assignments in CYANA. The resulting structure calculated yielded a structural ensemble with a much lower RMSD compared to the structure calculated without the input of the stereo assignments (paper IV, fig 1). This resolution improvement is in agreement with previous studies that likewise have reported lower RMSD values after employing stereospecific assignments.[122, 124, 139] The software programs HABAS and GLOMSA developed by Peter Güntert and coworkers provides stereo specific assignments based on scalar couplings, NOEs and distance restraints and does not require any additional input to the structure calculations programs than otherwise would be provided. They are therefore easy to implement in structure determination protocols and are consequently very extensively used. However, they are not capable of providing a complete assignment of the stereopairs and can therefore be supplemented by e.g. the method developed in paper IV.

Our method differs to most other methods for stereo specific assignments in that it do not requires any time consuming advanced isotope labeling schemes which often will be out of proportions with the importance of structure calculations of small proteins and peptides. However, because the structure of many small proteins and peptides are determined by NMR there is still a need for developing methods that can complement and improve the calculated structures, although the main focus in the NMR community have shifted towards much larger systems.

Part II

Structural studies of autotransporters

Introduction

Outer Membrane Proteins

The cell membrane of Gram negative bacteria consist of two phospholipid bilayers divided by a periplasmic space containing a relative small peptideglycan layer (see section Bacterial cell membrane and figure 5). The two lipid membranes are termed the outer membrane and inner membrane. Besides from LPS there is a substantial amount of proteins in the outer membrane of bacteria and in *E. coli* approximately 50 % of the membrane mass is estimated to originate from proteins.[140] Studies have shown that from a quantitative perspective the outer membrane proteins (OMPs) in *E. coli* are largely made up of only four constituent; OmpA, OmpF, OmpC and OmpX.[141] However, a multitude of other proteins are expressed although to a much lesser extent.[142] The structure of the proteins in the outer and inner membrane differs considerably. Proteins in the inner membrane are typically membrane spanning in the form of hydrophobic α-helices whereas integral OMPs are typically antiparallel β-strands that fold into cylindrical β-strands. These OMPs are amphiphatic structures with hydrophilic interiors and hydrophobic residues facing the lipid tails of the phospholipids.[140] In contrast to the inner membrane the outer membrane are not energized by a proton gradient and ATP is not present in the periplamic space. Consequently are most transport across the outer membrane passive diffusion via the OMPs which allows for non-specific passage of typically small hydrophilic compounds (<600 Da).[143]

X-ray crystallography have played a dominating role in structural determination of proteins and protein complexes, however inherent problems with crystallizing lipid and detergent imbedded proteins have meant that this technique until now have been very inadequate for this type of studies. Crystallization studies of small nano-discs have show promising results although the use of these has been sparse and remain to prove themselves for a wider use.[144] Solid state NMR have long been proposed as a leading candidate for solving the structures of membrane protein, although considerable improvement must be made to spectral resolution before the method can really fulfill its potential.[145] For solution state NMR the dominating obstacle for structural determination of membrane proteins is the dramatic size increase when proteins become imbedded into membrane mimicking systems where even small micelles adds approximately 20 kDa to the overall weight of the proteins. This causes the overall correlation time to go up whereby the relaxation rate goes up according to equation 7, 8 and 9. A number of different NMR methods have been developed for studying larger protein systems and membrane proteins which have effectively pushed the envelope of what can be studied. The most significant improvements have been achieved through the application of transverse relaxation-optimized spectroscopy (TROSY)[146], RDCs[147], spectrometer hardware improvements and more or less advanced isotope labeling schemes.[148] Despite these improvement and tremendous amount of

work, the structures of only 7 unique membrane β-barrels have been solved using NMR until now (http://www.drorlist.com/nmr/MPNMR.html).

Autotransporters

Autotransporters are a growing family of OMPs frequently found in pathogenic Gram-negative bacteria.[149] They consist of a signal peptide, a passenger domain and a C-terminal called the β-domain.[150] The signal peptide direct the inner membrane transport of the pro-protein where the C-terminal β-domain is then inserted into the outer membrane. It adapts a β-barrel structure through which the passenger domain can be transported to the extracellular space before it is cleaved of by an autocatalytic mechanism.[151] Thus all information necessary for secretion across the outer membrane is contained within a single polypeptide in contrast to other bacterial secretion systems. The β-domains are generally between 250 and 300 amino acid residues long, and are typically highly homologous in contrast to the passenger domains that varies greatly both with respect to sequence, structure and biological functions although all of them are implicated in virulence.[149] The structure of five different passenger domains have been solved using x-ray diffraction and they reveal different structural properties which is not surprising considering their functional diversity (see figure 12).[152] However, common for them is the presence of either β-helices or β-rolls which also has been predicted to be a general trait for autotransporters.[149]
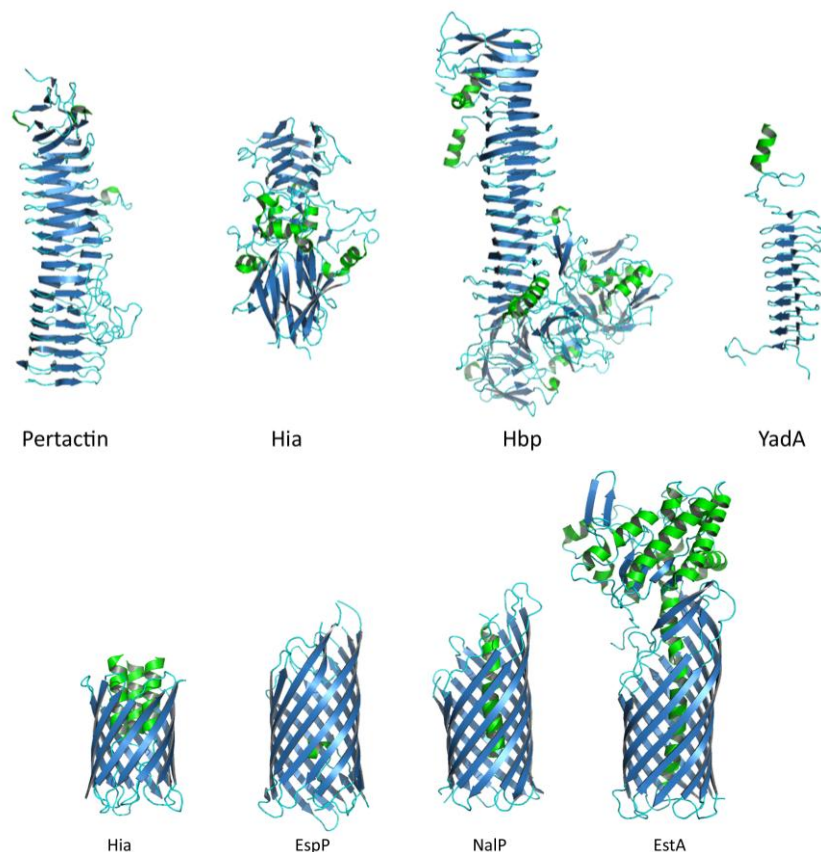

Figur 12. Crystal structures of autotransporter passenger domains on the top and β-barrel structures below.

Crystal structures of four autotransporters β-domains have been solved of which one is part of a full-length autotransporter (EstA).[140, 151, 153] All of them reveal a 12 stranded anti parallel β-barrel structure with the strands tilted approximately 45° which are typically seen for OMPs (see figure 12).[152, 154] A unique feature which is seen in all of the autotransporter β-domain structures are the presence of an α-helix positioned within the barrel lumen to which it is connected through hydrogen bonds.[151] Because the α-helix remains within the barrel subsequent to cleavage it has been speculated that it acts as a plug preventing undesirable influx or efflux from the bacteria after separation from the passenger domain.[151]

AIDA

Adhesin involved in diffuse adherence (AIDA) is an afimbrial adhesion protein and a member of the autotransporter family. By presenting the passenger domain on the surface of certain pathogenic strains of *E. Coli* the bacteria become capable of adhering to the intestinal lining and thereby to colonize the gut. This can cause diarrhea that contributes significantly to the high mortality rate among infants in developing countries.[155] AIDA furthermore possesses a major role in the development of diarrhea in piglets and studies have shown that more than 25 % of porcine *E. coli* isolates contain the AIDA operon.[156]

AIDA is synthesized as a pre-pro-protein consisting of 1286 amino acids divided into three domains as is seen for all autotransporter.[157] The 49 amino acid N-terminal signal peptides is cleaved from the remaining protein after transport to the periplasmic space. After insertion of the β-domain into the outer membrane and subsequent translocation of the passenger domain to the extracellular matrix, the passenger domain is cleaved from the barrel between residue 846 and 847 most likely through an autocatalytic mechanisms.[158]

The passenger domain consists of 31 sequential repeats of a 19 amino acids sequence[157] and based on sequential analysis the domain are predicted to form a β-helix which coincide both with the published structure of autotransporters (see figure 12) and with the biological function as an adhesion.[159] In several instances the passenger domain of AIDA have been replaced, thereby using the autotransporter secretion mechanism for displaying foreign protein on the cell surface of the bacteria.[160]

The C-terminal β-domain consists of two subdomains termed the β_1 (residues 847-949) and β_2 (residues 950-1286) and the two subdomains are defined as the part that can be proteolytic degraded (β_1) and the membrane embedded part that is protected from degradation (β_2).[157] There exist no high resolution structure of the AIDA β-domain but it most likely fold into a β-barrel structure based on both bioinformatic and experimental studies.[158, 161] The exact number of β-strands is however not known but calculations based on amphipathic properties of the protein predict roughly 14 β-strands which are in contrast to the previously published β-domain structures.[162]

The smaller β_1 act as a linker region between the barrel and the passenger domain and the tertiary structure (if any) is largely unknown. It has been predicted to form two β-strands at the

bilayer which presumably is part of the also predicted β-helix structure of the passenger domain.[158]

Material and Methods

Expression and purification

The expression and purification of the β_2-domain of AIDA were largely carried out as described previously.[163] *E. coli* BL21(DE3)pLysS transformed with the plasmid DT4 coding for the β_2-domain were grown on LB-agar plates and single colonies were transferred to 10 ml LB media containing 100 μg/mL ampicillin and grown overnight a 37 $^{\circ}$C with agitation. The overnight cultures were used to inoculated either 1 l LB, (>98%) ^{15}N Spectra 9 or M9 minimal media (3 g/l KH_2PO_4, 7.5 g/l $Na_2HPO_4 \cdot 2H_2O$, 5 g/l NaCl, 10 ml 100x MEM vitamins (VWR, USA), 1 mM $MgSO_4$, 1,5 g/l ^{15}N-$(NH_4)_2SO_4$, (Spectra Stable Isotopes, USA), 4 g/l glucose) containing 0.1 g ^{15}N-Phe and 0.1 g of each of the unlabeled variants of the remaining 19 natural amino acids. For growth in ^{2}H^{13}C^{15}N M9 minimal media with ^{13}C-glucose and >99% D_2O were used. The cells were adjusted to D_2O by growing the overnight culture in LB media with 100 μg/mL ampicillin and 25 % (v/v) D_2O and then transferring 100 μL to a second overnight culture containing 50 % D_2O which were used to inoculate the ^{2}H^{13}C^{15}N M9 minimal media. All media were grown at 37 $^{\circ}$C until OD$_{600 nm}$ ~ 0.8 was reached and the culture was induced with IPTG to a final concentration of 1 mM. The cells subsequently grew for four hours before they were harvested at 6000 g for 10 min at 4 $^{\circ}$C and flash frozen in liquid N_2 before they were resuspended in 10 ml/l culture TEN buffer (50 mM Tris, 2 mM EDTA, 100 mM NaCl, pH 8). DNase (0.1 mg/mL) was added and the samples incubated for 45 min at room temp. One *Complete Protease Inhibitor Cocktail Tablets* (Roche Diagnostics, Germany) were added pr 50 ml of buffer and the cells were sonicated for 5 x 30 s on ice. Inclusion bodies were collected by centrifugation at 4000 g for 1 h at 4 $^{\circ}$C and subsequently washed with TEN buffer (10 mL/L culture) containing 2% (w/w) Triton X-100 for 2 h at 37 $^{\circ}$C. The inclusion bodies were then washed with TEN buffer, sedimented and washed again with TN buffer (50 mM Tris, 100 mM NaCl, pH 8).

The inclusion bodies were solubilized in TN buffer containing 8 M urea and incubated for 2 h at 37 $^{\circ}$C then centrifuged at 32,000 g for 1 h. The dissolved protein was mixed 1:1 (v/v) with TN buffer containing either 10% (w/v) oPOE or 50 mM DPC or 10% (w/v) SDS sonicated 30 min? on ice. 1:10 (v/v) Ni-NTA beads were added and incubated for 2 h. The solution were applied to a Parmacia PD-10 gravity column and excess proteins were washed off with TN buffer containing either 0.5% (w/v) oPOE, 2.5 mM DPC, 0.5 % (w/v) SDS depending on the detergent wherein the protein was folded. AIDA-β_2 was eluted from the column with 0.5 M imidazole in TN buffer containing either 0.5% (w/v) oPOE, 2.5 mM DPC, 0.5 % (w/v) SDS again depending on the detergent wherein the protein was folded. For NMR samples the protein was concentrated on a Amicon Ultra (Milipore, USA)(MWCO 30 kDa) spin filter while the buffer was exchanged to 10 mM sodium phosphate, 5% D_2O, 0.05% NaN$_3$, pH 6.

The gene coding for the β_1 subunit from AIDA has been synthesized de novo (GenScript, Piscataway, USA), and subsequently re-designed by Finn L. Aachmann (NTNU, Trondheim,

Norway) The N-terminal threonine was mutated to alanine for optimal cleavage from the fusion protein during purification. The synthetic gene was inserted into the pTYB11 (from IMPACT-CN system, New England BioLabs) vector using the restriction sites SapI and EcoRI, hereafter purified via gel electrophoresis and ligated with T4 ligase at 289K over night resulting in the plasmid pFA11. The construct pFA11 was verified by restriction mapping. This plasmid was transformed into the *E. coli* production strain ER2566. To uniformly label the β_1 subunit with $^{13}C/^{15}N$, cells were grown in M9 minimal medium prepared with 99% $(^{15}NH_4)_2SO_4$ and 99% $^{13}C_6$-D-glucose (Spectra Stable Isotopes). The fusion protein was overexpressed by growing the cells at 37 °C until an OD_{600nm} of 0.8 was reached, followed by induction of the protein synthesis with 1 mM IPTG and subsequent incubation at 25 °C for 16 h. Cells were collected by centrifugation and disrupted by sonication in 20 mM HEPES buffer pH 6.9, containing 500 mM NaCl and 0.05 % Triton X-100 (Sigma-Aldrich). Following centrifugation, the supernatant was applied onto a Chitin bead column (NEB). The column was washed with 20 mM HEPES buffer pH 6.9, containing 500 mM NaCl, followed by cleavage with 50 mM dithiothretiol (DTT) at room temperature over ~16 h, resulting in the release of the β_1 subunit (93 amino acid) from the chitin bound intein tag. The β_1 subunit was further purified by dialysis in order to remove a 1.6 kDa peptide that occurred as a by-product from the cleavage reaction.

Circular dichroism

All experiments were recorded on a Jasco J-715 spectropolarimeter (Jasco Spectroscopic, Japan) in a 1 mm quartz cell at room temperature. Ellipticity was recorded in the 250 – 200 nm range with 5 increments per CD spectra. A spectrum of 20 μM AIDA-β2 dissolved in 10 mM sodium phosphate pH 6 and either 0, 5, 10, 20, 40 or 80 μM AIDA-β_1. Spectra of 16 μM AIDA-β_1 in 10 mM sodium phosphate pH 6 were also recorded and with the same conditions but in the presence of either 100 mM Ca^{2+}, 50 mM DPC, 50 mM SDS or 30% TFE.

NMR

All NMR spectra were recorded at 310 K on a BRUKER DRX600 spectrometer operating at a field strength of 14.1 T, equipped with a TXI(H/C/N) probe. All spectra were processed using Topspin version 1.3. Analysis of all NMR spectra were performed using the program CARA version 1.5.5[164]

^{15}N AIDA-β_2 samples were prepared in, 0.5% oPOE, 50 mM DPC, 0.5% SDS and 100 μM protein respectively. $^1H,^{15}N$-HSQC spectra were recorded for each sample using standard pulse sequences taken from the Bruker Topspin pulse sequence library.

A sample with selectively labeled ^{15}N-Phe AIDA-β_2 was prepared in 10 mM sodium phosphate, 5% D_2O, 0.05% NaN_3, pH 6 with 0.5% oPOE to a final protein concentration of 35 μM.

A $^2H^{15}N$ AIDA-β_2 sample was prepared in 10 mM sodium phosphate, 5% D_2O, 0.05% NaN_3, pH 6 with 0.5% oPOE. TROSY $^1H,^{15}N$-HSQC spectra were recorded.

A $^{13}C^{15}N$ AIDA-β_1 sample was prepared in 10 mM sodium phosphate, 5% D_2O, 0.05% NaN_3 to a final concentration of 0.84 mM. $^1H^{13}C$ HSQC, $^1H^{15}N$ HSQC, CBCA(CO)NH, CBCANH,

HBHA(CBCACO)NH, HBHANH, HNCA, HN(CA)CO, HNCO, HN(CO)CA and ^{1}H^{15}N TOCSY-HSQC were recorded. 90 mM d38-DPC were added and a second ^{1}H^{15}N HSQC were recorded.

Crystallization

Crystallization trials were performed using the sitting drop vapor diffusion method at 278, 293 and 298 ^{o}K with a protein concentration of 1.4 mg/ml in 0.5% oPOE or 1.3 mg/ml in 50 mM DPC. Screening was conducted using 24 well plates, with a drop volume of 1 µl protein and either 1 or 0.5 µl reservoir solution. The screening was conducted using Molecular Dimensions Structure Screen 1 and 2 (ww.moleculardimensions.com) and the drops were mixed by aspiration.

Modeling

Homology models of AIDA-β$_2$ was produced with the β-domain crystal structures of the autotransporters NalP and EspP from *E. coli* (PDB ID: 1UYN and 2QOM) as a template using MODELLER 9v2.[165] The models were subsequently optimized with respect to the Discrete Optimized Potential Energy (DOPE) score using the looprefine module of MODELLER.

The best AIDA-β$_2$ homology model obtained was energy minimized using the program Gromacs 3.3.1 [166] with the GROMOS96 force field [167] and done with the steepest descents method in steps of 1 femtoseconds with a cutoff for Vander Waals interactions of 1.4 nm.

Results

Purification of AIDA-β$_2$

AIDA β$_2$ was successfully expressed in LB media, isotope labeled Spectra 9 and M9 minimal media and the inclusion bodies were essentially purified in accordance with the previously established purification protocol.[163] For refolding and preparation of samples for NMR studies it was necessary to optimize the refolding process with respect to the used amounts of detergent used for refolding. For screening many different detergent conditions optimal for NMR experiments the cost of detergents would rapidly increase to unacceptable levels when using other detergents than oPOE which have a relative low cost (~180 EUR for 25 g) compared to detergents more suitable for NMR (e.g. DPC ~1600 EUR for 25 g). Because the use of deuterated detergents reduces the relaxation of membrane proteins significantly it was desirable to find detergents which could be obtained in this state. However, the costs of deuterated detergents are considerable higher than non-deuterated (e.g. d38-DPC ~25000 EUR for 25 g) emphasizing the need for a reduction of detergent in the refolding protocol.

It has been shown that OMPs are generally resistant to the detergent SDS and that denaturation requires heat treatment. Consequently will protein in a boiled sample migrate slower on a SDS-polyacrylamide gel compared to protein in a non-boiled sample due to the larger radius to mass ratio of denatured proteins. This phenomenon is called heat-modifiability.[168] To see whether AIDA-β$_2$ were folded correctly the folded protein were subjected to a heat-modifiability test after each refolding (see figure 13)
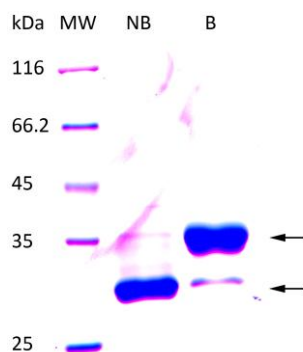
Figur 13. AIDA-β_2 purified in oPOE not subjected to heat-treatment (NB) or subjected to heat-treatments (B). A clear band shift is observed which is typical for correctly folded OMPs

Although no systematic investigation of the required amount of detergent needed for correct folding of AIDA-β_2 was carried out, it appears that at least 10 times the cmc values of the detergent were needed to get as much AIDA-β_2 refolded into its correct state as possible. Attempts to reduce the amounts of detergents needed were carried out by reducing the buffer volume when AIDA-β_2 was refolded to less than 10 mL/g of inclusion body pellet as described by Mogensen et al.[163] Unfortunately such a volume reduction causes the protein to precipitate into an insoluble white substance.

Circular dichroism

The far-UV CD spectrum of AIDA-β_2 in oPOE showed a typical β-sheet signal with a single minimum at ~220 nm as have been observed previously (see figure 14).[163] This is a clear indication that the protein is folded into a β-barrel structure as is seen for autotransporters in general and hence is considered to be the correct folded protein state for AIDA-β_2.
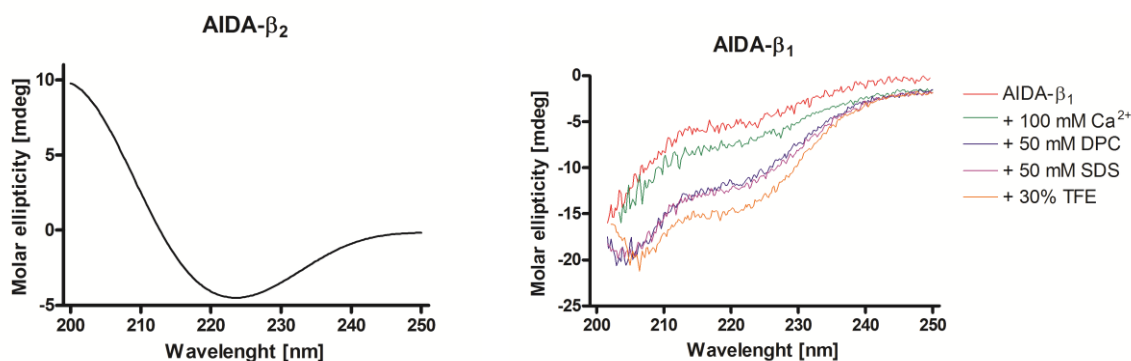
Figur 14. Far-UV CD spectra of AIDA-β_2 (left) and AIDA-β_1 (right). AIDA-β_1 were carried out with identical protein concentration and either 100 mM Ca^{2+}, 50 mM DPC, 50 mM SDS or 30% (v/v) TFE. A clear shift from an unfolded state to a more α-helix state is observed for AIDA-β_1 is solutions containing amphipathic molecules.

The far-UV CD spectrum of AIDA-β1 dissolved in buffer showed a typical random coil profile whereas the presence of 50 mM DPC or SDS induced and more typical α-helical pattern with minima at 208 and 222 nm (see figure 14) The addition of 30 % TFE appear to stimulate the α-helix formation even further and was used as an control experiment to observed the maximal inducible α-helix. From the combined experiments it is clear that the presence of micelles

stimulate a partial formation of α-helix in the part of the β-domain linking the β-barrel with the passenger domain located outside the membrane.

NMR

A ^{1}H,^{15}N-HSQC spectrum were recorded on AIDA-β$_2$ dissolved in oPOE (see figure 15). The peaks in the spectrum were with few exceptions impossible to distinguish from each other and peaks with very high intensity were located in the ^{1}H ppm range between 8 and 8.5 ppm. When dissolved in SDS micelles the ^{1}H,^{15}N-HSQC spectrum revealed a few more unambiguous peaks and there were especially a distinguishing difference in the ^{15}N 108-111 ppm range which is often populated by glycine residues.[111] In DPC micelles further peaks were observable in a ^{1}H,^{15}N-HSQC spectrum, however the best result was as expected obtained by recording a TROSY ^{1}H,^{15}N-HSQC on a deuterated sample of AIDA-β$_2$. Unfortunately the majority of the peaks were ambiguous with very broad line width and the sample could therefore not be used for recording of triple resonance spectra and subsequent assignment of the signals.
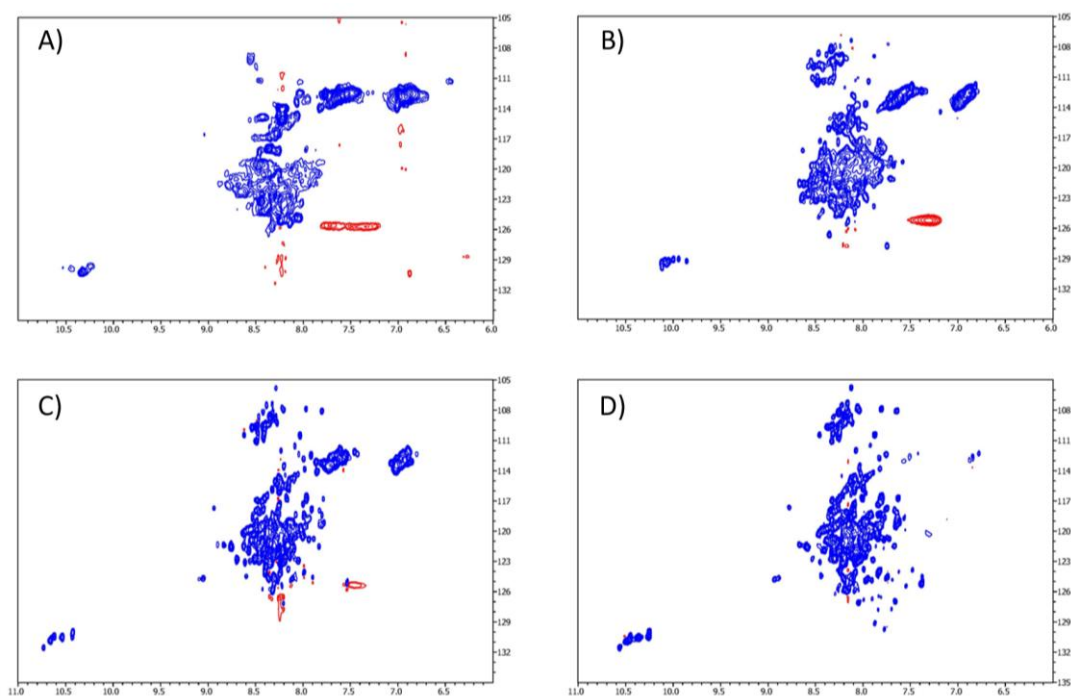

Figur 15. ^{1}H,^{15}N-HSQC spectra of AIDA-β$_2$ dissolved in 0.5 % oPOE (A), 0.5 % SDS (B), 50 mM DPC (C). TROSY-^{1}H,^{15}N-HSQC spectrum of AIDA-β$_2$ dissolved in DPC

In an attempt to assess whether the broad line width originated from part of the protein being unfolded we selectively labeled the 11 phenylalanines in the protein. We were however not able to obtain a high protein concentration (~35 μM) due to a low protein yield from the expression and consequently we could not detect any signals in the recorded ^{1}H,^{15}N-HSQC spectrum.

A ^{1}H,^{15}N-HSQC spectrum were recorded on AIDA-β$_1$ which showed a nicely resolved spectrum with ~120 peaks (see figure 16) of which 15 residues are expected to originate from a small cleavage peptide from the purification. The protein appears to be unfolded as all the peaks are located in a narrow ^{1}H ppm range and this observation is confirmed by the CD-spectra which

shows a typical random coil profile. After the addition of DPC the signals were still located in a narrow ^{1}H ppm range and the addition of DPC did only cause minor changes in the spectra which are a clear indication that most of the protein remains unfolded. We did therefore not proceed with a structural determination of the protein despite have recorded a complete set of triple resonance spectra.
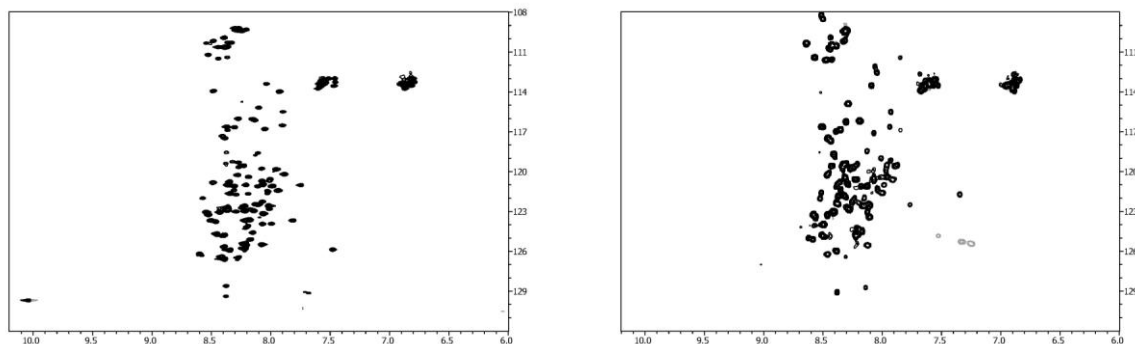
Figur 16. ^{1}H,^{15}N-HSQC spectra of AIDA-β$_1$ recorded without (left) or with (right) the presence of DPC micelles. The peaks are in both spectra clearly clustered in the ^{1}H 8-8.5 ppm range indication that the protein is not folded into a globular fold.

Crystallization

The wells were visually checked for crystals regularly for a period of over six month. Although a few instances of micro crystals were observed they did not evolve into larger crystals and there was no coherence between the salt types and concentrations in the reservoirs of the isolated instances. There were therefore no obvious derived experiments and we did not conduct further crystal screenings.

Homology model

A homology model of AIDA-β$_2$ was calculated based on the β-domain crystal structure of the autotransporter NalP. The calculated AIDA-β$_2$ structure contains 12 β-strands folded in an antiparallel β-barrel (see figure 17) with a α-helix located in the center of the barrel as is also seen in the structures of the four β-domains of autotransporters that have been solved. However, in contrast to the other β-domain structures the AIDA-β$_2$ structure contains three long loops between residue 110-132, 151-168 and 207-222. The lengths of these loops are sufficiently long to form a β-strands and it is likely that they do so in nature. A topology model predicts between 12 and 15 β-strand (data not shown) and because the number of strands in all solved OMPs are even numbers[154] 13 and 15 strands can most likely be ruled out. Because the model is based on a 12 β-strand domain it can be speculated that the modeler program have mistaken two of the extra β-strands with loops and that the actual count is 14, however a tertiary structure must be solved to answer that question.

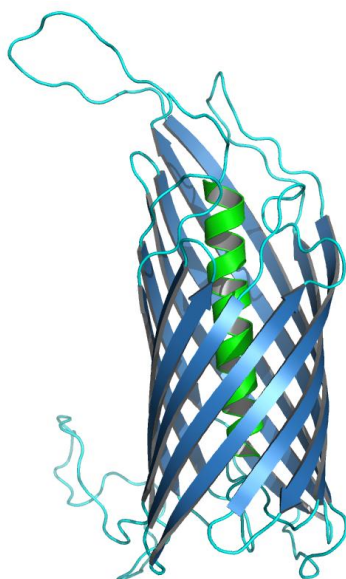**Figure 17. Homology model of AIDA-β₂ based on the crystal structures of crystal structures of the autotransporters NalP and EspP from *E. coli***

Discussion

The purpose of this part of the thesis is to preserve some knowledge about the experiments we have performed on AIDA-β2 and AIDA-β1 in case someone will reattempt to work on the β-domain using NMR spectroscopy. As mentioned in the introduction, despite a major improvement of methods and hardware the structure of only 36 unique membrane proteins have been solved using NMR. Of these only one monomer have been more than 30 kDa (human VDAC-1[169]) like AIDA-β₂ which clearly illustrates the tremendous tasks that lies ahead before solving NMR structures of membrane proteins become trivial. By using heat modifiability and CD-spectroscopy we were able to determine whether the AIDA-β₂ protein was correctly folded after refolding. However, because none of these methods are residue specific we were not able to determine if (small) parts of the protein like a tail region were unfolded which is not unlikely as AIDA-β₂ is merely a part of the complete AIDA autotransporter. Such an unfolded region would give rise to very strong signal located in the ^{1}H 8-8.5 ppm as is seen in the AIDA-β₂ HSQC spectra.

Due to difficulties with bringing down the required amount of needed detergent for refolding we have not been able to screen a large number of detergents for optimal NMR conditions with respect to AIDA-β₂ NMR spectra. Neither have we observed such promising spectra with the limited amount of detergents we have recorded in, that we could justify spending several thousand euro on deuterating the detergents. As expected we observed an increase in the unambiguous signals when recording a ^{1}H^{15}N HSQC on a perdeuterated AIDA-β₂ sample. Nonetheless, we have as mentioned not been able to obtain highly resolved NMR spectra that would be adequate for structural studies.

References

[1]   M. Botta, *Eur J Inorg Chem* **2000**, *2000*(3), 399-407.
[2]   D. M. Engelman, *Nature* **2005**, *438*(7068), 578-580.
[3]   M. R. Yeaman, N. Y. Yount, *Pharmacol Rev* **2003**, *55*(1), 27-55.
[4]   M. T. Cabeen, C. Jacobs-Wagner, *Nat Rev Microbiol* **2005**, *3*(8), 601-610.
[5]   R. E. W. Hancock, D. Knowles, *Current Opinion in Microbiology* **1998**, *1*(5), 493-494.
[6]   W. Spink, V. Ferris, *J Clin Invest.* **1947**, *26*(0021-9738 (Print)), 379-393.
[7]   WHO, *http://apps.who.int/medicinedocs/pdf/s7920e/s7920e.pdf* **2005**.
[8]   C. Lee, *International Journal of Antimicrobial Agents* **2008**, *32*(Supplement 4), S197-S199.
[9]   R. E. W. Hancock, *Nat Rev Drug Discov* **2006**, *6*, 28.
[10]   D. J. Payne, M. N. Gwynn, D. J. Holmes, D. L. Pompliano, *Nat Rev Drug Discov* **2007**, *6*(1), 29-40; H. Breithaupt, *Nat Biotechnol* **1999**, *17*(12), 1165-1169.
[11]   B. G. Spratt.
[12]   E. P. Abraham, E. Chain, *Nature* **1940**, *146*, 837-837.
[13]   R. L. Juliano, V. Ling, *Biochim Biophys Acta* **1976**, *455*(1), 152-162.
[14]   H. G. Boman, *Annu Rev Immunol* **1995**, *13*, 61-92.
[15]   M. Zasloff, *Nature* **2002**, *415*(6870), 389-395.
[16]   M. Simmaco, G. Mignogna, D. Barra, *Biopolymers* **1998**, *47*(6), 435-450.
[17]   R. Gennaro, M. Zanetti, *Biopolymers* **2000**, *55*(1), 31-49.
[18]   M. Zanetti, R. Gennaro, M. Scocchi, B. Skerlavaj, *Adv Exp Med Biol* **2000**, *479*, 203-218.
[19]   M. Zanetti, R. Gennaro, D. Romeo, *FEBS Lett* **1995**, *374*(1), 1-5.
[20]   K. A. Brogden, *Nat Rev Microbiol* **2005**, *3*(3), 238-250.
[21]   A. Tossi, L. Sandri, A. Giangaspero, *Biopolymers* **2000**, *55*(1), 4-30.
[22]   A. Jasanoff, A. R. Fersht, *Biochemistry* **1994**, *33*(8), 2129-2135.
[23]   G. Baumann, P. Mueller, *J Supramol Struct* **1974**, *2*(5-6), 538-557.
[24]   Y. Shai, Z. Oren, *Peptides* **2001**, *22*(10), 1629-1641.
[25]   L. Yang, T. M. Weiss, R. I. Lehrer, H. W. Huang, *Biophys J* **2000**, *79*(4), 2002-2009.
[26]   C. S. Chia, J. Torres, M. A. Cooper, I. T. Arkin, J. H. Bowie, *FEBS Lett* **2002**, *512*(1-3), 47-51.
[27]   A. Tossi, *http://www.bbcm.units.it/~tossi/amsdb.html*.
[28]   L. S. Chesnokova, S. V. Slepenkov, S. N. Witt, *FEBS Lett* **2004**, *565*(1-3), 65-69; L. Otvos, Jr., *J Pept Sci* **2000**, *6*(10), 497-511.
[29]   F. G. Oppenheim, T. Xu, F. M. McMillian, S. M. Levitz, R. D. Diamond, G. D. Offner, R. F. Troxler, *J Biol Chem* **1988**, *263*(16), 7472-7477; F. G. Oppenheim, Y. C. Yang, R. D. Diamond, D. Hyslop, G. D. Offner, R. F. Troxler, *J Biol Chem* **1986**, *261*(3), 1177-1182; J. J. Pollock, L. Denepitiya, B. J. MacKay, V. J. Iacono, *Infect Immun* **1984**, *44*(3), 702-707.
[30]   D. J. Schibli, P. M. Hwang, H. J. Vogel, *Biochemistry* **1999**, *38*(51), 16749-16755; M. E. Selsted, M. J. Novotny, W. L. Morris, Y. Q. Tang, W. Smith, J. S. Cullor, *J Biol Chem* **1992**, *267*(7), 4292-4295; G. Del Sal, P. Storici, C. Schneider, D. Romeo, M. Zanetti, *Biochem Biophys Res Commun* **1992**, *187*(1), 467-472.
[31]   R. C. Skarnes, D. W. Watson, *J Exp Med* **1956**, *104*(6), 829-845; R. C. Skarnes, *Nature* **1967**, *216*(5117), 806-808.
[32]   T. Ganz, *Nat Rev Immunol* **2003**, *3*(9), 710-720.
[33]   P. H. Mygind, R. L. Fischer, K. M. Schnorr, M. T. Hansen, C. P. Sonksen, S. Ludvigsen, D. Raventos, S. Buskov, B. Christensen, L. De Maria, O. Taboureau, D. Yaver, S. G. Elvig-Jorgensen, M. V. Sorensen, B. E. Christensen, S. Kjaerulff, N.

Frimodt-Moller, R. I. Lehrer, M. Zasloff, H. H. Kristensen, *Nature* **2005**, *437*(7061), 975-980.

[34]   R. I. Lehrer, *Nat Rev Microbiol* **2004**, *2*(9), 727-738.

[35]   Y. Q. Tang, J. Yuan, G. Osapay, K. Osapay, D. Tran, C. J. Miller, A. J. Ouellette, M. E. Selsted, *Science* **1999**, *286*(5439), 498-502.

[36]   J. R. Fromm, R. E. Hileman, E. E. Caldwell, J. M. Weiler, R. J. Linhardt, *Arch Biochem Biophys* **1995**, *323*(2), 279-287.

[37]   T. Ganz, M. E. Selsted, D. Szklarek, S. S. Harwig, K. Daher, D. F. Bainton, R. I. Lehrer, *J Clin Invest* **1985**, *76*(4), 1427-1435; D. Ghosh, E. Porter, B. Shen, S. K. Lee, D. Wilk, J. Drazba, S. P. Yadav, J. W. Crabb, T. Ganz, C. L. Bevins, *Nat Immunol* **2002**, *3*(6), 583-590; T. Ganz, *Infect Immun* **1987**, *55*(3), 568-571.

[38]   T. Ayabe, D. P. Satchell, C. L. Wilson, W. C. Parks, M. E. Selsted, A. J. Ouellette, *Nat Immunol* **2000**, *1*(2), 113-118.

[39]   F. Niyonsaba, I. Nagaoka, H. Ogawa, *Crit Rev Immunol* **2006**, *26*(6), 545-576.

[40]   W. C. Wimley, M. E. Selsted, S. H. White, *Protein Sci* **1994**, *3*(9), 1362-1373.

[41]   T. Schneider, T. Kruse, R. Wimmer, I. Wiedemann, V. Sass, U. Pag, A. Jansen, A. K. Nielsen, P. H. Mygind, D. S. Raventos, S. Neve, B. Ravn, A. M. Bonvin, L. De Maria, A. S. Andersen, L. K. Gammelgaard, H. G. Sahl, H. H. Kristensen, *Science*, *328*(5982), 1168-1172.

[42]   A. D. Befus, C. Mowat, M. Gilchrist, J. Hu, S. Solomon, A. Bateman, *J Immunol* **1999**, *163*(2), 947-953.

[43]   J. L. Dimarcq, P. Bulet, C. Hetru, J. Hoffmann, *Biopolymers* **1998**, *47*(6), 465-477.

[44]   B. Schittek, R. Hipfel, B. Sauer, J. Bauer, H. Kalbacher, S. Stevanovic, M. Schirle, K. Schroeder, N. Blin, F. Meier, G. Rassner, C. Garbe, *Nat Immunol* **2001**, *2*(12), 1133-1137; K. A. Brogden, M. Ackermann, K. M. Huttner, *Infect Immun* **1998**, *66*(12), 5948-5954.

[45]   K. A. Brogden, A. J. De Lucca, J. Bland, S. Elliott, *Proc Natl Acad Sci U S A* **1996**, *93*(1), 412-416.

[46]   F. Harris, S. R. Dennison, D. A. Phoenix, *Curr Protein Pept Sci* **2009**, *10*(6), 585-606.

[47]   K. Putsep, C. I. Branden, H. G. Boman, S. Normark, *Nature* **1999**, *398*(6729), 671-672.

[48]   G. Wang, *J Biol Chem* **2008**, *283*(47), 32637-32643.

[49]   H. N. Hunter, A. R. Demcoe, H. Jenssen, T. J. Gutteberg, H. J. Vogel, *Antimicrob Agents Chemother* **2005**, *49*(8), 3387-3395.

[50]   A. Szyk, Z. Wu, K. Tucker, D. Yang, W. Lu, J. Lubkowski, *Protein Sci* **2006**, *15*(12), 2749-2760.

[51]   B. Cornet, J. M. Bonmatin, C. Hetru, J. A. Hoffmann, M. Ptak, F. Vovelle, *Structure* **1995**, *3*(5), 435-448.

[52]   H. Jung, S. Yang, J. Kim, **2010**.

[53]   A. Rozek, C. L. Friedrich, R. E. Hancock, *Biochemistry* **2000**, *39*(51), 15765-15774.

[54]   S. A. Kristian, M. Durr, J. A. Van Strijp, B. Neumeister, A. Peschel, *Infect Immun* **2003**, *71*(1), 546-549; A. Peschel, R. W. Jack, M. Otto, L. V. Collins, P. Staubitz, G. Nicholson, H. Kalbacher, W. F. Nieuwenhuizen, G. Jung, A. Tarkowski, K. P. van Kessel, J. A. van Strijp, *J Exp Med* **2001**, *193*(9), 1067-1076.

[55]   M. R. Yeaman, A. S. Bayer, S. P. Koo, W. Foss, P. M. Sullam, *J Clin Invest* **1998**, *101*(1), 178-187.

[56]   C. Friedrich, M. G. Scott, N. Karunaratne, H. Yan, R. E. Hancock, *Antimicrob Agents Chemother* **1999**, *43*(7), 1542-1548.

[57]   R. K. Ernst, E. C. Yi, L. Guo, K. B. Lim, J. L. Burns, M. Hackett, S. I. Miller, *Science* **1999**, *286*(5444), 1561-1565.

[58]   J. N. Weiser, M. Shchepetov, S. T. Chong, *Infect Immun* **1997**, *65*(3), 943-950.

[59]   E. S. Lysenko, J. Gould, R. Bals, J. M. Wilson, J. N. Weiser, *Infect Immun* **2000**, *68*(3), 1664-1671.

[60]   T. Guina, E. C. Yi, H. Wang, M. Hackett, S. I. Miller, *J Bacteriol* **2000**, *182*(14), 4077-4086.

[61]   K. Sugimura, T. Nishihara, *J Bacteriol* **1988**, *170*(12), 5625-5632.

[62]   W. M. Shafer, X. Qu, A. J. Waring, R. I. Lehrer, *Proc Natl Acad Sci U S A* **1998**, *95*(4), 1829-1833.

[63]   A. C. Andrade, J. G. Van Nistelrooy, R. B. Peery, P. L. Skatrud, M. A. De Waard, *Mol Gen Genet* **2000**, *263*(6), 966-977.

[64]   G. Bell, P. H. Gouyon, *Microbiology* **2003**, *149*(Pt 6), 1367-1375.

[65]   D. A. Steinberg, M. A. Hurst, C. A. Fujii, A. H. Kung, J. F. Ho, F. C. Cheng, D. J. Loury, J. C. Fiddes, *Antimicrob Agents Chemother* **1997**, *41*(8), 1738-1742.

[66]   L. Zhang, J. Parente, S. M. Harris, D. E. Woods, R. E. Hancock, T. J. Falla, *Antimicrob Agents Chemother* **2005**, *49*(7), 2921-2927.

[67]   Y. Ge, D. L. MacDonald, K. J. Holroyd, C. Thornsberry, H. Wexler, M. Zasloff, *Antimicrob Agents Chemother* **1999**, *43*(4), 782-788.

[68]   J. Li, R. L. Nation, R. J. Owen, S. Wong, D. Spelman, C. Franklin, *Clin Infect Dis* **2007**, *45*(5), 594-598.

[69]   M. Vaara, *Curr Opin Pharmacol* **2009**, *9*(5), 571-576; Y. J. Gordon, E. G. Romanowski, A. M. McDermott, *Curr Eye Res* **2005**, *30*(7), 505-515.

[70]   M. McMillan, T. M. L. Price, D. M. Maclaren, G. W. Scott, *The Lancet* **1962**, *280*(7259), 737-739.

[71]   J. M. Streit, R. N. Jones, H. S. Sader, *J Antimicrob Chemother* **2004**, *53*(4), 669-674.

[72]   C. A. Olsen, H. L. Ziegler, H. M. Nielsen, N. Frimodt-Moller, J. W. Jaroszewski, H. Franzyk, *Chembiochem*; D. Wade, A. Boman, B. Wahlin, C. M. Drain, D. Andreu, H. G. Boman, R. B. Merrifield, *Proc Natl Acad Sci U S A* **1990**, *87*(12), 4761-4765.

[73]   V. Dartois, J. Sanchez-Quesada, E. Cabezas, E. Chi, C. Dubbelde, C. Dunn, J. Granja, C. Gritzen, D. Weinberger, M. R. Ghadiri, T. R. Parr, Jr., *Antimicrob Agents Chemother* **2005**, *49*(8), 3302-3310.

[74]   M. Dathe, H. Nikolenko, J. Klose, M. Bienert, *Biochemistry* **2004**, *43*(28), 9140-9150.

[75]   M. V. Sawai, A. J. Waring, W. R. Kearney, P. B. McCray, Jr., W. R. Forsyth, R. I. Lehrer, B. F. Tack, *Protein Eng* **2002**, *15*(3), 225-232.

[76]   Z. Liu, A. Brady, A. Young, B. Rasimick, K. Chen, C. Zhou, N. R. Kallenbach, *Antimicrob Agents Chemother* **2007**, *51*(2), 597-603.

[77]   D. M. Bowdish, D. J. Davidson, Y. E. Lau, K. Lee, M. G. Scott, R. E. Hancock, *J Leukoc Biol* **2005**, *77*(4), 451-459; R. Bucki, D. B. Namiot, Z. Namiot, P. B. Savage, P. A. Janmey, *J Antimicrob Chemother* **2008**, *62*(2), 329-335.

[78]   J. Broughton, *Food Technol* **1990**, *44*, 100-113.

[79]   R. P. Ross, S. Morgan, C. Hill, *Int J Food Microbiol* **2002**, *79*(1-2), 3-16.

[80]   L. J. de Arauz, A. F. Jozala, P. G. Mazzola, T. C. Vessoni Penna, *Trends in Food Science & Technology* **2009**, *20*(3-4), 146-154.

[81]   L. B. Sousa, M. J. Mannis, I. R. Schwab, J. Cullor, H. Hosotani, W. Smith, J. Jaynes, *Clao J* **1996**, *22*(2), 114-117.

[82]   J. L. Nussbaum, R. Bieth, P. Mandel, *Nature* **1963**, *198*, 586-587.

[83]   S. Singer, G. Nicolson, *Science* **1972**, *175*(4023), 720-731.

[84]   G. van Meer, D. R. Voelker, G. W. Feigenson, *Nat Rev Mol Cell Biol* **2008**, *9*(2), 112-124; A. A. Spector, M. A. Yorek, *J Lipid Res* **1985**, *26*(9), 1015-1035.

[85]   M. T. Cabeen, C. Jacobs-Wagner, *Nat Rev Micro* **2005**, *3*(8), 601-610.

[86]   K. H. Schleifer, O. Kandler, *Bacteriol Rev* **1972**, *36*(4), 407-477.

[87]   Y. Kamio, H. Nikaido, *Biochemistry* **1976**, *15*(12), 2561-2570.

[88]   D. C. Morrison, L. F. Kline, *J Immunol* **1977**, *118*(1), 362-368.
[89]   Y. Kanemasa, Y. Akamatsu, S. Nojima, *Biochim Biophys Acta* **1967**, *144*(2), 382-390.
[90]   M. J. Osborn, J. E. Gander, E. Parisi, J. Carson, *J Biol Chem* **1972**, *247*(12), 3962-3972.
[91]   H. Goldfine, *Curr Top Membr Trans* **1982**, *17*, 1-43.
[92]   M. J. Rosen, *Surfactants and interfacial phenomena*, Wiley, New York :, **1978**.
[93]   J. Lauterwein, C. Bosch, L. R. Brown, K. Wuthrich, *Biochim Biophys Acta* **1979**, *556*(2), 244-264.
[94]   E. W. Anacker, H. E. Gerry, P. T. Jacobs, I. Petrariu, *Journal of Colloid and Interface Science* **1977**, *60*(3), 514-518.
[95]   S. Marrink, D. Tieleman, A. Mark, *J Phys Chem B* **2000**, *104*(51), 12165-12173.
[96]   C. R. Sanders, 2nd, G. C. Landis, *Biochemistry* **1995**, *34*(12), 4030-4040.
[97]   C. R. Sanders, 2nd, J. P. Schwonek, *Biochemistry* **1992**, *31*(37), 8898-8905.
[98]   P. Ram, J. H. Prestegard, *Biochim Biophys Acta* **1988**, *940*(2), 289-294.
[99]   N. Tjandra, A. Bax, *Science* **1997**, *278*(5340), 1111-1114.
[100]   R. R. Vold, R. S. Prosser, A. J. Deese, *J Biomol NMR* **1997**, *9*(3), 329-335.
[101]   C. R. Sanders, R. S. Prosser, *Structure* **1998**, *6*(10), 1227-1234.
[102]   A. D. Bangham, R. W. Horne.
[103]   V. P. Torchilin, *Nat Rev Drug Discov* **2005**, *4*(2), 145-160.
[104]   W. H. Pitcher, 3rd, W. H. Huestis, *Biochem Biophys Res Commun* **2002**, *296*(5), 1352-1355.
[105]   F. Szoka, Jr., D. Papahadjopoulos, *Proc Natl Acad Sci U S A* **1978**, *75*(9), 4194-4198.
[106]   L. A. Bagatolli, T. Parasassi, E. Gratton, *Chem Phys Lipids* **2000**, *105*(2), 135-147.
[107]   F. M. Menger, J. S. Keiper, *Curr Opin Chem Biol* **1998**, *2*(6), 726-732.
[108]   D. A. Kendall, R. C. MacDonald, *J Biol Chem* **1982**, *257*(23), 13892-13895.
[109]   J. Keeler, *Wiley-Interscience* **2005**.
[110]   K. Wüthrich, *Wiley-Interscience* **1986**.
[111]   J. Cavanagh, W. Fairbrother, A. Palmer III, N. Skelton, *Academic Press, San Diego* **1996**.
[112]   I. Solomon, *Phys. Rev.* **1955**, *99*, 559 - 565.
[113]   K. Wuthrich, *Biosci Rep.* **2003**, *23*(4), 119-168.
[114]   I. Solomon, N. Bloembergen, *J Chem Phys* **1956**, *25*, 261-266; N. Bloembergen, L. O. Morgan, *J Chem Phys* **1961**, *34*, 842-850.
[115]   R. B. Lauffer, *Chemical Reviews* **1987**, *87*(5), 901-927.
[116]   G. Cornilescu, F. Delaglio, A. Bax, *J Biomol NMR* **1999**, *13*(3), 289-302.
[117]   P. Guntert, C. Mumenthaler, K. Wuthrich, *J Mol Biol* **1997**, *273*(1), 283-298.
[118]   K. Wuthrich, M. Billeter, W. Braun, *J Mol Biol* **1983**, *169*(4), 949-961.
[119]   D. Neri, T. Szyperski, G. Otting, H. Senn, K. Wuthrich, *Biochemistry* **1989**, *28*(19), 510-7516; H. Senn, B. Werner, B. A. Messerle, C. Weber, R. Traber, K. Wüthrich, *FEBS Letters* **1989**, *249*(1), 113-118.
[120]   R. W. Curley, Jr., M. J. Panigot, A. P. Hansen, S. W. Fesik, *J Biomol NMR* **1994**, *4*(3), 335-340; G. Ostler, A. Soteriou, C. M. Moody, J. A. Khan, B. Birdsall, M. D. Carr, D. W. Young, J. Feeney, *FEBS Lett* **1993**, *318*(2), 177-180.
[121]   S. G. Hyberts, W. Marki, G. Wagner, *Eur J Biochem* **1987**, *164*(3), 625-635; E. R. P. Zuiderweg, R. Boelens, R. Kaptein, *Biopolymers* **1985**, *24*(4), 601-611; R. X. Xu, E. T. Olejniczak, S. W. Fesik, *FEBS Lett* **1992**, *305*(2), 137-143.
[122]   M. Nilges, G. M. Clore, A. M. Gronenborn, *Biopolymers* **1990**, *29*(4-5), 813-822.
[123]   T. Carlomagno, W. Peti, C. Griesinger, *J Biomol NMR* **2000**, *17*(2), 99-109.
[124]   P. Guntert, W. Braun, M. Billeter, K. Wuthrich, *J Am Chem Soc* **1989**, *111*, 3997 - 4004.

[125]   P. Guntert, W. Braun, K. Wuthrich, *J Mol Biol* **1991**, *217*(3), 517-530.

[126]   V. C. Kalfa, H. P. Jia, R. A. Kunkle, P. B. McCray, Jr., B. F. Tack, K. A. Brogden, *Antimicrob Agents Chemother* **2001**, *45*(11), 3256-3261.

[127]   C. T. Gottlieb, L. E. Thomsen, H. Ingmer, P. H. Mygind, H. H. Kristensen, L. Gram, *BMC Microbiol* **2008**, *8*, 205.

[128]   R. Wimmer, K. K. Andersen, B. Vad, M. Davidsen, S. Molgaard, L. W. Nesgaard, H. H. Kristensen, D. E. Otzen, *Biochemistry* **2006**, *45*(2), 481-497.

[129]   C. B. Park, K. S. Yi, K. Matsuzaki, M. S. Kim, S. C. Kim, *Proc Natl Acad Sci U S A* **2000**, *97*(15), 8245-8250.

[130]   N. Pathak, R. Salas-Auvert, G. Ruche, M. H. Janna, D. McCarthy, R. G. Harrison, *Proteins* **1995**, *22*(2), 182-186.

[131]   A. Makovitzki, D. Avrahami, Y. Shai, *Proc Natl Acad Sci U S A* **2006**, *103*(43), 15997-16002.

[132]   D. Avrahami, Y. Shai, *Biochemistry* **2002**, *41*(7), 2254-2263.

[133]   M. Respondek, T. Madl, C. Gobl, R. Golser, K. Zangger, *J Am Chem Soc* **2007**, *129*(16), 5228-5234.

[134]   G. Pintacuda, G. Otting, *J Am Chem Soc* **2002**, *124*(3), 372-373.

[135]   E. E. Ambroggio, F. Separovic, J. H. Bowie, G. D. Fidelio, L. A. Bagatolli, *Biophys J* **2005**, *89*(3), 1874-1881.

[136]   J. D. Gehman, F. Luc, K. Hall, T. H. Lee, M. P. Boland, T. L. Pukala, J. H. Bowie, M. I. Aguilar, F. Separovic, *Biochemistry* **2008**, *47*(33), 8557-8565; I. Marcotte, K. L. Wegener, Y. H. Lam, B. C. Chia, M. R. de Planque, J. H. Bowie, M. Auger, F. Separovic, *Chem Phys Lipids* **2003**, *122*(1-2), 107-120.

[137]   D. C. Carter, F. Rüker, J. X. Ho, K. Lim, K. Keeling, G. Gilliland, J. Xinhua, *Protein Pept Lett* **1994**, *1*(4), 175-178.

[138]   K. Zangger, M. Respondek, C. Gobl, W. Hohlweg, K. Rasmussen, G. Grampp, T. Madl, *J Phys Chem B* **2009**, *113*(13), 4400-4406.

[139]   P. C. Driscoll, A. M. Gronenborn, G. M. Clore, *FEBS Lett* **1989**, *243*(2), 223-233.

[140]   R. Koebnik, K. P. Locher, P. Van Gelder, *Mol Microbiol* **2000**, *37*(2), 239-253.

[141]   M. P. Molloy, B. R. Herbert, M. B. Slade, T. Rabilloud, A. S. Nouwens, K. L. Williams, A. A. Gooley, *Eur J Biochem* **2000**, *267*(10), 2871-2881.

[142]   W. C. Wimley, *Curr Opin Struct Biol* **2003**, *13*(4), 404-411.

[143]   H. Nikaido, *Microbiol Mol Biol Rev* **2003**, *67*(4), 593-656.

[144]   I. G. Denisov, Y. V. Grinkova, A. A. Lazarides, S. G. Sligar, *J Am Chem Soc* **2004**, *126*(11), 3477-3487.

[145]   S. J. Opella, *Nat Meth* **2009**, *6*(3), 197-198.

[146]   K. Pervushin, R. Riek, G. Wider, K. Wuthrich, *Proc Natl Acad Sci U S A* **1997**, *94*(23), 12366-12371.

[147]   N. Tjandra, S. Grzesiek, A. Bax, *Journal of the American Chemical Society* **1996**, *118*(26), 6264-6272.

[148]   G. Wagner, *J Biomol NMR* **2009**, *46*(1), 1-2.

[149]   I. R. Henderson, F. Navarro-Garcia, M. Desvaux, R. C. Fernandez, D. Ala'Aldeen, *Microbiol Mol Biol Rev* **2004**, *68*(4), 692-744.

[150]   J. Jose, F. Jahnig, T. F. Meyer, *Mol Microbiol* **1995**, *18*(2), 378-380.

[151]   T. J. Barnard, N. Dautin, P. Lukacik, H. D. Bernstein, S. K. Buchanan, *Nat Struct Mol Biol* **2007**, *14*(12), 1214-1220.

[152]   P. Emsley, I. G. Charles, N. F. Fairweather, N. W. Isaacs, *Nature* **1996**, *381*(6577), 90-92; B. R. Otto, R. Sijbrandi, J. Luirink, B. Oudega, J. G. Heddle, K. Mizutani, S. Y. Park, J. R. Tame, *J Biol Chem* **2005**, *280*(17), 17339-17345; H. Nummelin, M. C. Merckel, Y. el Tahir, P. Ollikka, M. Skurnik, A. Goldman, *Adv Exp Med Biol* **2003**,

529, 85-88; H. J. Yeo, S. E. Cotter, S. Laarmann, T. Juehne, J. W. St Geme, 3rd, G. Waksman, *Embo J* **2004**, *23*(6), 1245-1256.

[153]   C. J. Oomen, P. van Ulsen, P. van Gelder, M. Feijen, J. Tommassen, P. Gros, *Embo J* **2004**, *23*(6), 1257-1266; G. Meng, N. K. Surana, J. W. St Geme, 3rd, G. Waksman, *Embo J* **2006**, *25*(11), 2297-2304.

[154]   G. E. Schulz, *Curr Opin Struct Biol* **2000**, *10*(4), 443-447.

[155]   J. P. Nataro, J. B. Kaper, *Clin Microbiol Rev* **1998**, *11*(1), 142-201.

[156]   U. Niewerth, A. Frey, T. Voss, C. Le Bouguenec, G. Baljer, S. Franke, M. A. Schmidt, *Clin Diagn Lab Immunol* **2001**, *8*(1), 143-149.

[157]   I. Benz, M. A. Schmidt, *Mol Microbiol* **1992**, *6*(11), 1539-1546.

[158]   M. P. J. Konieczny, I. Benz, B. Hollinderbaumer, C. Beinke, M. Niederweis, M. A. Schmidt, *Antonie Van Leeuwenhoek* **2001**, *80*(1), 19-34.

[159]   P. Bradley, L. Cowen, M. Menke, J. King, B. Berger, *Proc Natl Acad Sci U S A* **2001**, *98*(26), 14819-14824; A. V. Kajava, N. Cheng, R. Cleaver, M. Kessel, M. N. Simon, E. Willery, F. Jacob-Dubuisson, C. Locht, A. C. Steven, *Mol Microbiol* **2001**, *42*(2), 279-292.

[160]   M. P. Konieczny, M. Suhr, A. Noll, I. B. Autenrieth, M. Alexander Schmidt, *FEMS Immunol Med Microbiol* **2000**, *27*(4), 321-332; C. T. Lattemann, J. Maurer, E. Gerland, T. F. Meyer, *J Bacteriol* **2000**, *182*(13), 3726-3733; J. Jose, R. Bernhardt, F. Hannemann, *J Biotechnol* **2002**, *95*(3), 257-268; J. Jose, S. von Schwichow, *Chembiochem* **2004**, *5*(4), 491-499.

[161]   M. Suhr, I. Benz, M. A. Schmidt, *Mol Microbiol* **1996**, *22*(1), 31-42; J. Maurer, J. Jose, T. F. Meyer, *J Bacteriol* **1999**, *181*(22), 7014-7020.

[162]   J. Maurer, J. Jose, T. F. Meyer, *J Bacteriol* **1997**, *179*(3), 794-804.

[163]   J. E. Mogensen, D. Tapadar, M. A. Schmidt, D. E. Otzen, *Biochemistry* **2005**, *44*(11), 4533-4545.

[164]   R. Keller, 'OPTIMIZING THE PROCESS OF NUCLEAR MAGNETIC RESONANCE SPECTRUM ANALYSIS AND COMPUTER AIDED RESONANCE ASSIGNMENT' obtained from the website www.nmr.ch.

[165]   A. Sali, T. L. Blundell, *J Mol Biol* **1993**, *234*(3), 779-815.

[166]   E. Lindahl, B. Hess, D. van der Spoel, *Journal of Molecular Modeling* **2001**, *7*(8), 306-317.

[167]   W. F. van Gunsteren, P. Kruger, S. R. Billeter, A. E. Mark, A. A. Eising, W. R. P. Scott, P. H. Huneberger, I. G. Tironi, *Biomos Hochschulverlag AG an der ETH Zurich, Groningen* **1996**.

[168]   P. Alexander, S. Fahnestock, T. Lee, J. Orban, P. Bryan, *Biochemistry* **1992**, *31*(14), 3597-3603.

[169]   S. Hiller, R. G. Garces, T. J. Malia, V. Y. Orekhov, M. Colombini, G. Wagner, *Science* **2008**, *321*(5893), 1206-1210; M. Bayrhuber, T. Meins, M. Habeck, S. Becker, K. Giller, S. Villinger, C. Vonrhein, C. Griesinger, M. Zweckstetter, K. Zeth, *Proc Natl Acad Sci U S A* **2008**, *105*(40), 15370-15375.

Part III

Papers

Paper I

Co-author statement for Paper I

Magnus Franzmann, Daniel Otzen, Reinhard Wimmer: **Quantitative Use of Paramagnetic Relaxation Enhancements for Determining Orientations and Insertion Depths of Peptides in Micelles**

Chembiochem. 2009 Sep 21;10(14):2339-47.

- Magnus Franzmann performed all experiments and wrote the article
- Daniel Otzen co-supervised the experiments
- Reinhard Wimmer supervised overall design and execution of the experiments, contributed extensively to the writing of the article.

Daniel Otzen _____

Reinhard Wimmer _____

Quantitative Use of Paramagnetic Relaxation Enhancements for Determining Orientations and Insertion Depths of Peptides in Micelles

Magnus Franzmann,[a] Daniel Otzen,[b] and Reinhard Wimmer*[a]

We describe the background and implementation of a method to determine, at atomic resolution, the insertion depths and orientations of peptides embedded in micelles. A nonperturbing paramagnetic agent—Gd(DTPA–BMA)—was used to induce paramagnetic relaxation enhancements (PREs) of peptide atoms inside the micelle. By calibrating these PREs it was possible to translate them into distance restraints that could be used for structure calculation. We demonstrate this here on the antimicrobial peptides novicidin and novispirin. Characterization of the interactions between antimicrobial peptides and membranes is important for understanding of their biological activities and functions, and a further development of tools to study these interactions is described.

Introduction

Considerable work has been put into the characterization and understanding of the interactions of proteins and peptides with biological membranes in order to further elucidate their biological functions. [1–3] Because biological membrane lipids are expensive, frequently ill-defined, and generally difficult to work with, peptides are often embedded in membrane-mimicking environments such as surfactant micelles and bicelles.[1,3,4] Determination of the orientations and insertion depths of proteins in lipid aggregates is also essential for understanding the mechanisms of the rapidly growing number of identified antimicrobial peptides (AMPs). These peptides are very promising candidates for alternative treatment of an increasing number of microbial infections that cannot be treated with conventional antibiotics as a consequence of growing resistance. A wide variety of such peptides has been discovered in a multitude of different organisms, and they display great diversity in their primary sequences and tertiary structures.[5]

One large group of AMPs does not adopt secondary structures in the absence of lipid aggregates, but in the presence of lipids they form small amphiphatic α helices. It has been suggested that they disrupt the cell membranes of the target organisms either by forming pores ("toroidal" or "barrel-stave") or by binding to the surfaces of the microbes in a detergent-like manner, leading to displacement of a part of the membrane.[6] Often, a single mutation that does not change the overall structure of a peptide can lead to large changes in antimicrobial behavior. It is therefore desirable to have a tool for obtaining detailed information on interactions between AMPs and membranes/surfactants for the determination of the mechanisms of action of the individual peptides.

Various optical spectroscopic techniques such as Fourier transform infrared (FTIR), Raman, fluorescence, and oriented circular dichroism have been used to characterize lipid-peptide interactions at low resolution.[7] Computational biology methods such as molecular dynamics have provided valuable information at atomic resolution.[8] A considerable amount of proteins and peptides have been simulated in lipid bilayers to provide valuable spatial information concerning their arrangements in membrane-mimicking environments. The results of this effort have been made available in the "Orientation of Proteins in Membranes" (OPM) Database.[9] However, many of these simulations have not been validated by experimental data, and there is therefore a need for the development of new high-resolution techniques to probe lipid–peptide interactions. The most commonly used experimental methods for studying membrane proteins and peptides at high resolution include electron paramagnetic resonance (EPR),[10] solid-state NMR[11] and solution-state NMR with the aid of chemical shifts,[12] NOEs,[1] and the attachment of various paramagnetic spin labels to the peptides.[13] In addition, ^{19}F has been incorporated into peptides as an NMR probe. These various approaches have also been combined with measurement of the paramagnetic effect of apolar oxygen to measure the immersion depths of peptides in bicelles under high pressure.[14] Furthermore, both the line-broadening effect and the reduced signal intensity induced by titration with paramagnetic species such as Mn^{II} in solution have been used to determine which residues are facing the solution.[15,16] It is, however, likely that positively charged metal ions would to some degree be associ-

[a] M. Franzmann, Prof. Dr. R. Wimmer
Department of Biotechnology
Chemistry and Environmental Engineering, Aalborg University
Sohngaardsholmsvej 49, 9000 Aalborg (Denmark)
Fax: (+45) 98141808
E-mail: rw@bio.aau.dk

[b] Prof. Dr. D. Otzen
Interdisciplinary Nanoscience Center (iNANO)
Department of Molecular Biology, Aarhus University
Gustav Wieds Vej 10 C, 8000 Aarhus C (Denmark)

Supporting information for this article is available on the WWW under
http://dx.doi.org/10.1002/cbic.200900347.

ated with the proteins or the micelles, especially when anionic detergents such as SDS are used, and this specific association can significantly bias the results obtained.

Studies of peptides in aligned media have also been extensively used to yield information on their global orientations and thereby also the orientations of peptides in membranes.[17] These studies rely on hydrogen–nitrogen couplings, and ^{15}N-isotopically labeled peptides are therefore needed. These can be very expensive, however, especially in the case of AMPs, which, because of their very natures, often cannot be expressed in their active forms in bacterial and fungal expression systems.

Chelated paramagnetic metals such as the electrically neutral Gd(DTPA–BMA) are highly water soluble and do not appear to interact either with phospholipids or with proteins.[18,19] Because we have not observed any chemical shift changes either in the peptide or in the DPC signals, but merely attenuation of the signals upon addition of Gd(DTPA–BMA), we have concluded that neither our peptides nor detergent interact with this chelate. This is consistent with a previously published observation that Gd(DTPA–BMA) does not interact with lipid membranes[18] or with ubiquitin.[19] Gd(DTPA–BMA) is more strongly paramagnetic than similarly used nitroxide agents such as HyTEMPO, and smaller amounts are therefore needed in the experiments; this further reduces chances of binding.[19] In more recent years the role of Gd(DTPA–BMA) has therefore been adapted from that of a contrast agent in MRI-type experiments to investigation of the solvent exposure of micelle-bound proteins, because it can be used in a nonperturbing manner.[19–21]

Relaxation enhancements caused by paramagnetic ions can be described by inner-sphere, second-sphere, and outer-sphere models. The inner-sphere model describes the relaxation of atoms within the same molecular framework as the paramagnetic center, the outer-sphere model describes the relaxation enhancement of atoms not bound and rotationally uncorrelated to the paramagnetic center, and the second-sphere interaction model describes an intermediate situation in which there is no specific interaction between the molecule carrying the paramagnetic center and the molecule carrying the nucleus in which the relaxation is enhanced, but the two molecules are still rotationally correlated.[22]

Relaxation enhancement arises from modulation of the dipolar interaction between the electron and nuclear spins. In the inner-sphere model, this modulation is caused by the rotational diffusion of the molecular framework containing both the paramagnetic center and the nuclear spin. In the outer-sphere model, this modulation is caused by translational diffusion of the molecule containing the paramagnetic center and the molecule containing the nuclear spin.[23] In the second-sphere interaction model, both rotational and translational diffusion enter into the equations.

Although one would intuitively expect the relaxation enhancement of proteins in solution by a Gd complex in solution to follow an outer-sphere model, it has been shown that the relaxation enhancements caused by Gd(DTPA–BMA) can be more accurately described by a "second-sphere interaction"

model, which gives a highly distance-dependent paramagnetic effect[19] [Equation (1)]:

$$\frac{1}{T_1} = \frac{2}{15}\left(\frac{\mu_0}{4\pi}\right)^2 \frac{\gamma_H^2 (g_J \mu_B)^2 J(J+1)}{r^6}\left(\frac{3\tau_C}{1+\omega_H^2\tau_C^2} + \frac{7\tau_C}{1+\omega_S^2\tau_C^2}\right) \quad (1)$$

where J is the electronic spin, τ_C is a correlation time dependent on the T_1 of the electron spin and the rotational and diffusional correlation times of the molecules in question,[19] r is the distance between the electron and ^1H spin, T_1 is the longitudinal relaxation time, μ_0 is the induction constant, γ_H the ^1H gyromagnetic ratio, g_J the Landé factor, μ_B the Bohr magneton, r the distance between the electron and the ^1H spin, and ω_H and ω_S the Larmor frequencies of the ^1H and electron spin, respectively.

However, this relationship holds only for the interaction between fixed nuclear and electron spins. If the moiety carrying the electron spin is free to move, the interactions need to be integrated over the volume in which the electron spin can be located.[21,24] This leads to a dependence of the PRE on the inverse third power of the distance between nuclear and electron spin.

To the best of our knowledge, chelated paramagnetic agents and other paramagnetic agents in solution have until recently only been used in a qualitative manner, only providing relative comparisons of different parts of the peptide. Although it is possible to estimate a peptide's orientation in a micelle, no absolute information about immersion depths could be obtained. Zangger and co-workers developed a method to measure the orientations and immersion depths of small helical peptides in micelles and bicelles with the aid of paramagnetic agents in solution.[21,25] This technique relies on quantitative use of PRE values to calculate the tilt and azimuth angles of a straight-helical peptide without the need for isotope labeling of the protein. In a recent paper, a method that allowed peptides of any structure to be oriented in a micelle by a least-squares fitting of observed versus calculated PREs was proposed.[25]

Here we present a different method for obtaining information relating to immersion depths and orientations of all types of secondary and tertiary structures of proteins at atomic resolution. Our method is readily implemented in existing structure calculation programs, and allows the straightforward incorporation of PREs into the structure calculation as experimental data equal to NOEs and dihedral angles. From Gd(DTPA–BMA) titration experiments we have determined the PREs for the atoms of interest in our model peptides—novicidin and novispirin—in [D$_{38}$]dodecylphosphocholine (DPC) micelles. To convert these PREs into quantitative distance information, we have calibrated PRE data for DPC in micelles with distances obtained from simulated DPC micelles. We were thus able to convert the PRE values of our model peptides into detailed information on the distances between the centers of the micelles and the atoms in the peptides. Because this PRE/distance correlation is completely independent of the structural properties of the molecules, this method should be directly applicable for all types of micelle-embedded peptides and proteins, for

which it can provide accurate orientation and immersion depth information at atomic resolution.

Results and Discussion

Calibration of micelle distances from PRE values

From a 1D NMR spectrum we have identified six unambiguous proton signals (H1–3, H5, H6, H12, H13, and H23; see Scheme 1) of DPC micelles in solution. To obtain distance information for atoms in micelles, we titrated DPC micelles with Gd-(DTPA–BMA), which is known not to interact with peptides and micelles.[19,21] The PRE values of an atom depend on the inverse
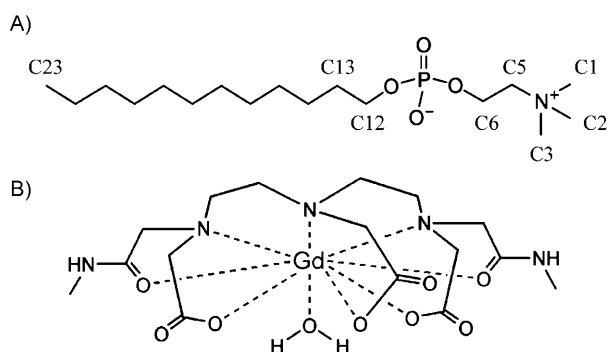
Scheme 1. A) Chemical structure of DPC showing the (arbitrary) numbering used in the text. B) Chemical structure of Gd(DTPA–BMA).[19]

Table 1. Distances between the hydrogen atoms of DPC and the micelle center.

Atom(s)	Average PRE value [$s^{-1} mM^{-1}$]	Average distance to center $\pm$ sd [Å]
H1–3	0.55 ± 0.032	22.55 ± 0.25
H5	0.45 ± 0.029	21.86 ± 0.21
H6	0.40 ± 0.046	21.64 ± 0.19
H12	0.21 ± 0.0018	18.40 ± 0.17
H13	0.15 ± 0.0085	17.19 ± 0.19
H14	–	16.47 ± 0.17
H15	–	15.42 ± 0.20
H16	–	14.70 ± 0.18
H17	–	13.85 ± 0.18
H18	–	13.20 ± 0.17
H19	–	12.48 ± 0.16
H20	–	12.01 ± 0.14
H21	–	11.43 ± 0.17
H22	–	11.12 ± 0.18
H23	0.091 ± 0.0057	10.75 ± 0.20

Calculated distances between the hydrogen atoms of DPC and the center of the micelle. For the distinguishable atoms the PRE values are listed.

$$PRE = a + k \times (g + R - r)^{-3} \qquad (2)$$

where Equation (1) has been integrated as described previously,[21] and all constants have been combined into the single constant k. The distance between the electron and the ^{1}H spin is split into three distances, where g is the average distance of a Gd atom from the surface of the micelle, R is the micelle radius, and r is the distance between the atom in question and the center of the micelle.

of the sixth power of the distance between the affected nucleus and a fixed paramagnetic center.[26] However, for a nuclear spin surrounded by a mobile, noninteracting paramagnetic probe the relaxation depends on the inverse of the third power between the atoms.[21,24]

The PRE values for the atoms of DPC are given in Table 1. Scheme 1 shows the DPC molecule with the numbering used. To convert the PRE values into distance information, the PRE values were correlated with distances obtained from an MD-simulated micelle. For each DPC atom we measured the distance of the atom from the center of mass of the micelle to which it belonged until the average distances became stable. This part of the simulation was considered an equilibration phase and was discarded for the subsequent calculations. We then continued the simulation of the micelle and averaged over the DPC atoms in all molecules in all the snapshots. As expected, this shows that the methyl protons of the DPC choline group are located furthest away from the micelle center, whereas the methyl groups of the acyl chain are closest to the center, despite the carbon chains being bent and flexible, which can be seen in the average distance of 10.75 Å between the micelle center and the DPC H23 atoms. The PRE values for the DPC protons identified in the NMR spectra were plotted against the calculated average distances of the corresponding atoms and the values were fitted to Equation (2) (see Figure 1):

Figure 1. PRE values for well-resolved DPC protons plotted against distance information relating to the corresponding atoms in a MD-simulated micelle. The values were fitted to Equation (2), giving an "*a*" value of 0.057 ± 0.017 $s^{-1} mM^{-1}$, a $g + R$ value of 30.5 ± 0.9 Å [with the maximum distance from the center of the DPC micelles obtained in the MD simulation ($R = 22.55$ Å); this yields a "*g*" value of 7.98 Å], and a k value of 253.1 ± 91.95 $s^{-1} mM^{-1} Å^3$. d corresponds to the distance to the center of the DPC micelle.

It had previously been estimated that the Gd(DTPA–BMA) complex has to diffuse approximately 10 Å away from the interacting partner in order not to contribute to relaxation.[19] Our g value of 8 ± 0.9 Å lies between this value and the radius

of the Gd complex making up the distance of closest approach, so it seems realistic.

We furthermore had to introduce the constant "*a*" into Equation (2), because the measured PREs do not tend towards zero with decreasing distances to the micelle center. This is probably due to the fact that the DPC molecules in this system exist in equilibrium between a monomeric form in solution and the aggregated form in the micelle, because DPC has a critical micelle concentration (cmc) of 1.1 mм,[27] which means that 1.1 mм of the total 90 mм DPC molecules are at any time located outside the micelle, where they experience a greater relaxation enhancement than inside the micelle. Exchange between these two states is fast on the NMR timescale, as shown by the fact that no sharp signals for DPC can be seen in the NMR spectrum of a micellar solution–-only the broad signals from micellar DPC.

Structure calculation

The proton signals of the 18-residue peptides novicidin and novispirin in DPC micelles were assigned with the aid of standard sets of homonuclear 2D spectra, and the C^α and C^β shifts of the residues were assigned with the aid of $^1H,^{13}C$ HSQC spectra. A set of 80 structures was calculated for each peptide, and the 20 structures with the lowest residual target functions can be seen in Figure 2.

Key values from the structure calculations are listed in Table 2. As can be seen from Figure 2, both novicidin and novispirin form highly similar slightly curved α helices that are clearly amphiphatic, because the hydrophobic residues Leu3, Ile6, -7, -11, -13, and -14, and Tyr17 are located on one side whereas Arg4, -5, and -8, Lys9, -15, and -16, and His12 are located on the opposite side. This has also been reported previously for novispirin and for the highly similar peptide ovispirin in other lipidic environments.[16, 28]

Qualitative interpretation of PRE values—paramagnetic relaxation wave

Figure 3 shows a plot of the PRE values of the H^α atoms of novicidin and novispirin against the residue numbers of the peptides; it features wavelike patterns with wavelengths of either three or four residues between the maxima of the PRE curves. These patterns are characteristic for α helices lying parallel to the surfaces of the micelles, as previously described.[21] The maximum PREs of novicidin are experienced by the residues Asn2, Arg5, Lys9, His12, and Lys16, all located on the hydrophilic side of the amphipathic helix. For novispirin the maxima are located at residues Asn2, Arg5, Lys9, His12, and Tyr17, showing a slight deviation in the C-terminal part of the peptide, where the mutation is located. Because the Gd(DTPA–BMA) is located in the solution surrounding the micelles, the relatively high PRE values confirm that the hydrophilic sides of the helices are facing the outsides of the micelles, as would be expected. The PRE values for novispirin residues 2–13 are very similar to the values for novicidin, but for residues 14, 15, 17, and 18 the values for novispirin are noticeably higher (see

Figure 2. Overlay of novicidin (black) and novispirin (gray) structures in the presence of DPC. The bundles of the 20 structures with the lowest residual target functions are shown, with N, C′, and C^α from residues 2–17 aligned.

Table 2. Quality criteria for the calculated novicidin structures.

	Novicidin	Novispirin
number of distance constraints	210	211
– of which intraresidual	130	135
– of which sequential	42	41
– of which medium-range ($2 \leq \Delta_{res} \leq 4$)	38	35
number of angle constraints[a]	26	26
– of which ϕ	13	13
– of which ψ	13	13
CYANA residual target function [Å²]	0.74 ± 0.05	0.60 ± 0.04
distance restraints violated by more than 0.2 Å	0	0
angle restraints violated by more than 5°[b]	0	0
rmsd residues 2–17 [Å][c]	0.17 ± 0.08	0.13 ± 0.05
% of residues in Ramachandran plot[d]		
– in most favored regions	86.6	89.7
– less favored regions	13.4	9.0
– generously allowed regions	0	1.0
– disallowed regions	0	0.3

[a] Only those derived from Talos. [b] Per molecule. [c] For backbone atoms C′, C$^\alpha$, and N, as calculated by CYANA from the pairwise rmsd values of each of the 20 structures against a mean structure. [d] As calculated by PROCHECK_NMR.
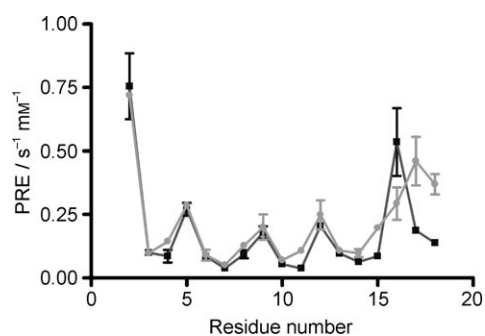
Figure 3. PRE values for H$^\alpha$ nuclei of novicidin (■, black) and novispirin (●, gray) as a function of residue number. Error bars indicate variations in PRE values obtained from fitting several peaks.

Figure 3). Because the Gly to Phe mutation from novispirin to novicidin is located at the C-terminal ends of the peptides, it is possible to observe this mutation and hence to distinguish the two peptides by their PRE values. Because the PRE values for residues 14, 15, 17, and 18 are higher in novispirin than in the corresponding novicidin residues it is most likely that the more hydrophobic Phe pulls the C-terminal part of novicidin into the micelle and further away from the Gd-containing buffer than is the case in novispirin.

Quantitative use of PRE values

In order to use PRE values quantitatively for determining the positioning of a peptide in a micelle, we need to convert them into distances from the center or the surface of the micelle. The center of a micelle represents a single point in space, whereas the surface of the micelle represents a multitude of points. Structure calculation programs routinely accept distan-

ces between points in space as constraints for structure calculations, whereas the distance between a point in space and a spherical surface is not straightforward to implement. For that reason we sought to convert the PRE values into distances between the atoms in question and the centers of the micelles. This requires knowledge of the micellar radii, which has been reported in the literature both from experiments[27, 29] and from MD simulations.[30, 31] Simulations have shown that the shapes of the micelles are dependent on the DPC concentration, with high concentrations (460 mм) giving rodlike micelles and bilayers whereas lower concentrations (120 mм) give spherical micelles.[31] Because all our experiments are conducted at 90 mм, we can safely assume a spherical micelle shape with minor fluctuations. The method presented here is based on knowledge of the micellar radii. If the peptides and proteins investigated are so large that they start to influence the micellar radii significantly, the radii of the peptide-loaded micelles have to be determined independently. The method can still be used, however, but the *R* value in Equation (3) has to be adjusted accordingly.

Conversion of PRE values into distances is fairly straightforward with the calibration curve obtained from the titration of DPC. As mentioned above, a nonzero offset in the r^{-3} dependence of the PRE on the distance of an atom from the micelle center is caused by the presence of monomeric DPC molecules in the aqueous phase in equilibrium with DPC in the micelle. This offset does not have to be taken into account for peptide data, because the equilibrium between free and micelle-bound peptide is shifted strongly towards the micelle-bound form. This was substantiated by NMR spin diffusion measurements. The observed diffusion coefficient of 90 mм DPC is 1.07×10^{-10} m²s^{-1} and the diffusion coefficient of novicidin in the presence of 90 mм DPC is 0.97×10^{-10} m²s^{-1}, whereas the diffusion constant of novicidin in aqueous solution without detergents was measured as 1.98×10^{-10} m²s^{-1}. Therefore, in order to use the calibration curve obtained from DPC on the peptide atoms, the start value "*a*" can be eliminated from the calibration curve [see Eq. (2)], allowing us to calculate the distance from the PRE with Eq. (3):

$$r = (g + R) - \left(\frac{\text{PRE}}{k}\right)^{-1/3} \qquad (3)$$

Peptide PRE values can thus be converted into average distances between the atoms in question and the centers of the micelles. In order to account for experimental uncertainties, distances are allowed to vary within a range of two standard deviations from the value determined from the calibration curve. The distances thus calculated for novicidin and novispirin atoms can be seen in the Supporting Information.

It is crucial for the validity of this approach that the peptide is bound strongly to the micelle with only one conformation. Weak binding to the micelle would lead to significant fractions of the peptide in the bulk solution, in which it is in close contact with the paramagnetic center. This would yield too-high PRE values, and consequently too-low distances from the mi-

cellar surface. Conformational flexibility will likewise lead to an averaging of PRE values.

For the calculations, a range of linker residues consisting only of pseudoatoms was attached to the C terminus of the peptide. At the end of the chain of linker residues, the center of the micelle was attached as a pseudoatom. This approach builds on a previously described technique for introducing distance constraints obtained from metal ions in metalloproteins.[32] In CYANA, lower distance limits and upper distance limits were introduced for the distances between the pseudoatom defining the center of the micelle and every H^{α} atom for which PRE data were available (here all of them except Lys1).

In cases of high PRE values that would suggest distances from the micelle center larger than the radius of the micelle, it would be advantageous only to apply a lower distance limit corresponding to the micelle radius. Conversely, in the case of very low PREs with large experimental uncertainties only an upper distance limit should be applied.

In our samples, this only applies to the $H^{\alpha 3}$ atom of Gly10 in novicidin. Because this PRE is based on only one peak, it seemed impossible to estimate the experimental uncertainty, and the PRE was excluded from further calculations. For all other atoms we used both lower and upper distance limits defined by the average calculated distance to the center minus/plus one standard deviation obtained by calculating the distance from multiple H^{α} peak volumes (see the Supporting Information).

Structure calculation was then repeated with all experimental constraints (TALOS-derived angle constraints, NOESY cross peak intensities, and PRE-derived distance constraints) present in the calculation. The PRE-derived distance constraints were weighted by only 10% relative to the weighting for NOE-derived distance constraints in the calculation of the residual target function, in order not to allow PRE-derived distance limits to influence the structure of the peptide itself, but merely to position it correctly with respect to the center of the micelle. In cases in which PRE data are available only for a limited number of amino acids, increasing the weight of the PRE-derived distance constraints should be considered.

Figure 4 shows the PRE-derived distance limits from each H^{α} atom to the center of the micelle, together with the ranges of distances for the calculated ensemble of structures.

As can be seen from Figure 4, the distance constraints positioning the peptide in the micelle derived from PRE values are mostly fulfilled, and for those that are not fulfilled the violations are negligible. Increasing the acceptable deviation of the distance between a specific H^{α} and the center of the micelle has no influence on the overall positioning and orientation of the peptide, but reduces or eliminates the violations. The result of the simultaneous structure/positioning calculation can be seen in Figure 5.

The structures and positioning of both novicidin and novispirin in DPC show that the charged groups of the sidechains of the hydrophilic residues (Lys1, Asn2, Arg4, Arg5, Lys9, His12, Lys15, and Lys16), together with the N and C termini, are located at the DPC/solution interface, whereas the hydrophobic side chains of Ile7, Ile11, and Ile14 are further away from the surface of the micelle. Novicidin appears to be more deeply buried in the sphere than novispirin, as would be expected from the lower PRE values. Furthermore, novispirin is rotated approximately 20° around the helix axis in relation to novicidin, in order to best accommodate the PRE restraints (see Figure 5).

Conclusions

PREs have been used here in a quantitative manner in combination with distance information from MD simulations to provide valuable long-range distance restraints to determine the insertion depths and orientations of small micelle-embedded α helices. In contrast with previous studies that used paramagnetic agents or oxygen for determining immersion depths, this method provides information with atomic resolution. For this study we have used PRE values of Hα atoms, because these provide the least flexible protons in the peptide backbone that are not affected by solvent exchange (as is the case with the H^{N} atoms). Dynamic light scattering (DLS) measurements on DPC micelles show no detectable size increase upon addition
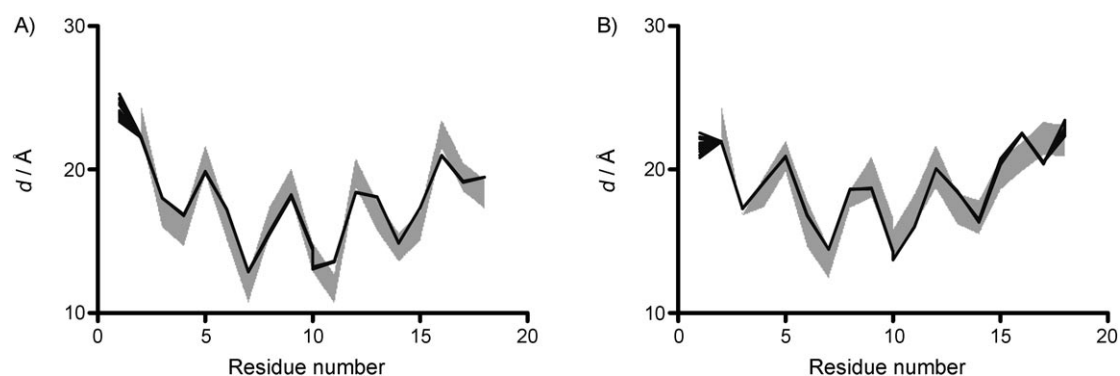
Figure 4. Black lines show the calculated distances between H^{α} atoms from the 20 structures with the lowest residual target function and the center of the micelle. The gray area defines the range between the upper and lower distance restraints, based on the PRE values of the H^{α} atoms. A) Restraints are obtained from the average PRE values ±one standard deviation of the multiple novicidin peaks. B) The same values for novispirin. *d* corresponds to the distance to the micelle center.
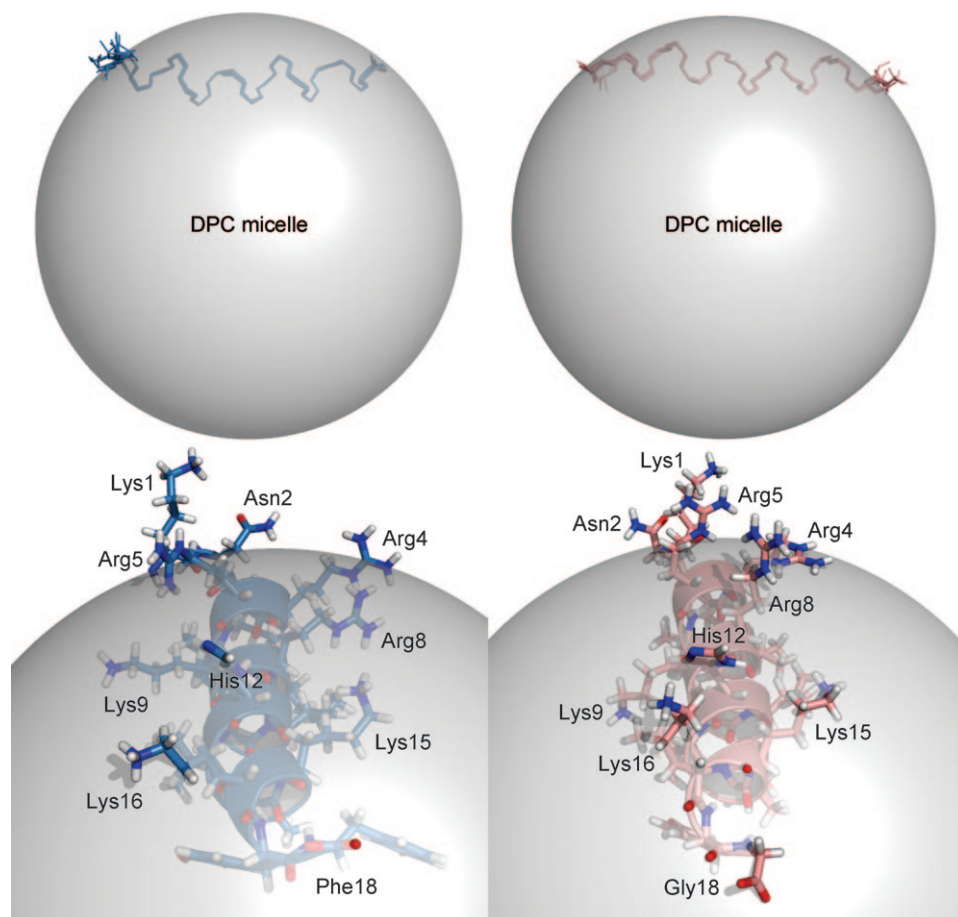
Figure 5. The bundles of A) the 20 novicidin and B) the 20 novispirin structures with the lowest residual target functions are shown with N, C′, and C$^\alpha$ from residues 2–17 aligned. The structures are calculated with PRE constraints between the micelle center and the Hα atoms. A 45.2 Å diameter sphere is shown to illustrate the approximate size of the DPC micelle. Note that the micelle in solution is not a perfect sphere but a mobile, continuously changing shape. However, on average, the micellar shape will be close to spherical, so the micelle is represented here in its simplest form as a sphere. Below are the structures of C) novicidin and D) novispirin with the lowest residual target functions and with visible side chain atoms.

toxicity. The ability to determine precise orientations is therefore a key technique for understanding of the modes of action of some of these peptides. The technique demonstrated here on two highly similar peptides provides this capability in a straightforward, generally applicable, and ready-to-implement way.

Experimental Section

Materials: DPC was purchased from Avanti Polar Lipids (Alabaster, AL, USA) and DPC-d$_{38}$ from Cambridge Isotope Laboratories, Inc. (Andover, MA, USA). Novicidin (sequence: KNLRRIIRKGIHIIKKYF) and novispirin (sequence: KNLRRIIRKGIHIIKKYG) were generously provided by Novozymes A/S, and Gd-(DTPA–BMA) was generously provided by Klaus Zangger.

NMR recording: All NMR spectra were recorded at 310 K on a BRUKER DRX 600 spectrometer operating at a field strength of 14.1 T, fitted with a TXI(H/C/N) probe with triple-axis gradients. Either novicidin or novispirin (2 mM) was dissolved in [D$_{38}$]DPC (90 mM, Cambridge Isotope Laboratories), phosphate buffer (10 mM), sodium azide (0.05 %), and D$_2$O (5 %) at pH 6 to a final volume of 500 μL. For structural determination of novicidin and novispirin in DPC micelles, the following spectra were recorded: 2D NOESY spectra with

of the peptide (data not shown), but if the technique were to be applied on larger systems or even membrane proteins this should be taken into consideration.

The only strictly quantitative approach for utilizing PREs so far was published very recently.[25] Our method has several advantages over that method. Firstly, our protocol is readily applicable in standard structure calculation protocols and does not need a separate fitting routine. Secondly, our method allows simultaneous determination of structure and lipid immersion. Incompatibilities between NOE data and PRE data will show up immediately and can be corrected during structure calculation. Thirdly, our protocol treats PRE data individually for each atom of the protein, instead of accumulating all PRE data for the whole peptide into one sum of squared errors function.

It is believed that precise orientations of some antimicrobial peptides in biological membranes are of vital importance for the antimicrobial action and to the absence/presence of cyto-

80 ms mixing times were recorded with Watergate water suppression,[33] [^{1}H,^{1}H] TOCSY spectra with 50 and 80 ms mixing times were recorded by use of a clean TOCSY pulse sequence with a 15 kHz spin-lock and Watergate water suppression.[34] 2QF COSY and [^{1}H,^{13}C] HSQC in the aromatic and aliphatic regions were recorded by use of standard sequences taken from the Bruker Topspin pulse sequence library. All spectra were processed with Topspin version 1.3. Assignments of all NMR spectra were achieved by use of the program CARA version 1.5.5[35] and NOE cross-peaks were subsequently integrated by use of CARA's NEASY subroutine.[36] Backbone torsion angle restraints were obtained from chemical shift values by use of the program TALOS,[37] and the CALIBA[38] subroutine in CYANA was used to convert integrated cross-peak intensities from the NOESY spectra into distance constraints. These combined constraints provided the input for structure calculation with the torsion angle dynamics program CYANA.[39] Structure calculations were started from 80 conformers with random torsion angle values and the 20 structures with the lowest CYANA target functions were collected and analyzed with the aid of Pymol.[40]

PRE measurements: For the PRE measurements on novicidin and novispirin, samples identical to those used for structural determination were titrated with Gd(DTPA–BMA) to give final concentrations of 2, 5, and 10 mM. Eight inversion recovery NOESY spectra with recovery delay times of 1, 50, 150, 400, 700, 1200, 2600, and 4000 ms were recorded for each titration point in order to obtain the T_1 relaxation time. For calibration, samples were prepared with DPC (90 mM) dissolved in D_2O (5%), phosphate buffer (10 mM), and sodium azide (0.05%) at pH 6. As above, the samples were titrated with Gd(DTPA–BMA) and eight 1D inversion recovery spectra with recovery delay times of 1, 50, 150, 400, 700, 1200, 2600, and 4000 ms were recorded for each titration point (including a set before the start of the titration). T_1 relaxation times were analyzed by use of TOPSPIN version 1.3. Relaxation rates ($1/T_1$) were plotted against the concentration of the Gd complex, and linear regression yielded the PRE values as the slope of the regression line. All molecular visualizations were made with Pymol.[40]

Diffusion measurements: Diffusion measurements on novicidin were recorded with novicidin (2 mM), DPC-d_{38} (90 mM), phosphate buffer (10 mM), and sodium azide (0.05%) dissolved in D_2O (100%) at pH 6, and also on an otherwise identical sample without [D_{38}]DPC. The diffusion constants were also measured on a sample containing only DPC (90 mM), phosphate buffer (10 mM), and sodium azide (0.05%) dissolved in D_2O (100%) at pH 6. Diffusion coefficients were determined by use of a double stimulated echo pulse sequence.[41] A total of 32 spectra were recorded, with increasing gradient strengths ranging from 7.1 to 40 G cm^{-1}. Novicidin or DPC signals were integrated at each gradient strength and diffusion constants were obtained by fitting to Equation (4) by use of Bruker TopSpin version 1.3.

$$I = I_0 \exp(-D_t(2\pi\gamma\delta G)^2 \times (\Delta - \delta/3) \times 10^4) \qquad (4)$$

with $\delta = 4$ ms, $\Delta = 140$ ms, and G being the gradient strength.[42]

Molecular dynamics simulations: The initial DPC micelle coordinates were taken from the homepage of Professor Peter Tieleman at the University of Calgary (http://moose.bio.ucalgary.ca).[30] The micelle was put into an 88×80×80 nm-sized box, extending 2 nm from the micelle along all three axes. The box was filled with 19405 TIP3P water, and sodium ions were iteratively placed at the coordinates with the lowest electrostatic potential by the YASARA MD protocol.[43] Simulation temperatures were 310 K, water densities 1003 g L^{-1}, and the pH was 6. The van der Waals pairs cutoff distance was 7.86 Å and particle mesh Ewald (PME) long-range electrostatics were employed.[44] The time steps chosen were 1.25 fs for bond, angle, dihedral, and planarity forces and 2.5 fs for the intermolecular forces. Simulations were started with a steepest descent minimization (until atom speed < 2200 m s^{-1}), followed by 500 steps of simulated annealing of the solvent to equilibrate the system. MD simulations were conducted with YASARA 8.9.11[43] with use of the YASARA MD protocol and the AMBER99 forcefield[45] at constant pressure (NPT ensemble). The MD simulations ran for 3.345 ns with a snapshot taken every 7.5 fs; this gave 446 micelle states. During the first ns the micelle expanded slightly, so this part of the simulation was considered an equilibration phase and these snapshots were discarded for the subsequent calculations.

Acknowledgements

[1] C. Fernández, C. Hilty, G. Wider, K. Wüthrich, *Proc. Natl. Acad. Sci. USA* **2002**, *99*, 13533–13537.

[2] E. E. Matthews, M. Zoonens, D. M. Engelman, *Cell* **2006**, *127*, 447–450; J. A. Whiles, R. Deems, R. R. Vold, E. A. Dennis, *Bioorg. Chem.* **2002**, *31*, 431–442; A. Arora, L. K. Tamm, *Curr. Opin. Struct. Biol.* **2001**, *11*, 540–547.

[3] C. R. Sanders, 2nd, G. C. Landis, *Biochemistry* **1995**, *34*, 4030–4040.

[4] R. R. Vold, R. S. Prosser, A. J. Deese, *J. Biomol. NMR* **1997**, *9*, 329–335; D. A. Kallick, M. R. Tessmer, C. R. Watts, C. Y. Li, *J. Magn. Reson. Ser. B* **1995**, *109*, 60–65.

[5] M. Zasloff, *Nature* **2002**, *415*, 389–395; K. A. Brogden, *Nat. Rev. Microbiol.* **2005**, *3*, 238–250; Y. Shai, A. Makovitzky, D. Avrahami, *Curr. Protein Pept. Sci.* **2006**, *7*, 479–486.

[6] Y. Shai, *Biochim. Biophys. Acta Biomembr.* **1999**, *1462*, 55–70; L. Yang, T. M. Weiss, T. A. Harroun, W. T. Heller, H. W. Huang, *Biophys. J.* **1999**, *77*, 2648–2656; K. Matsuzaki, *Biochim. Biophys. Acta Biomembr.* **1999**, *1462*, 1–10.

[7] L. J. Lis, S. C. Goheen, J. W. Kauffman, D. F. Shriver, *Biochim. Biophys. Acta Nucleic Acids Protein Synth.* **1976**, *443*, 331–338; W. K. Surewicz, H. H. Mantsch, *Biochem. Biophys. Res. Commun.* **1988**, *150*, 245–251; N. V. Strashnikova, N. Medvedeva, G. I. Likhtenshtein, *J. Biochem. Biophys. Methods* **2001**, *48*, 43–60; Y. Wu, H. W. Huang, G. A. Olah, *Biophys. J.* **1990**, *57*, 797–806.

[8] H. Khandelia, Y. N. Kaznessis, *J. Phys. Chem. B* **2005**, *109*, 12990–12996; S. K. Kandasamy, R. G. Larson, *Chem. Phys. Lipids* **2004**, *132*, 113–132; F. Dancea, K. Kami, M. Overduin, *Biophys. J.* **2008**, *94*, 515–524.

[9] M. A. Lomize, A. L. Lomize, I. D. Pogozheva, H. I. Mosberg, *Bioinformatics* **2006**, *22*, 623–625.

[10] C. Altenbach, T. Marti, H. G. Khorana, W. L. Hubbell, *Science* **1990**, *248*, 1088–1092.

[11] B. Bechinger, L. M. Gierasch, M. Montal, M. Zasloff, S. J. Opella, *Solid State Nucl. Magn. Reson.* **1996**, *7*, 185–191; F. M. Marassi, A. Ramamoorthy, S. J. Opella, *Proc. Natl. Acad. Sci. USA* **1997**, *94*, 8551–8556.

[12] H. Matsuo, H. Li, A. M. McGuire, C. M. Fletcher, A. C. Gingras, N. Sonenberg, G. Wagner, *Nat. Struct. Biol.* **1997**, *4*, 717–724.

[13] J. L. Battiste, G. Wagner, *Biochemistry* **2000**, *39*, 5355–5365; K. Bhargava, J. B. Feix, *Biophys. J.* **2004**, *86*, 329–336.

[14] R. S. Prosser, P. A. Luchette, P. W. Westerman, *Proc. Natl. Acad. Sci. USA* **2000**, *97*, 9967–9971; F. Evanics, P. M. Hwang, Y. Cheng, L. E. Kay, R. S. Prosser, *J. Am. Chem. Soc.* **2006**, *128*, 8256–8264.

[15] M. Lindberg, A. Graslund, *FEBS Lett.* **2001**, *497*, 39–44.

[16] R. Wimmer, K. K. Andersen, B. Vad, M. Davidsen, S. Molgaard, L. W. Nesgaard, H. H. Kristensen, D. E. Otzen, *Biochemistry* **2006**, *45*, 481–497.

[17] J. J. Chou, J. D. Kaufman, S. J. Stahl, P. T. Wingfield, A. Bax, *J. Am. Chem. Soc.* **2002**, *124*, 2450–2451; M. F. Mesleh, S. J. Opella, *J. Magn. Reson.* **2003**, *163*, 288–299; M. F. Mesleh, G. Veglia, T. M. DeSilva, F. M. Marassi, S. J. Opella, *J. Am. Chem. Soc.* **2002**, *124*, 4206–4207.

[18] A. M. Petros, L. Mueller, K. D. Kopple, *Biochemistry* **1990**, *29*, 10041–10048; G. L. Jendrasiak, R. L. Smith, A. A. Ribeiro, *Phys. Med. Biol.* **2000**, *45*, 3109–3122; T. I. Smirnova, A. I. Smirnov, R. L. Belford, R. B. Clarkson, G. L. Jendrasiak, R. L. Smith, A. A. Ribeiro, *Acta Chem. Scand.* **1997**, *51*, 562–566.

[19] G. Pintacuda, G. Otting, *J. Am. Chem. Soc.* **2002**, *124*, 372–373.

[20] A. Bernini, V. Venditti, O. Spiga, A. Ciutti, F. Prischi, R. Consonni, L. Zetta, I. Arosio, P. Fusi, A. Guagliardi, N. Niccolai, *Biophys. Chem.* **2008**, *137*, 71–75; J. Dittmer, L. Thogersen, J. Underhaug, K. Bertelsen, T. Vosegaard, J. M. Pedersen, B. Schiott, E. Tajkhorshid, T. Skrydstrup, N. C. Nielsen, *J. Phys. Chem. A* **2009**, *113*, 6928–6937; V. Venditti, A. Bernini, A. De

Simone, O. Spiga, F. Prischi, N. Niccolai, *Biochem. Biophys. Res. Commun.* **2007**, *356*, 114–117.

[21] M. Respondek, T. Madl, C. Gobl, R. Golser, K. Zangger, *J. Am. Chem. Soc.* **2007**, *129*, 5228–5234.

[22] M. Botta, *Eur. J. Inorg. Chem.* **2000**, *2000*, 399–407.

[23] I. Bertini, C. Luchinat, G. Parigi, *Elsevier Science* **2001**; D. Kruk, J. Kowalewski, I. Bertini, G. Cavallaro, M. Cosenza, R. Kummerle, C. Luchinat, M. Piccioli, L. Poggi, L. Banci, I. Bertini, G. Cavallaro, A. Giachetti, C. Luchinat, G. Parigi, *J. Chem. Phys.* **2009**, *130*, 174104.

[24] Z. Luz, S. Meiboom, *J. Chem. Phys.* **1964**, *40*, 2686–2692; Z. Luz, S. Meiboom, *J. Chem. Phys.* **1964**, *40*, 1058–1066.

[25] K. Zangger, M. Respondek, C. Gobl, W. Hohlweg, K. Rasmussen, G. Grampp, T. Madl, *J. Phys. Chem. B* **2009**, *113*, 4400–4406.

[26] I. Solomon, *Phys. Rev.* **1955**, *99*, 559–565.

[27] J. Lauterwein, C. Bosch, L. R. Brown, K. Wüthrich, *Biochim. Biophys. Acta Biomembr.* **1979**, *556*, 244–264.

[28] M. V. Sawai, A. J. Waring, W. R. Kearney, P. B. McCray, Jr., W. R. Forsyth, R. I. Lehrer, B. F. Tack, *Protein Eng.* **2002**, *15*, 225–232; V. C. Kalfa, H. P. Jia, R. A. Kunkle, P. B. McCray, Jr., B. F. Tack, K. A. Brogden, *Antimicrob. Agents Chemother.* **2001**, *45*, 3256–3261.

[29] K. Zangger, M. Respondek, C. Gobl, W. Hohlweg, K. Rasmussen, G. Grampp, T. Madl, *J. Phys. Chem. B* **2009**.

[30] D. P. Tieleman, D. van der Spoel, H. J. C. Berendsen, *J. Phys. Chem. B* **2000**, *104*, 6380–6388.

[31] S. Marrink, D. Tieleman, A. Mark, *J. Phys. Chem. B* **2000**, *104*, 12165–12173.

[32] L. Banci, I. Bertini, G. Cavallaro, A. Giachetti, C. Luchinat, G. Parigi, *J. Biomol. NMR* **2004**, *28*, 249–261; L. Banci, I. Bertini, M. A. Cremonini, G. Gori-Savellini, C. Luchinat, K. Wüthrich, P. Güntert, *J. Biomol. NMR* **1998**, *12*, 553–557; I. Bertini, G. Cavallaro, M. Cosenza, R. Kummerle, C. Luchi-nat, M. Piccioli, L. Poggi, L. Banci, I. Bertini, G. Cavallaro, A. Giachetti, C. Luchinat, G. Parigi, *J. Biomol. NMR* **2002**, *23*, 115–125.

[33] M. Piotto, V. Saudek, V. Sklenár, *J. Biomol. NMR* **1992**, *2*, 661–665.

[34] C. Griesinger, G. Otting, K. Wuethrich, R. Ernst, *J. Am. Chem. Soc.* **1988**, *110*, 7870–7872.

[35] "Optimizing the Process of Nuclear Magnetic Resonance Spectrum Analysis and Computer Aided Resonance Assignment", R. Keller, obtained from the website http://www.nmr.ch.

[36] C. Bartels, T. Xia, M. Billeter, P. Güntert, K. Wüthrich, *J. Biomol. NMR* **1995**, *6*, 1–10.

[37] G. Cornilescu, F. Delaglio, A. Bax, *J. Biomol. NMR* **1999**, *13*, 289–302.

[38] P. Guntert, W. Braun, K. Wüthrich, *J. Mol. Biol.* **1991**, *217*, 517–530.

[39] P. Guntert, C. Mumenthaler, K. Wüthrich, *J. Mol. Biol.* **1997**, *273*, 283–298.

[40] W. L. DeLano, The PyMOL Molecular Graphics System, http://www.pymol.org **2002**.

[41] A. Jerschow, N. Müller, *J. Magn. Reson.* **1997**, *125*, 372–375; A. Jerschow, N. Müller, *J. Magn. Reson.* **1998**, *132*, 13–18; K. Wüthrich, *NMR of Proteins and Nucleic Acids*, Wiley, New York, **1986**.

[42] E. O. Stejskal, J. E. Tanner, *J. Chem. Phys.* **1965**, *42*, 288–292.

[43] E. Krieger, T. Darden, S. B. Nabuurs, A. Finkelstein, G. Vriend, *Proteins Struct. Funct. Bioinf.* **2004**, *57*, 678–683.

[44] U. Essman, L. Perera, M. Berkowitz, T. Darden, H. Lee, L. Pedersen, *J. Chem. Phys.* **1995**, *103*, 8577–8593.

[45] J. Wang, P. Cieplak, P. A. Kollman, *J. Comput. Chem.* **2000**, *21*, 1049–1074.

CHEMBIOCHEM

Supporting Information

Supporting Information

for

Quantitative Use of Paramagnetic Relaxation Enhancements for Determining Orientation and Insertion Depth of Peptides in Micelles

Magnus Franzmann, Daniel Otzen, and Reinhard Wimmer*

Table S1. Novicidin PRE values.

Residue number	PRE [s^{-1}mM^{-1}]	Dist. to micelle center [Å]	Dist standard diviation [Å]	Lower distance restraints [Å]	Upper distance restraints [Å]
2	0.75	23.54	0.57	22.96	24.11
3	0.10	16.97	1.15	15.82	18.12
4	0.09	15.68	2.35	13.33	18.03
5	0.27	20.69	0.65	20.04	21.33
6	0.09	16.13	0.66	15.47	16.79
7	0.04	11.73	0.61	11.12	12.34
8	0.09	16.41	1.54	14.87	17.95
9	0.18	19.05	1.60	17.45	20.64
10(2HA)	0.05	13.89	0.98	12.91	14.87
10(3HA)	0.02	6.83	0.98	5.86	7.81
11	0.04	11.69	0.98	10.72	12.67
12	0.21	19.80	0.26	19.54	20.06
13	0.10	16.76	0.47	16.29	17.23
14	0.06	14.60	0.95	13.64	15.55
15	0.09	16.05	1.43	14.62	17.49
16	0.54	22.49	1.29	21.20	23.78
17	0.19	19.48	0.16	19.32	19.63
18	0.14	18.29	0.98	17.31	19.27

Average values of PRE values from multiple H$^{\alpha}$ peaks and average calculated distances between the H$^{\alpha}$ atoms and the center of the micelle. As only one distance has been obtained from residue 10(2HA), 10(3HA), 11 and 18 an average of the remaining standard deviations have been used.

Table S2. Novispirin PRE values.

Residue number	PRE [s^{-1}mM^{-1}]	Dist. to micelle center [Å]	Dist standard diviation [Å]	Lower distance restraints [Å]	Upper distance restraints [Å]
2	0.72	23.47	1.06	22.41	24.53
3	0.098	16.82	0.01	16.81	16.83
4	0.14	18.45	1.06	17.39	19.51
5	0.29	20.93	1.06	19.87	21.99
6	0.09	16.25	1.61	14.63	17.86
7	0.05	13.51	1.06	12.45	14.56
8	0.13	17.95	0.61	17.34	18.56
9	0.20	19.45	1.42	18.04	20.87
10(2HA)	0.076	15.59	1.06	14.53	16.65
10(3HA)	0.064	14.73	1.06	13.67	15.79
11	0.11	17.22	1.06	16.16	18.28
12	0.25	20.20	1.49	18.71	21.69
13	0.11	17.25	1.06	16.19	18.31
14	0.098	16.68	1.17	15.51	17.85
15	0.20	19.66	1.06	18.60	20.72
16	0.29	20.91	1.00	19.91	21.91
17	0.46	22.15	1.16	20.99	23.31
18(2HA)	0.41	22.01	1.06	20.95	23.07
18(3HA)	0.33	21.37	1.06	20.31	22.43

Average values of PRE values from multiple H$^{\alpha}$ peaks and average calculated distances between the H$^{\alpha}$ atoms and the center of the micelle. As only one distance has been obtained from residue 2, 4, 5, 7, 10(2HA), 10(3HA), 11, 13, 15, 18(2HA), 18(3HA) an average of the remaining standard deviations have been used.

Paper II

Co-author statement for Paper II

Brian Vad., Line Aagot Thomsen, Jan Mondrup Pedersen, Kresten Bertelsen, Thomas Vosegaard, Zuzana Valnickova, Magnus Franzmann, Reinhard Wimmer, Troels Skrydstrup, Jan J. Enghild, Niels Chr. Nielsen, Daniel Otzen .: **Divorcing Folding from Function: How Acylation Affects the Membrane-perturbing Properties of an Anti-microbial Peptide**

Biochim Biophys Acta. 2010 Apr;1804(4):806-20. Epub 2009 Dec 22.

- Brian Vad performed all liposome calcein release work, Stopped flow fluorescence, Confocal Laser microscopy, Circular dichroism, fluorescence anisotropy measurements and wrote the bulk of the article
- Kresten Bertelsen performed, described and discussed the Solid state NMR experiments under supervision of Thomas Vosegaard and Niels Chr. Nielsen.
- Line Aagot Thomsen did preliminary purification and characterization of Novicidin.
- Magnus Franzmann did the solution state NMR and wrote the associated part of the article under the supervision of Reinhard Wimmer
- Jan Mondrup Pedersen performed the peptide synthesis under the supervision of Troels Skrydstrup.
- Zuzana Valnickova performed the β-galactosidase assay under the supervision of Jan Enghild.
- Niels Nielsen contributed to the interpretation of NMR data and writing of the article.
- Daniel Otzen supervised overall design and execution of the experiments, contributed extensively to the writing of the article and submitted the article.
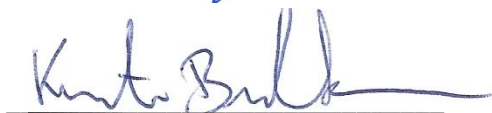
Jan Mondrup Pedersen   _____

Line Aagot Thomsen   _____

Kresten Bertelsen   _____

Thomas Vosegaard   _____

Zuzana Valnickova   _____

Reinhard Wimmer   _____

Jan J. Enghild

Niels Chr. Nielsen
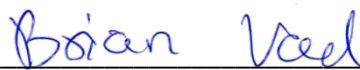
Daniel Otzen

Brian Stougaard Vad

Divorcing folding from function: How acylation affects the membrane-perturbing properties of an antimicrobial peptide

Brian Vad [a,b], Line Aagot Thomsen [b], Kresten Bertelsen [c], Magnus Franzmann [b], Jan Mondrup Pedersen [c], Søren B. Nielsen [a,d], Thomas Vosegaard [c], Zuzana Valnickova [a], Troels Skrydstrup [c], Jan J. Enghild [a], Reinhard Wimmer [b], Niels Chr. Nielsen [c,*], Daniel E. Otzen [a,b,*]

[a] Center for Insoluble Protein Structures (inSPIN), Interdisciplinary Nanoscience Center (iNANO) and Department of Molecular Biology, Gustav Wieds Vej 10C, University of Aarhus, DK – 8000 Aarhus C, Denmark
[b] Department of Biotechnology, Chemistry and Environmental Engineering, Aalborg University, Sohngaardsholmsvej 49, DK – 9000 Aalborg, Denmark
[c] Center for Insoluble Protein Structures (inSPIN), Interdisciplinary Nanoscience Center (iNANO) and Department of Chemistry, Langelandsgade 140, University of Aarhus, DK – 8000 Aarhus C, Denmark
[d] Department of Food Science, Faculty of Agricultural Sciences, University of Aarhus, Blichers Allé, DK – 8830 Tjele, Denmark

ARTICLE INFO

ABSTRACT

Many small cationic peptides, which are unstructured in aqueous solution, have antimicrobial properties. These properties are assumed to be linked to their ability to permeabilize bacterial membranes, accompanied by the transition to an α-helical folding state. Here we show that there is no direct link between folding of the antimicrobial peptide Novicidin (Nc) and its membrane permeabilization. N-terminal acylation with C8–C16 alkyl chains and the inclusion of anionic lipids both increase Nc's ability to form α-helical structure in the presence of vesicles. Nevertheless, both acylation and anionic lipids reduce the extent of permeabilization of these vesicles and lead to slower permeabilization kinetics. Furthermore, acylation significantly decreases antimicrobial activity. Although acyl chains of increasing length also increase the tendency of the peptides to aggregate in solution, this cannot rationalize our results since permeabilization and antimicrobial activities are observed well below concentrations where aggregation occurs. This suggests that significant induction of α-helical structure is not a prerequisite for membrane perturbation in this class of antimicrobial peptides. Our data suggests that for Nc, induction of α-helical structure may inhibit rather than facilitate membrane disruption, and that a more peripheral interaction may be the most efficient permeabilization mechanism. Furthermore, acylation leads to a deeper embedding in the membrane, which could lead to an anti-permeabilizing "plugging" effect.

© 2009 Elsevier B.V. All rights reserved.

1. Introduction

Over the past two decades, more than 800 antimicrobial peptides (AMPs) have been reported from sources as diverse as animals, plants, insects, and fungi [1–4]. As parts of the innate immune system in vertebrates, AMPs are often the first line of defence against an invading organism, and thus show activity against a broad range of targets. Microorganisms do not easily evolve resistance to them, making them of great interest as alternatives to small-molecule

antibiotics. Over the recent few years significant resources have been directed towards their commercialization. So far, only a few products have succeeded, while several promising candidates have been halted because of adverse effects or effects similar to existing antibiotics [5]. The lack of success most likely reflects limited understanding of their mechanism of action and microbial specificity. At present the common procedure is to search for naturally occurring AMPs and then subsequently mutate them to change their specificity [6–10]. More detailed insight into AMP activity may ultimately allow design *in silico* [11].

Many AMPs are understood to target the bacterial plasma membrane directly rather than through receptors (though there are a growing number of exceptions such as lantibiotic peptides that target lipids in the bacterial septum and thus inhibit cell division [12] and defensins with viral targets [13]). They do so in a variety of ways, including a barrel-stave model, a carpet model, and a toroidal-pore model [14]. In the barrel-stave model, the peptides completely traverse the membrane by pore formation, quickly ruining the

electrochemical gradient and killing the cell [15]. This mode of action is mostly driven by hydrophobic interactions between an amphipathic peptide and the lipid's acyl chains and is therefore less specific towards membranes of different lipid compositions [15]. A minimum of 22 and 8 amino acids is necessary to straddle the bacterial membrane for an α-helical- and a β-sheet peptide, respectively. In the carpet model, the positively charged peptides cover the membrane surface in a carpet-like fashion until they reach a concentration where they permeabilize the cell by disrupting the membrane curvature [16]. As opposed to the barrel-stave model, the peptide does not need to assume a specific oligomeric structure and the peptides are always in contact with the lipid headgroups at the interface with the acyl chains. This mode of action is more sensitive to the lipid headgroup charge, explaining why it is more specific towards the negatively charged surface of bacteria [17–19]. Finally, the toroidal-pore model is a mixture between the carpet model and the barrel-stave model. Defined pores are formed as in the barrel-stave model but the peptides lie in the lipid headgroup-acyl chain interface. This is possible because the peptides induce a sharp bending of the lipids so that lipid headgroups can line the interior of the pore.

It may be possible to modulate the mode of antimicrobial action, and thus the spectrum of applications, by modifying the AMPs with acyl chains, since this modification will increase AMP hydrophobicity and potentially also its membrane affinity. This has been studied in two different approaches: Makovitzki et al. [20] synthesized tetra-peptides with acyl chains of length 8–16 (number carbons in the acyl chain) and found that the tetrapeptides conferred bacterial species specificity while their aggressiveness correlated with acyl chain length. The same group also showed that conjugation of the AMP magainin with acyl chains of length 7, 11, and 16 had important effects on magainin activity, with the membrane permeabilizing ability increasing uniformly with chain length [21]. Furthermore, the attachment of the acyl chains also resulted in a change of the secondary structure of magainin-C11 and magainin-C16 (magainin with acyl chains of lengths 11 and 16, respectively) in solution from that of the wildtype magainin. While magainin-C7, like the wild type, was disordered and monomeric in solution, both magainin-C11 and magainin-C16 adopted α-helical structure. Magainin-C11 was only α-helical above a threshold concentration indicating detergent-like properties in which the protein assumed an α-helical structure in the micellar state. In contrast, magainin-C16 remained α-helical at all investigated concentrations, suggesting that the longer acyl chain was able to sequester the hydrophobic residues in the folded magainin at the monomer level. C-terminal modification with biotin through a single or tandemly coupled caproyl group had no significant effect on gramidicin structure or function [22], and modification with a palmitoyl only group slightly reduces the gramicidin's lipid-perturbing properties, consistent with the peptide's high tendency to associate with the lipid even in the unacylated form [23].

For non-acylated peptides that are unstructured in solution, membrane binding is generally accompanied by the formation of α-helical structure in order to satisfy hydrogen-bonding requirements in a less hydrophilic environment [24]. One might therefore expect that membrane-binding properties and thus antimicrobial properties should correlate with the ability to form α-helical structures in a membrane environment. However, it has been shown for designed antimicrobial peptides composed of a mixture of α- and β-amino acids [25] (but not for peptides containing β-amino acids alone [26]) that there is no correlation between helical propensity and antimicrobial activity.

To explore in greater detail how acylation can modulate membrane-binding properties, and whether helical propensities of peptides with α-amino acids correlate with membrane permeabilization, we report here a detailed study on the effect of acylation on the AMP Novicidin (Nc) [7,27–30]. This AMP is a variant of the 18-residue Ovispirin, which in turn is derived from the N-terminal region of the cathelicidin

peptide SMAP-29 from sheep. Ovispirin showed unacceptably high haemolytic activity, but the mutation Ile10→Gly (Novispirin) reduced this to more appropriate levels. Subsequently, the C-terminal mutation Gly18→Phe (giving the peptide Novicidin, abbreviated Nc, sequence KNLRR IIRKG IHIIK KYF) led to improved efficacy towards microorganisms (personal communication, Hans Henrik Kristensen). Novispirin and Nc are unstructured in solution but readily adopt α-helical structures in the presence of anionic lipids and detergents, as well as to a smaller extent in the presence of cationic and zwitterionic detergents [31], in agreement with its amphipathic character (Fig. 1A). We focus on the structural and vesicle-disruptive properties of Nc (denoted Nc wt in its unmodified form), its N-terminally acylated derivatives and a Dansyl-labelled version of Nc. Surprisingly, we find that the induction of measurable amounts of α-helical structure is not a prerequisite for membrane permeabilizing properties and that acylation actually reduces permeabilization efficiency. We suggest that a more peripheral membrane contact may be the most productive mode of action for at least some AMPs.

2. Materials and methods

2.1. Chemicals

DMPC (1,2-di-myristoyl-sn-glycero-3-phosphocholine), DHPC (1,2-di-hexanoyl-sn-glycero-3-phosphocholine), DMPG (1,2-di-myr-istoyl-sn-glycero-3-[phospho-rac-(1-glycerol)]), DOPC (1,2-di-oleoyl-sn-glycero-3-phosphocholine) and DOPG (1,2-di-oleoyl-sn-glycero-3-[phospho-rac-(1-glycerol)]) were from Avanti Polar Lipids (Alabaster, AL). Protected amino acids, 1,2-ethane dithiole (EDT), triisopropylsylane (TIPS), di-chloromethane (DCM), dimethylforma-mide (DMF), N,N-diisopropylethylamine (DIPEA), 1H-benzotriazolyl)-1,1,3,3-tetramethyl-uronium hexafluorophosphate (HBTU), octanoic, dodecanoic- and hexadecanoic acid, and O-(7-azabenzotriazol-1-yl)-N, N,N′,N′-tetramethyl-uronium hexafluorophosphate (HATU) were from Iris Biotech (Marktredwitz, Germany). Acetonitrile chromasolv gradient grade, trifluoroacetic acid (TFA), sucrose 99.5% purity and D (+) glucose 99.5% purity were from Sigma (St. Louis, MO). DiIC18(3), Alexa-488 hydrazide (Alexa[488]), Alexa-633 hydrazide (Alexa[633]) and BL21(DE3) were from Invitrogen (Carlsbad, California). Calcein disodium salt was from Fluka (Buchs, Switzerland). Deuterated dodecylphosphocholine (DPC-d[38]) was from Cambridge Isotope Laboratories Inc. (Andover, MA). Gd-(DTPA-BMA) was generously provided by Klaus Zangger. Recombinant Nc wt peptide (prepared as described [31] and used for all experiments that involved non-derivatized Nc) was generously provided by Dr. Hans Henrik Kristensen.

2.2. Peptide synthesis, acylation and purification

Synthesis of the acylated Nc peptides was carried out in two steps. Firstly, the 18-residue Nc peptide was synthesized on an automatic CEM liberty microwave assisted peptide synthesizer (Matthews, North Carolina) by solid-phase synthesis using standard Fmoc chemistry on Wang resin. Secondly, the fatty acid was attached to the N-terminus of the resin-bound peptide also using Fmoc chemistry. To prepare dansyl-Nc, Nc was manually acylated with the dansyl moiety. Further synthesis and purification details are provided in the Supplementary information.

2.2.1. Preparation of LUV liposomes
LUVs (large unilamellar vesicles) containing calcein were prepared from stock solutions of lipids dissolved in methanol and dried overnight in a Heto VR-1 centrifuge vacuum drier. Lipids were then resuspended by vortexing in 20 mM Tris HCl, pH 7.5 containing 40 mM calcein sodium salt, to a final concentration of 10 g/l (~14 mM), exposed to at least seven cycles of freezing in liquid nitrogen, followed by thawing in a 50 °C water bath, before extrusion through a 200 nm
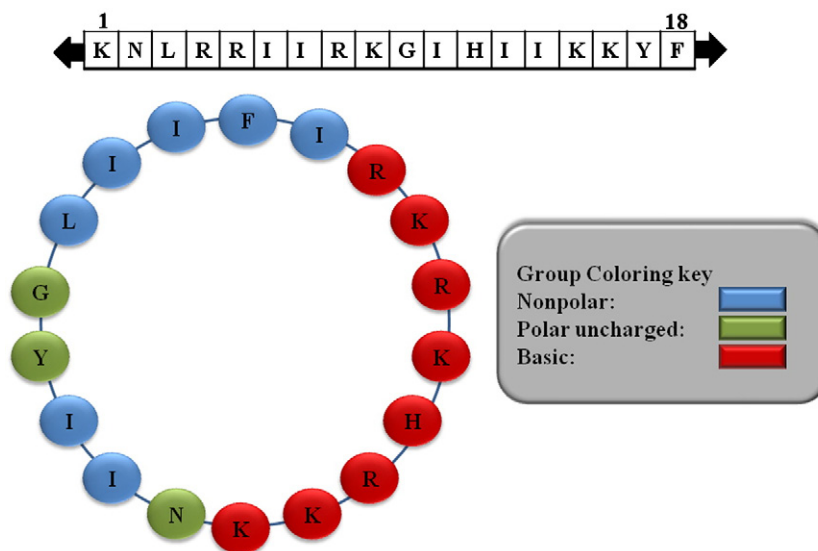
Fig. 1. Sequence of Novicidin and a helical projection highlighting its amphipathic character.

pore filter 12 times using a 10 ml thermo barrel extruder (Northern Lipids, Vancouver, Canada). The lipid solutions were run on a PD10 column pre-equilibrated with 20 mM Tris HCl, pH 7.5. Eluent fractions were gathered and tested by fluorescence measurements with and without the addition of Triton X-100 to test for calcein release. Those with the highest signal-to-background ratio were selected for further use. All extruded vesicles were used on the same day that they were made.

2.2.2. GUV liposomes and laser confocal microscopy measurements

GUVs (giant unilamellar vesicles) were prepared by the electro-formation method originally described by Angelova and Dimitrov [32] and observed with a LSM 510 scanning confocal microscope (Zeiss GmbH, Jena, Germany). Further details are provided in the Supplementary information.

2.3. Manual calcein release assay

All fluorescence measurements were conducted on an LS55 fluorimeter essentially as described [33]. Further details are provided in the Supplementary information.

2.4. Stopped-flow measurements

Kinetic experiments were carried out on an Applied Photophysics SX-18MV reaction analyzer (Applied Photophysics, Leatherhead, Surrey) in fluorescence detection mode. For the calcein release measurements, the solution was excited at 490 nm and a 510-nm glass filter was used to measure emission intensity. The calcein vesicles and peptides were mixed in 10:1 volume ratio and at least three measurements were averaged for each concentration. Final concentrations of lipid were around 50 μM while final peptide concentrations varied from 0.2 μM to 72 μM. In measurements using Dansyl-Nc, the samples were excited at 335 nm and a 530-nm glass filter was used. The lipid concentration was held constant at 20 μM while the peptide concentration was varied from 1 to 10 μM.

2.5. Secondary structural changes measured by CD spectroscopy

Circular dichroism studies were performed on a Jasco J-810 spectropolarimeter (Jasco Spectroscopic Co., Hachioji City, Japan) with a Jasco PTC-348W1 temperature control unit. Scan speed was set to 100 nm/min, slit width 2 nm. All experiments were carried out in 20 mM Tris–HCl pH 7.5, at 25 °C using a 1 mm quartz cuvette. The measurements were conducted as one-pot titrations with an initial peptide concentration of 200 μM and stepwise addition of lipids. After the addition of each new lipid aliquot, the sample was allowed to equilibrate for at least 1 min before a spectrum was recorded. Samples at each concentration were measured in three scans and averaged to yield the final spectrum. Background spectra without peptide were subtracted and the CD signal was corrected for dilution.

2.6. Differential scanning calorimetry (DSC)

LUVs for use in DSC experiments were prepared by dissolving and mixing appropriate amounts of DMPC and DMPG yielding pure DMPC and 80:20 w/w% DMPC:DMPG in 1:1 chloroform:methanol, respectively. 10 mg lipid was transferred to a glass vial and solvent was removed under a stream of nitrogen gas followed overnight incubation in a vacuum desiccator ($p < 60$ mbar) to remove trace amounts of solvent. Lipids were rehydrated in 10 mM sodium phosphate pH 8.0 to produce a 10 mg/ml lipid solution and LUVs were subsequently formed by extrusion through 100-nm polycarbonate filter by 15 passages through a MiniExtruder (Avanti Polar Lipids, Alabaster, CA). The phase behavior of LVUs was studied using a Microcal VP-DSC scanning microcalorimeter (Northampton, MA, USA). Samples were prepared by mixing peptide and buffer in appropriate ratios followed by addition of pre-formed LUVs to obtain a lipid concentration of 1 mg/ml and varying peptide content from pure lipid to 1:20 Nc:lipid (molar ratios). Heating and cooling scans were performed between 5 and 45 °C at a scan rate of 60 °C/h and prescan thermal equilibration for 15 min using 10 mM sodium phosphate buffer pH 8.0 as the reference sample. The high feedback mode was used to ensure correct recording of sharp peaks. The DSC cell was pressurized to ~30 psi throughout the experiment.

2.7. Peptide lipid binding measured by fluorescence anisotropy

The excitation was set to 335 nm and emission was measured at 515 nm in a 200 μl Hellma quartz cuvette. Slit width was set to 7.5 nm for both the vertical and horizontal filters. For each sample the G-Factor was measured before measuring the anisotropy. Dansyl-Nc concentration was held constant at 25 μM and increasing amounts of lipid was added. The samples were mixed by pipetting and allowed to equilibrate for 2 min before measuring anisotropy.

2.8. Interaction of Nc variants with E. coli cells

Cell permeabilization assays and minimal inhibitory concentration (MIC) assays were performed essentially as described [34,35] but with modifications described in the Supplementary information.

2.9. Solution-state NMR experiments

NMR samples containing 1 mM Nc-C16 or 2 mM Nc were dissolved in 90 mM DPC-d$_{38}$, 10 mM phosphate buffer, 0.05% sodium azide, 5% D$_2$O, pH 6 to a final volume of 500 μl. All NMR measurements were conducted at 37 °C on a Bruker DRX600 spectrometer (Bruker BioSpin, Rheinstetten, Germany) operating at a field strength of 14.1 T, equipped with a TXI(H/C/N) probe with triple-axis gradients. The PRE measurements of Nc-C16 were performed as previously described in detail [36]. Further details are provided in the Supplementary information.

2.10. Solid-state NMR

The NMR bicelle samples were made from DMPC, DHPC, and DMPG. All experiments were performed on a Bruker Avance 400 spectrometer operating at 9.4 T corresponding to 400 MHz for protons. Further details are provided in the Supplementary information.

3. Results

3.1. Interaction of Nc and acyl derivatives with lipids

We start by analyzing the degree to which zwitterionic (DOPC) and mixed, partially anionic (80DOPC:20DOPG) lipid vesicles induce structure in the different Nc variants. These vesicles were used as simple mimics of the mammalian plasma membrane (predominantly zwitterionic) and the outer leaflet of the bacterial cell membrane (at least 25% anionic lipid in E. coli). The secondary structure of Nc and the acylated derivatives (termed Nc-CX, where X refers to the number of carbon atoms in the acyl chain) was monitored by far-UV CD. Fig. 2A shows the CD spectra of Nc, Nc-C8, Nc-C12, and Nc-C16. Nc, Nc-C8, and low concentrations (40 μM) of Nc-C12 display CD spectra characteristic of a random coil. At high concentrations (200 μM), the CD spectrum of Nc-C12 changes to a distinct α-helical profile with minima at 209 and 222 nm. Nc wt and Nc-C8 remain unstructured at 200 μM (data not shown). The CD spectrum of Nc-C16 is primarily α-helical over the entire accessible concentration range (20–200 μM).

In the presence of 0–2 mg/ml DOPC, Nc shows only a slight change in its CD spectrum, retaining the features of a random coil structure (data not shown) though there is a small increase in ellipticity between 0 and 2 mg/ml lipid (Fig. 2B). This agrees with the observation that high (several hundred mM) concentrations of non-ionic and zwitterionic surfactant are required to induce helical structure in the closely related peptide Novispirin [31]. In contrast, Nc-C8 and Nc-C12 both change from random coil to α-helical structure with increasing concentrations of lipid over the range probed (the spectrum for Nc-C8 shown in Fig. 2A). In the presence of 80DOPC:20DOPG vesicles, the spectra of Nc, Nc-C8, and Nc-C12 changed dramatically from random coil to α-helix (representative spectra shown in Fig. 2A, summarized in Fig. 2C). The ellipticity at 208 nm, which is indicative of α-helical structure, shows a reasonably linear increase with lipid concentration, apart from a more hyperbolic behavior for Nc-C12 in DOPC (Fig. 2B). As we have previously reported for Novispirin [31], this slope most likely represents the initial linear stage of a hyperbolic binding curve, whose slope (summarized in Table 1) is directly proportional to the lipid binding affinity. To avoid artifacts from light scattering, we did not record data at higher lipid concentrations.

For both lipid compositions, Nc wt shows the lowest lipid affinity of all the peptides (measured in terms of α-helix induction), although
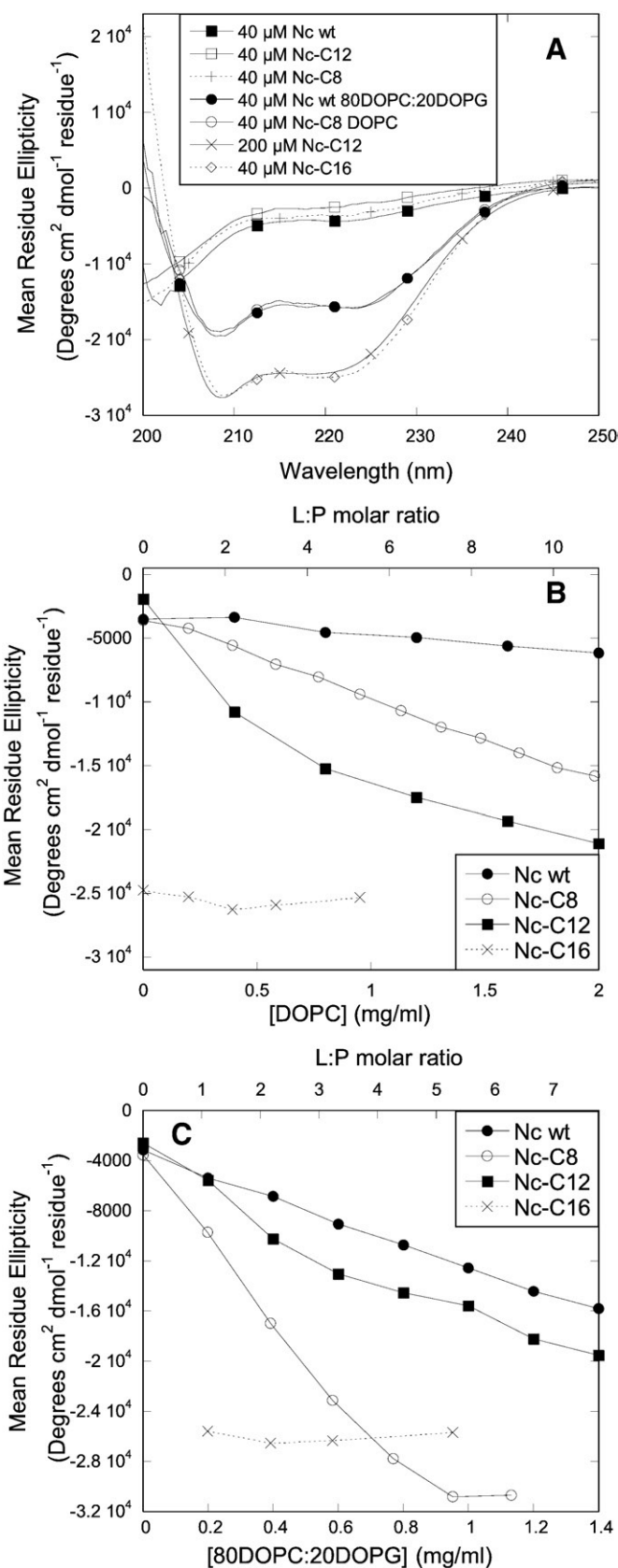
Fig. 2. (A) CD spectra of Nc and acylated derivatives in 20 mM Tris–Cl pH 7.5: 40 μM Nc wt, 40 μM Nc-C8, 40 μM Nc-C12, 200 μM Nc-C12, 40 μM Nc-C16, 40 μM Novicidin in 80DOPC:20DOPG vesicles and 40 μM Nc-C8 in pure DOPC vesicles. Development of CD spectra at 208 nm with the addition of increasing concentrations of (B) DOPC and (C) 80DOPC:20DOPG to Nc wt, Nc-C8, Nc-C12 and Nc-C16.

Table 1
Increase in ellipticity at 208 nm of Nc peptides as a function of lipid concentration (units of molar ellipticity per mg/ml lipid $\times 10^{-3}$).[a,b]

Peptide	DOPC	80DOPC:20DOPG
Nc wt	−1.21	−8.98
Nc-C8	−6.56	−29.56
Nc-C12	−8.84[c]	−11.87
Nc-C16	−0.58	−1.15

[a] All data carried out in 20 mM Tris–HCl pH 7.5 at 25 °C. Fits based on data shown in Fig. 2.
[b] These values are not actual affinity constants (since the ellipticity generally increases linearly and does not level off to a plateau level over the concentration range tested) but serve to illustrate the degree to which different lipids can increase the secondary structure of the Nc peptides over the experimentally accessible concentration range.
[c] Data have been fitted to a parabolic equation to derive the slope at zero molar lipid.

it has a clear preference for 80DOPC:20DOPG vesicles where the slope (corresponding to the binding affinity) is ~7 times higher. Nc-C12 has slightly greater affinity for DOPC than Nc-C8, but the switch to 80DOPC:20DOPG vesicles only increases Nc-C12 affinity by around 30% while that of Nc-C8 increases 5-fold. The CD spectra of Nc-C16 remained essentially unchanged by the addition of both lipid types. The reduced effect of anionic lipids likely reflects the increased propensity of the acylated peptides to form α-helical structures on their own (see Discussion).

3.2. Acylation leads to a marked decrease in the efficiency of lipid permeabilization

We now turn to a functional analysis of the Nc peptides, *i.e.* their ability to permeabilize vesicles, using a manual calcein release assay.
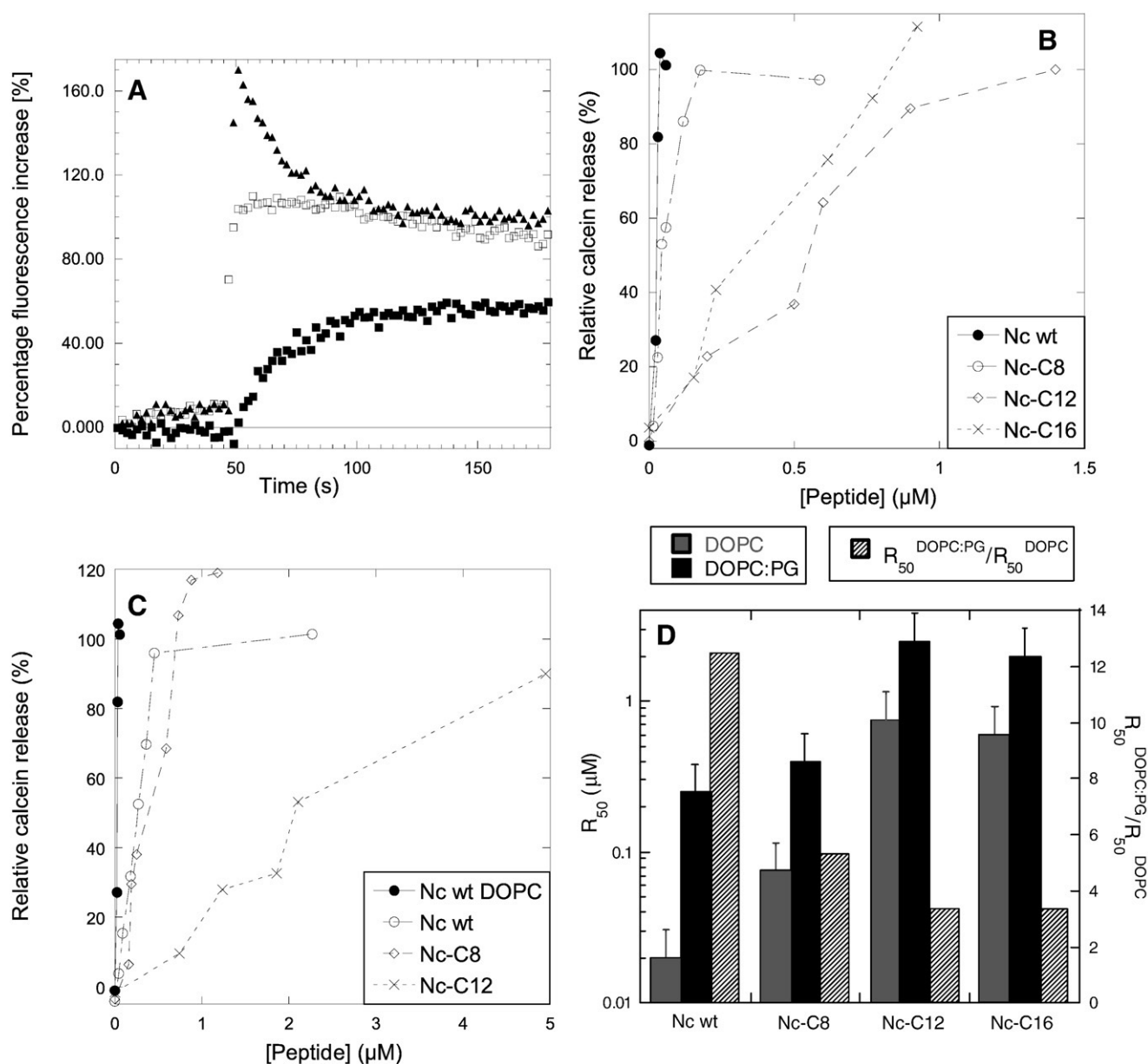
Fig. 3. (A) Typical time profile of calcein release by Nc and derivatives. Signal normalised relative to signal upon the addition of Triton X-100 (see Materials and methods). With the addition of Nc and acylated derivatives to calcein-loaded vesicles three distinct calcein release patterns are observed in steady-state fluorescence measurements. A slow release leading with the curve displaying second order characteristics (■), a fast release with a fluorescence increase between 0- and 100% (□), and finally a fast release with an overshoot which after ~1 min reach decreases to 100% (▲). Injection occurs in all cases at 50 s. (B and C) Nc and the acylated derivatives were added to calcein-loaded vesicles composed of (B) DOPC and (C) 80DOPC:20DOPG (data for Nc in DOPC included for comparison). The normalised maximum fluorescence was plotted as a function of protein concentration. (D) Peptide concentrations needed for 50% calcein release (R_{50}) from DOPC vesicles and 80DOPC:20DOPG vesicles and the ratio between these two values. Errors based on duplicate measurements.

We prepared LUVs containing calcein at a concentration (50 mM) in which calcein fluorescence is self-quenched, and measured the release of calcein as function of peptide concentration, using the addition of Triton X-100 to obtain the fluorescence level associated with 100% release. The presence of calcein did not affect the ability of lipids to induce structural changes in the peptides (data not shown), nor did Triton X-100 influence the fluorescence of calcein (data not shown).

Three distinct calcein release patterns were observed (Fig. 3A): (*i*) instantaneous (<10 s) calcein release, followed by a steady base-line (mainly seen for acylated Nc), (*ii*) relatively rapid release of calcein which could be described by first order kinetics with a plateau being reached after a few minutes (mainly seen for wt Nc), or (*iii*) rapid overshoot of fluorescence to a value well above that of free calcein, followed by a decrease to a signal corresponding to roughly 100% calcein release (seen at high concentrations of all 4 peptides)The fraction of calcein released as a function of peptide concentration in the two different lipid compositions is illustrated in Fig. 3B–C. The efficacy of release is quantified by the amount of peptide needed to effectuate 50% calcein release (R_{50}). In all cases, very high concentrations of peptide lead to a drop in calcein release (data not shown), possibly due to vesicle aggregation (*vide infra*).

The ranking order of the lipolytic effect of the peptides is as follows (summarized in Fig. 3D): Nc > Nc-C8 > Nc-C16 > Nc-C12. For all of the peptides, it was apparent that R_{50} increased in 80DOPC:20DOPG vesicles. The ratio $R_{50}^{DOPC:DOPG}/R_{50}^{DOPC}$ (the higher this ratio, the greater the preference for DOPC) decreased in the order Nc > Nc-C8 > Nc-C12 ~ Nc-C16, reaching a plateau of around 3 for Nc-C12 and Nc-C16. This indicates that the more hydrophobic the peptide, the lower the preference for DOPC vesicles. For Nc-C8 and Nc-C12 these permea-bilization data contrast with the structural data provided by CD, which reveal that acylation decreases the preference for 80DOPC:20DOPG vesicles in terms of inducing α-helicity.

3.3. Exposure of E. coli to Nc variants shows that acylation reduces the efficacy of Nc as an antimicrobial peptide

To compare the data on synthetic vesicles with Nc's biological targets, *i.e.* bacteria, we measured the lysis of *E. coli* at different concentrations of the Nc variants. Lysis was measured by the release of cytosolic β-galactosidase, monitored by the hydrolysis of the chromogenic substrate *o*-nitrophenyl galactose. All peptides lead to the same level of release at concentrations around 20–40 μM (Fig. 4A), but differ at lower concentrations. When we quantify this as [Nc-X]$^{50\%}$, the concentration of Nc at which release is 50% of the maximal value, we obtain a value of ~1 μM for Nc wt and values of 5–7 μM for all 3 acylated peptides. An even clearer picture emerges from MIC (minimal inhibitory concentration) assays (Fig. 4B), which reveal that Nc-C8 has a ~3-fold reduction in efficacy compared to Nc wt, while Nc-C12 and Nc-C16 hardly have any inhibitory effect at all. Thus, both in calcein assays and biological assays, unacylated Nc permeabilizes membranes more efficiently than acylated Nc. This membrane-lysing activity does not have any unwanted side effect, since hemolysis assays do not reveal any of the Nc peptides to have lytic activities against red blood cells at concentrations up to several mM (data not shown).

3.4. Fluorescence anisotropy measurements show that Nc mobility is decreased upon mixing with DOPC and 80DOPC:20DOPG vesicles

The calcein release measurements indicate that Nc binds to and permeabilizes both neutral and partially anionic vesicles, although CD titration data show that α-helical structure is only induced in the partially anionic vesicles. This suggests that induction of α-helix structure in peptides that are unstructured in solution is not a prerequisite for AMP action. To monitor binding independent of
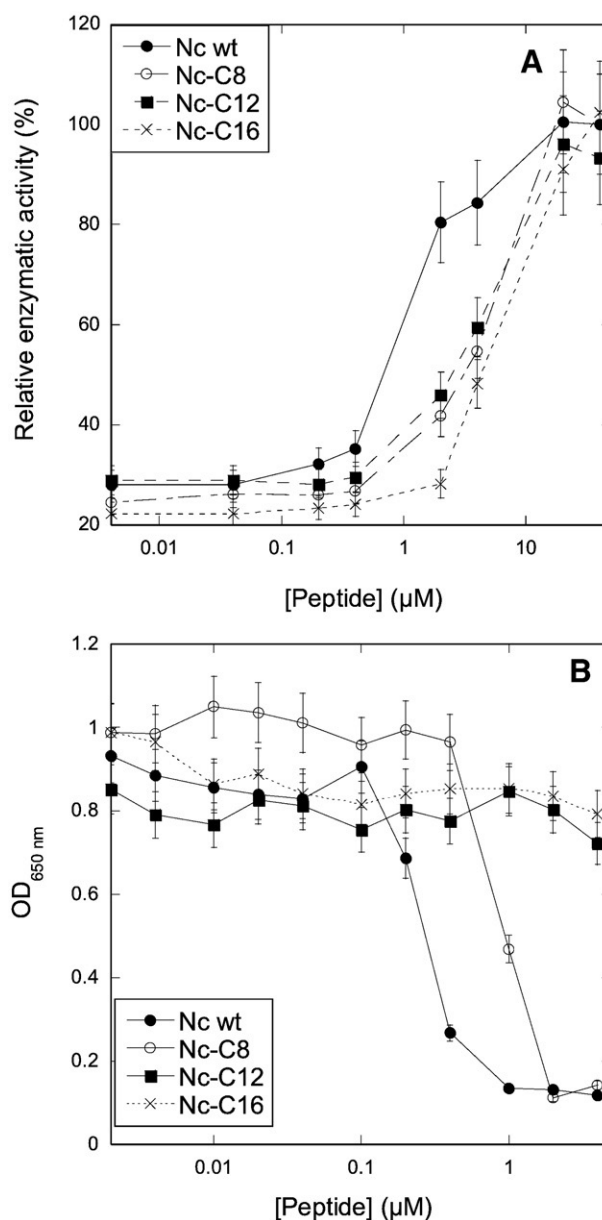
Fig. 4. (A) Degree of release of β-galactosidase from *E. coli* by different concentrations of Nc and acylated variants hereof. Errors in individual measurements ~7% based on duplicate measurements. (B) MIC assay performed on *E. coli* using different con-centrations of Nc and acylated variants hereof. Errors in individual measurements ~15% based on duplicate measurements. Clearly Nc wt is the most effective at reducing *E. coli* growth while Nc-C12 and Nc-C16 hardly have any effect at all.

folding, we used a Dansyl-labelled variant of unacylated Nc (Dansyl-Nc) to measure how the fluorescence anisotropy of the dansyl group changes as lipid is added. Immobilization of the peptide on the vesicle surface is expected to lead to a significant increase in anisotropy. Upon increasing the concentrations of lipid, we observe a hyperbolic binding curve which for both DOPC and 80DOPC:20DOPG vesicles reaches a plateau at a lipid:protein molar ratio of ~250 (Fig. 5A). Lipids were added stepwise to a single Dansyl-Nc solution. We were able to probe higher lipid:peptide ratios than in the CD experiments because of the low concentrations of Dansyl-Nc required for these experiments. To obtain reproducible results, we had to let the system equilibrate for a few minutes before recording anisotropy, particularly at the lower concentrations. This is most likely due to reorganization of the lipids into micellar-like structures as we can see from our calcein release measurements that the binding happens on a much
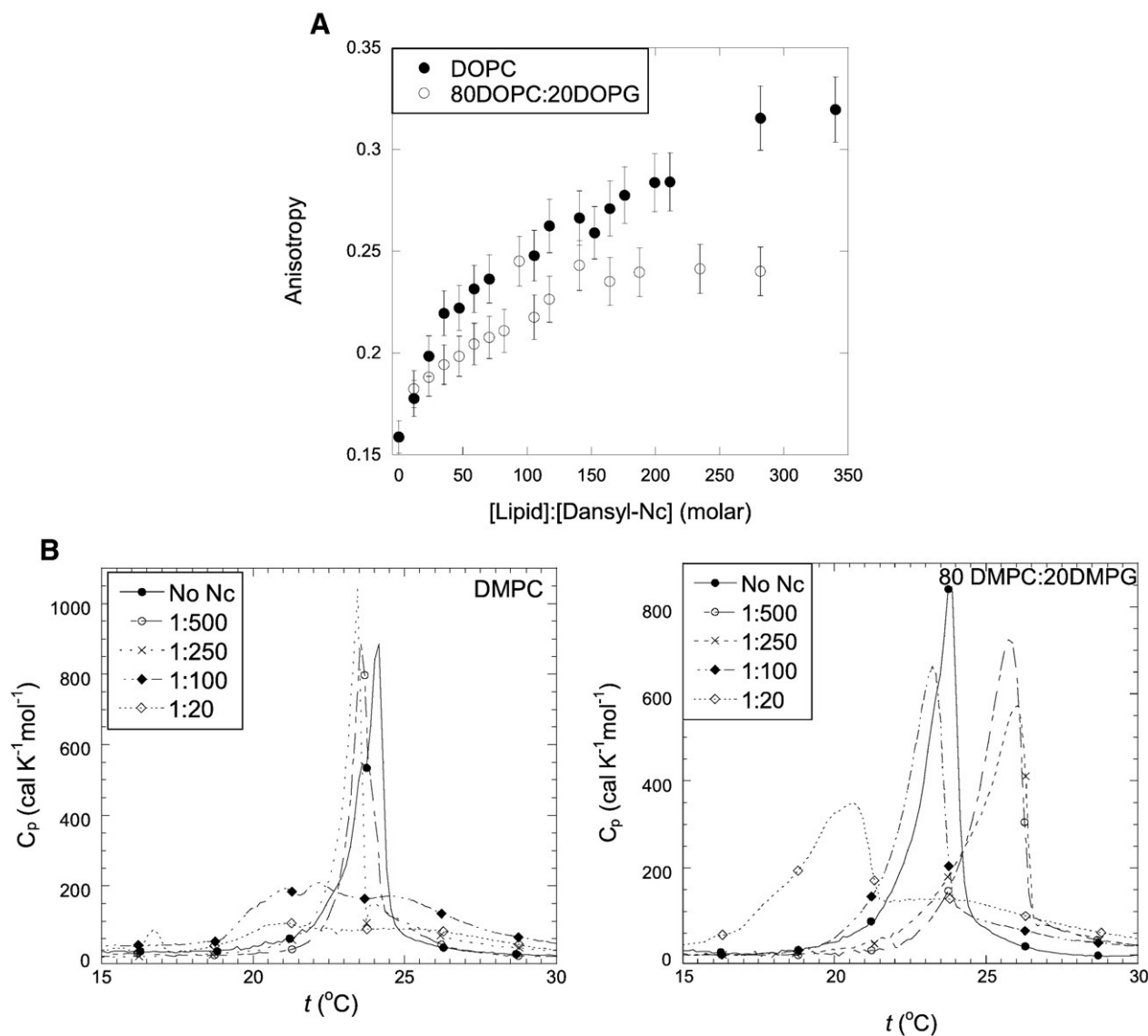
Fig. 5. (A) Anisotropy measurements of Dansyl-Nc in increasing concentrations of pure DOPC and 80DOPC:20DOPG. The vesicles were allowed to equillibrate for 1 min before each measurement. (B) DSC scans of DMPC and 80DMPC:20DMPG at different peptide–lipid ratios. Legend indicates Nc wt:lipid ratio (molar ratio).

faster timescale. We observe a slightly larger increase in fluorescence anisotropy for the DOPC vesicles. This could tentatively be interpreted as increased propensity to aggregate and thus permeabilize these vesicles compared to 80DOPC:20DOPG vesicles (cf. Fig. 3D). Alternatively, the peptide could be localized in a deeper and more ordered part of the bilayer in the DOPC vesicles, leading to a more pronounced effect on the lipid transition (see below).

3.5. DSC experiments reveal Nc interactions with both lipid types

Further evidence for the strong interaction of Nc with zwitterionic as well as partially anionic vesicles comes from differential scanning calorimetry experiments, where we monitor the phase transition temperature t_m in the presence of different concentrations of Nc. Here we use DMPC and 80DMPC:20DMPG where the transition temperature (23 °C in the absence of peptide) is experimentally accessible. Even at P:L ratios as low as 1:500, Nc wt has a marked effect on the transition (Fig. 5B) but the details are different for the two lipids: for DMPC, t_m declines by a few degrees as we go from 1:500 to 1:250 P:L and is replaced by a much broader transition at 1:100 and 1:25 P:L. For 80DMPC:20DMPG, there is a rise in t_m at the two lowest P:L ratios

followed by a decline; the broad transition is only observed at the highest P:L.

3.6. Dansyl-labelled Nc highlights differences in peptide insertion into different lipids

We combined the time-resolution of stopped-flow kinetics with the environmental sensitivity of a Dansyl fluorophor, attached to the N-terminus of unacylated Nc, to investigate the coupling between peptide binding and calcein release. The Dansyl probe increases the hydrophobicity of Nc and this might be expected to lead to an increased partitioning into the membrane. Accordingly, Dansyl-Nc shows a ~3-fold higher affinity towards DOPC and 80DOPC:20DOPG vesicles compared to Nc wt, measured in terms of increased α-helicity (data not shown). However, Dansyl-Nc shows the same 6–7 fold preference for 80DOPC:20DOPG over DOPC as Nc wt does (Table 1), making it a valid probe for measuring binding to different membrane types. When Dansyl-Nc is mixed with DOPC vesicles, we observe a slight increase in Dansyl fluorescence prior to vesicle disruption (indicated by the increase in calcein fluorescence), indicating a modest degree of peptide interaction with the membrane before disruption (Fig. 6A). However,

when Dansyl-Nc is added to 80DOPC:20DOPG vesicles, we observe a 10-fold higher increase in Dansyl fluorescence (compared to DOPC), which also precedes vesicle disruption (Fig. 6B). This increased Dansyl fluorescence in 80DOPC:20DOPG vesicles compared to DOPC vesicles indicates that Novicidin undergoes a greater change in environmental polarity when it inserts into 80DOPC:20DOPG vesicles. This suggests that Nc inserts more deeply into the 80DOPC:20DOPG membrane than into the pure DOPC membrane. We also observe an additional increase in Dansyl fluorescence during the process of calcein release from 80DOPC:20DOPG vesicles, suggesting a further rearrangement of Dansyl-Nc in the 80DOPC:20DOPG membrane upon vesicle disruption.

3.7. Nc peptides cause vesicle leakage, aggregation and lysis

Confocal laser scanning microscopy (CLSM) with giant unilamellar vesicles (GUVs) provides an alternative way of elucidating the
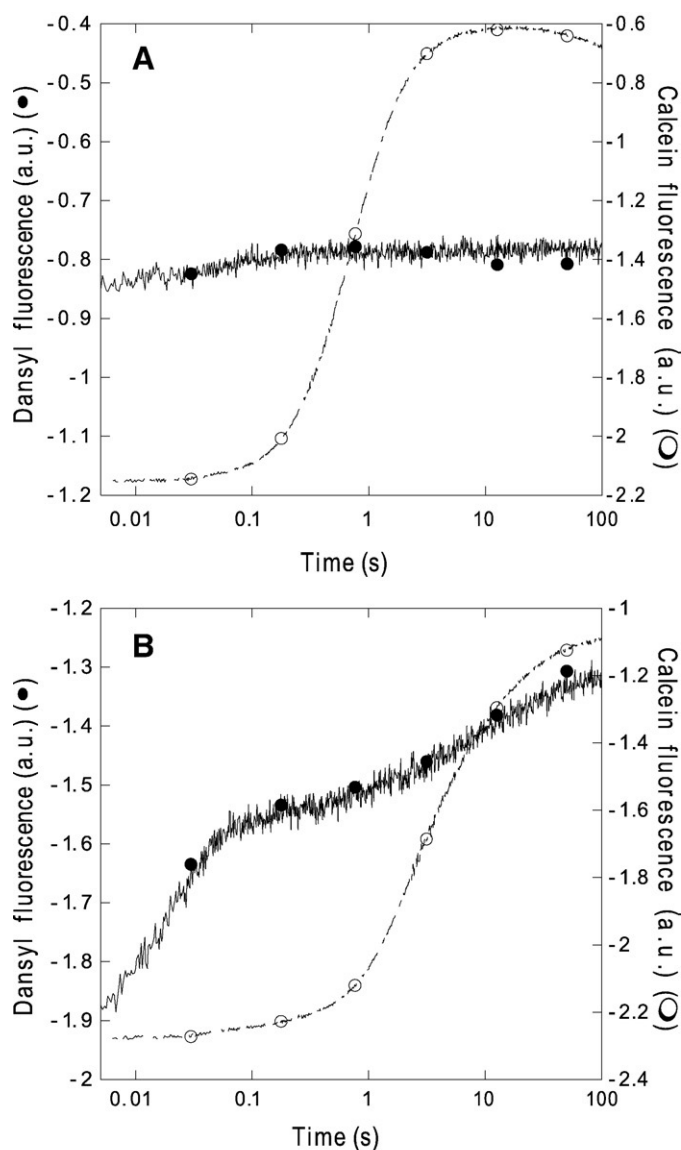
Fig. 6. Stopped-flow analysis of Nc interactions with lipids. Upon the addition of Dansyl-Nc we observe an increase for the dansyl fluorescence for both vesicles composed of DOPC (A) and 80DOPC:20DOPG (B) before an increase in the calcein fluorescence. In DOPC vesicles, there is a small increase in dansyl fluorescence due to binding (up to 0.1 s) followed by release of vesicle contents over 0.1–10 s. For the 80DOPC:20DOPG vesicles, there is a large fluorescence increase from the dansyl probe up to ~0.1 s and an additional slower increase up to 100 s (possibly due to lipid rearrangements) while calcein release occurs over the period 1–100 s.

mechanism of action of the different peptides, since we can focus on individual vesicles rather than measuring ensemble changes. The GUVs contained a lipid fluorophor (DiIC18) and were loaded with membrane impermeable water-soluble fluorophors (Alexa[488] for 80DOPC:20DOPG vesicles and Alexa[633] for DOPC vesicles), allowing us to monitor changes in both membrane integrity and permeability. The increased imaging facilities come at the expense of kinetic resolution, because diffusion limitation led to typical lag times of 10–15 min until the added peptide reached the field of vision, which makes it unrealistic to compare with the time profile provided by stopped-flow experiments. As illustrated in Fig. 7 and summarized in Table 2, the interactions between peptide and vesicle could be classified into three groups: (i) slow leakage that led to complete release of the vesicle content over 5–10 min, leaving an empty but intact vesicle behind; (ii) vesicle aggregation where the vesicles clump together, without necessarily facilitating the release of trapped fluorophor and (iii) vesicle lysis, causing immediate release of the vesicle content and complete loss of vesicle structure. Within the framework of current models for AMP action, (i) is most simply interpreted as pore formation and (iii) as the carpet model for membrane lysis, whereas (ii) represents an alternative class of interactions which do not occur in the absence of Nc and which to our knowledge has not been described before using CLSM. Images recorded at different stages of the process are provided in the Supplementary material.

Nc wt added to DOPC vesicles caused both vesicle lysis and aggregation (Table 2). The fused vesicles seemed partially stabilized, as they were the last to rupture and little to no leakage was observed. For Nc, it was clear that there was a higher degree of vesicle aggregation when the vesicles contained 20% DOPG. The aggregation of both vesicle types caused partial entrapment of the water-soluble probe and leads to larger particles with greater light-scattering properties. This could very well explain the overshoot in steady-state measurements at high concentrations that was more prominent with 80DOPC:20DOPG vesicles. For both vesicle types, both lysis of the vesicles and slow leakage was observed during and after the aggregation of the vesicles. The increase in vesicle aggregation observed with 80DOPC:20DOPG vesicles might be explained by favorable electrostatic interactions between adsorbed (cationic) Nc and neighbouring (anionic) vesicles. We have also observed aggregation of the related peptide Novispirin in the presence of different concentrations of SDS [31].

The addition of Nc-C8 to either DOPC vesicles or 80DOPC:20DOPG vesicles did not cause vesicle aggregation to any observable degree, but we did observe vesicle lysis. Vesicle leakage was only evident for 80DOPC:20DOPG vesicles. The leaky vesicles retained their structural integrity despite the fact that they did not aggregate, in contrast to observations with Nc. Nc-C12 did not cause slow leakage from neither DOPC nor 80DOPC:20DOPG vesicles but resulted in vesicle lysis, and, in contrast to Nc-C8, also led to vesicle aggregation. Thus, vesicle aggregation seems to be independent of whether the peptide causes lysis or leakage. For Nc-C16 the vesicle leakage behavior was comparable to that of Nc for both DOPC and 80DOPC:20DOPG vesicles but Nc-C16 caused an equally high degree of aggregation of vesicles irrespective of their lipid composition.

We also investigated the behavior of Nc when presented with a mixed population of different vesicles. In the presence of both DOPC and 80DOPC:20DOPG vesicles, we see a clear preference for the vesicles containing DOPG. We distinguish between the two vesicle types by filling them separately with different water-soluble fluorophores (Alexa[488] for DOPC versus Alexa[633] for 80DOPC:20-DOPG). While the 80DOPC:20DOPG vesicles behave more or less in the vesicle mixture as we have observed for neat 80DOPC:20DOPG vesicles (both aggregation, lysis and leakage are observed), we only observe rupturing of a few of the DOPC vesicles in the mixture. This indicates that the 80DOPC:20DOPG vesicles compete effectively
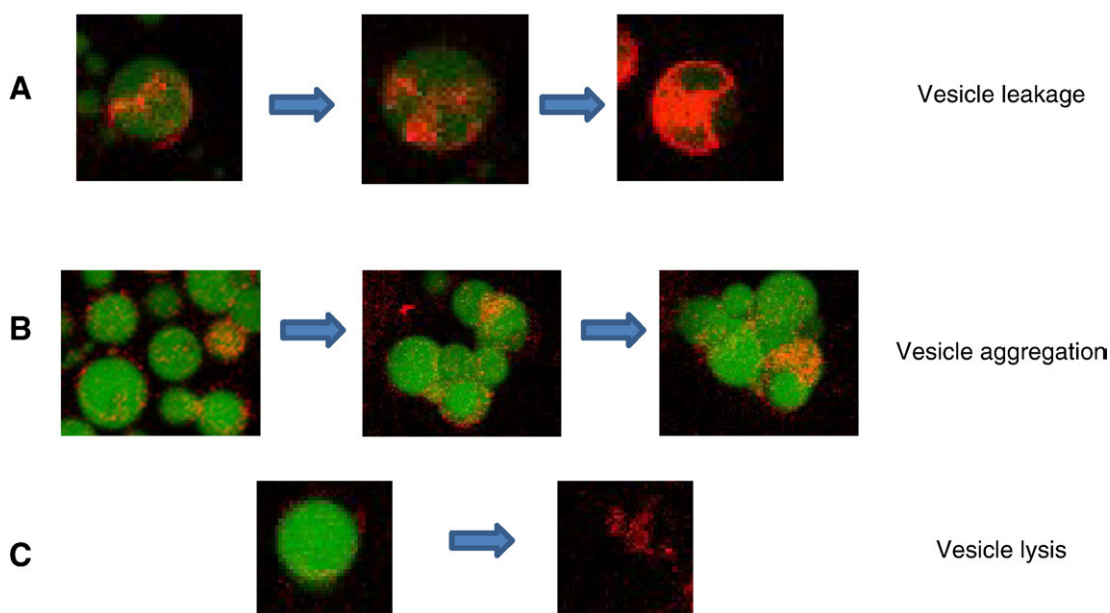
Fig. 7. Representative multicolour fluorescence images of Alexa[488] (green colour) loaded lipid vesicles with DiIC18 (red colour) incorporated in the membrane obtained by confocal laser scanning microscopy. In the presence of Nc and acylated derivatives, we observe three distinct modes of action, namely (A) vesicle leakage, (B) vesicle aggregation and (C) vesicle lysis. The relative preferences for the three modes of action are summarized in Table 2. The arrows represent the flow of time, but the length of time is not specified due to different kinetics with different peptides and lipids.

with pure DOPC vesicles in attracting free Nc (see Supplementary material).

3.8. Nc-C16 is more deeply embedded in micelles than Nc wt

In order to analyze the effect of acylation on Nc's anchoring in amphiphilic environments, we have used solution-state NMR to determine the structure and extent of insertion of Nc-C16 in zwitterionic (DPC) micelles. The structure was determined with traditional homonuclear 2D-spectra for the proton shift assignment and ^1H–^{13}C-HSQC natural abundance spectra for the C^α and C^β shift assignment. Key values of the structure calculation are listed in Table 3. The structure of Nc-C16 consists of a single slightly bent amphipathic α-helix with the acyl chain attached to the N-terminal

part of the peptide (Fig. 8A). Similar structures have been reported for the homologous peptides Ovispirin and Novispirin in SDS micelles [37–39]. The only NOE cross peaks between the peptide and the attached acyl group that could be assigned were the correlation between the H^N of residues 1–3 and the protons located on the fatty acid α-carbon atom. In the calculated structures the acyl chain therefore appears highly flexible without this necessarily being correct.

To determine the relative insertion depths of Nc and Nc-C16 in DPC micelles, samples with the micelle bound peptides were titrated with the paramagnetic agent Gd(DTPA-BMA) that is known not to interact with peptides and micelles [36,40]. T_1 relaxation values for the H^α protons in the peptides were calculated from peak volumes of cross peaks with the H^α atom appearing in the indirect dimension of inversion-recovery weighted NOESY spectra. The R_1 relaxation rates of the H^α atoms measured at different concentration of Gd(DTPA-

Table 2
Summary of confocal laser scanning microscopy experiments with Nc and acylated derivatives, indicating the propensities of the peptides for three different kinds of vesicle interactions (illustrated in Fig. 7).[a]

Peptide	DOPC vesicles	80DOPC:20DOPG vesicles
Vesicle leakage		
Nc wt	+	+++
Nc-C8	−	+
Nc-C12	−	−
Nc-C16	+	+++
Vesicle aggregation		
Nc wt	+	+++
Nc-C8	−	−
Nc-C12	++	+
Nc-C16	+++	+++
Vesicle lysis		
Nc wt	++	+
Nc-C8	+++	++
Nc-C12	+++	+++
Nc-C16	++	+

[a] For practical reasons, all experiments were performed at pH 6 and at 15 °C. The degree of leakage, aggregation and lysis was based on a relative comparison between the different samples.

Table 3
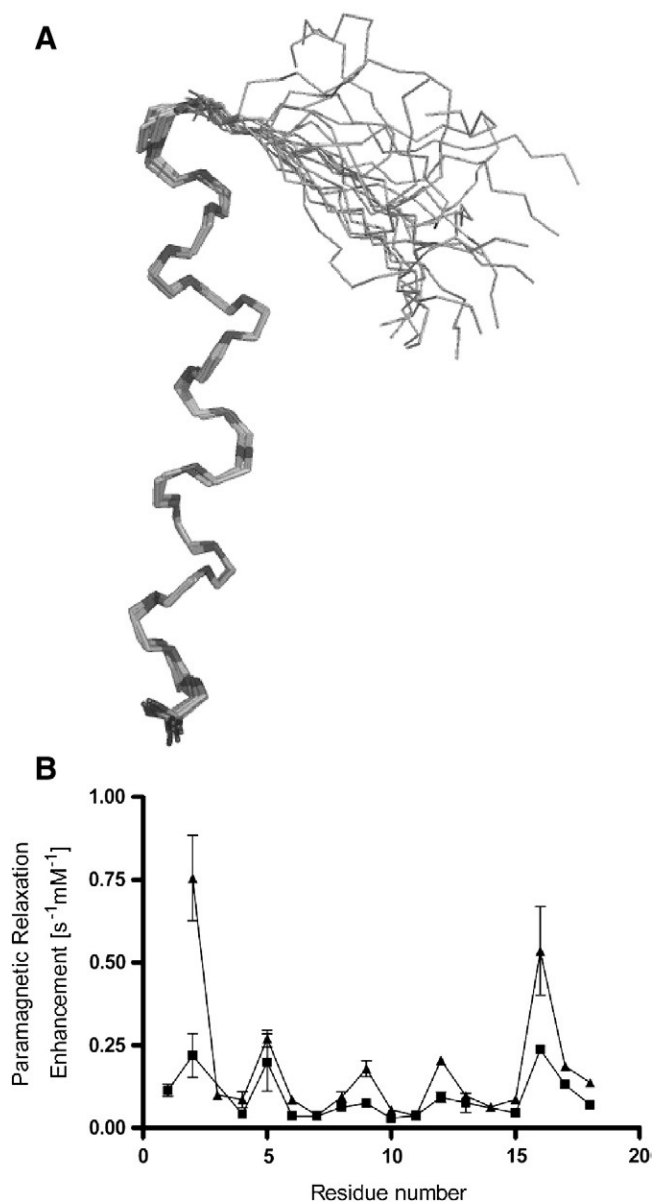Quality criteria for the calculated Nc-C16 structures.

Number of distance constraints	271
Of which intraresidual	136
Of which sequential	69
Of which medium-range ($2 \leq \Delta_{res} \leq 4$)	66
Number of angle constraints[a]	26
Of which φ	13
Of which ψ	13
CYANA residual target function	$0.89 \pm 0.04\ \text{Å}^2$
Distance restraints violated by more than 0.2 Å	0
Angle restraints violated more than 5°[b]	0
rmsd residues 2–17[c]	$0.13 \pm 0.08\ \text{Å}$
% of residues in Ramachandran plot[d]	
In most favored regions	91.5
Less favored regions	7.6
Generously allowed regions	0.9
Disallowed allowed regions	0

[a] Only those derived from TALOS.
[b] Per molecule.
[c] For backbone atoms C′, C^α and N, as calculated by CYANA from the pairwise rmsd values of each of the 20 structures against a mean structure.
[d] As calculated by PROCHECK_NMR.

deeper into the micelles. This difference is most pronounced for Asn2 in the N-terminal part of the peptides where the acyl chain of Nc-C16 is attached, which suggests that the hydrophobic acyl chain of Nc-C16 is pulling the N-terminus of the peptide towards the hydrophobic core of the micelle. This increased immersion then appears to be transmitted along the helix backbone to the rest of the peptide all the way to the C-terminus, probably reflecting an overall increase in the membrane partitioning coefficient.

3.9. Solid-state NMR experiments reveal stronger interactions of acylated Nc with lipids

We now turn from Nc–detergent to Nc–lipid interactions using oriented-sample solid-state NMR spectroscopy. Atomic-resolution details on the insertion of the different variants of Nc into different phospholipids may be obtained by recording ^{1}H–^{13}C PISEMA spectra [41] of natural abundance samples with the peptides reconstituted into bicelles (formed by DMPC:DMPG:DHPC lipids at different ratios) produce bicelles with the right size and charge properties. Note that DMPC:DMPG based membranes was chosen instead of DOPC:DOPG membranes to follow known recipes [42] for production of stable bicelles. To the best of our knowledge, such recipes are not established for DOPC/DOPG membranes. Accordingly, direct comparison of biophysical and solid-state NMR data has to be conducted under the precaution that lipid chain-length and saturation may influence details of the membrane–peptide interactions. The DMPC:DMPG: DHPC bicelles orient in a strong magnetic field with the bicelle normal perpendicular to the field direction, enabling measurement of anisotropic (i.e., orientation-dependent) chemical shift and dipole–dipole coupling interactions for the various CH$_n$ groups in the lipids. Accordingly, the ^{1}H–^{13}C PISEMA experiments may be used correlate orientation-dependent ^{13}C chemical shifts with ^{1}H–^{13}C dipole–dipole couplings for the abundant lipid molecules as demonstrated previously for other systems by Ramamoorthy and coworkers [43,44]. By monitoring the positions and lineshapes of the resonances for various lipid carbons in 2D PISEMA spectra, it is possible to probe small differences in local dynamics and orientation of the lipid functional groups and thereby get information about the influence of the peptides on the various parts of the lipids. This is illustrated in Fig. 9, with Fig. 9A showing a representative full 2D PISEMA spectrum of DMPC:DHPC bicelles containing Nc wt (molar ratios Nc wt:DMPC: DHPC 1:57:18), Fig. 9B the molecular structure of DMPC with indication of three representative functional groups, and Fig. 9C–H excerpts for these functional groups from 2D PISEMA spectra recorded using different lipid:peptide systems. The full PISEMA spectrum demonstrates correlation between ^{1}H–^{13}C dipole–dipole couplings (giving rise to multiplets/splittings in the horizontal direction) and ^{13}C chemical shifts for the highly abundant lipid CH$_n$ groups. Variations in the orientation-dependent dipole–dipole coupling and chemical shifts upon mixing in peptides to the membranes will probe peptide:lipid interactions with spatial resolution through observation of distinct signals for the various lipid carbons.

The PISEMA spectrum excerpts (Fig. 9C–H) originate from samples with pure lipid (red line), lipid and Nc wt (green line), lipid and Nc-C8 (blue line), and lipid and Nc-C16 (magenta line) with the lipids being either pure zwitterionic bicelles (DMPC together with DHPC, Fig. 9C–E) or a mixtures of zwitterionic and anionic bicelles (molar ratios Nc:DMPC:DMPG:DHPC 1:46:10.6:17.7, Fig. 9F–H). The spectra report the perturbation of headgroup (C$_\alpha$), a central carbon (C$_3$), and a terminal acyl carbon (C$_{14}$) according to the structural model given in Fig. 9B. In addition to contour plots from relevant parts of the 2D PISEMA spectra for the four different samples, the individual panels also contain sum projections (left and top) onto the ^{13}C chemical shift axis (vertical) and the ^{1}H–^{13}C dipolar axis (horizontal). The individual panels also contain (right and bottom) the corresponding traces taken through the maximum point of the 2D spectra for the peptide-free

Fig. 8. (A) Structure of Nc-C16 in the presence of DPC. Superposition of the 20 backbone conformers with the lowest cyana target function representing the 3D NMR structure. The bundle is obtained by superimposing the backbone C$^\alpha$, C, and N atoms of residues 2–17. The carbon atoms of the acyl chain are clearly seen extending from the N-terminal part of the peptide. (B) PRE values of H$^\alpha$ nuclei of Nc (▲) and Nc-C16 (■) as a function of residue numbers. Error bars indicate variations in PRE values obtained from fitting several peaks.

BMA) were subsequently plotted against the concentration of the paramagnetic agents giving the paramagnetic relaxation enhancement (PRE) values of the atoms.

In Fig. 8B the H$^\alpha$ PRE values of Nc and Nc-C16 can be seen as a function of the residue numbers. The PRE curves of both peptides give a wavelike pattern with a wavelength of either 3 or 4 residues between the maxima of the PRE curves which for both peptides are located at the residues Asn-2, Arg-5, Lys-9, His-12 and Lys-16 corresponding to the hydrophilic side of the amphipathic helix.
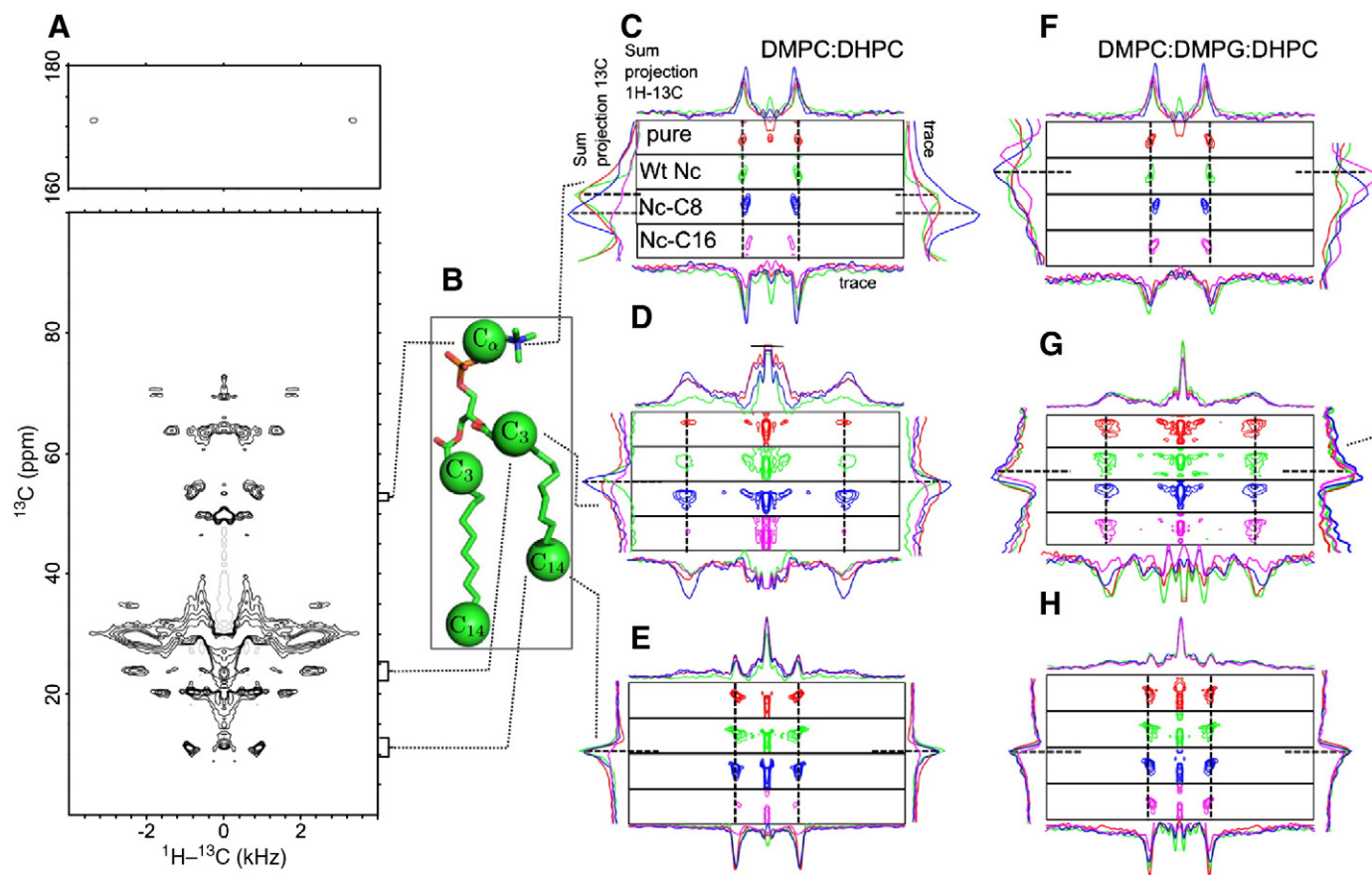
As the PRE values depend on the inverse of the sixth power of the distance between the hydrogen and the paramagnetic atom [40], the results shows that the hydrophilic side of the helix is facing the outside of the micelle as expected. The PRE values of the Nc atoms are significantly larger than the corresponding atoms in Nc-C16 which clearly indicates that the acylated variant of Novicidin is buried

Fig. 9. Solid-state NMR spectra of Novicidin and acetylated variants in pure and mixed lipids. (A) Full ^{1}H–^{13}C dipole–dipole couplings versus ^{13}C chemical shift correlated PISEMA spectrum of DMPC:DHPC bicelles including Nc wt (molar ratios Nc:DMPC:DHPC of 1:57:18). (B) Molecular model of DMPC with indication of the C_α, C_3, and C_{14} carbons through which excerpts of PISEMA spectra (C–H) are taken. (C–H) Each panel describes four different bicelle samples containing either; pure lipid bicelle (red), lipid and Nc wt (green), lipid and Nc-C8 (blue) and lipid with Nc-C16 (magenta). Each panel consists of an excerpt from 2D ^{1}H–^{13}C PISEMA spectra of DMPC:DHPC or DMPC:DMPG:DHPC bicelles as well as sum projections and traces along the position of the pure bicelle for both the ^{1}H dimension and the ^{13}C dimension. (C–E) describe the spectral changes observed for zwitterionic bicelles. (F–H) describe the spectral changes observed for a mixture of zwitterionic and anionic bicelles (molar ratios Nc:DMPC:DMPG:DHPC 1:46:10.6:17.7). The focus is on three representative regions describing the lipid head group (C, F), the central part of the lipid molecule (D, G), and the lipid tail region (E, H).

bicelles. While changes in the local environment (structure/orientation and time averaged dynamics) may be monitored from the 2D contours as well as the projections, it is evident that most sensitivity towards minor changes in peak positions will be probed through the traces. Note that all samples were prepared with approximately the same peptide concentration. Furthermore, the calcein release data (Fig. 3) suggest that Nc will display stronger interactions with zwitterionic vesicles than with the mixed zwitterionic and anionic vesicles. However, the CD data (Fig. 2) suggest that 80DOPC:20DOPG vesicles bind Nc more strongly.

From the upper panels in Fig. 9C–H, it becomes evident that Nc as well as the acylated Nc variants interact with the headgroup of both types of lipids. This is seen from the position and shape of the contours, and very clearly from the traces taken at the position of the resonance in the pure lipid spectra. A closer inspection of the spectra provides a more diverse set of observations for a deeper penetration of the peptides into the various lipids. From Fig. 9C–E column, it is seen that Nc-C16 interacts with all carbon sites of the zwitterionic lipids and thereby may adapt a transmembrane (or transiently transmembrane) configuration with significant effect on the carbons on the central region of the lipids. Note that in the absence of NMR signals from the peptide, we cannot determine whether it is the acyl chain or the peptide backbone that is transmembrane. In contrast, it appears that largely only the headgroup region (C_α and C_3 carbons) are affected by the peptides with shorter or no acylation. Turning to the DMPC:DMPG:DHPC lipid bicelles (Fig. 9F–H column), it appears

that the perturbing effect from the various peptides on the local environment of the lipids are somewhat less pronounced (weaker interactions) and to a large extend only influence the headgroup region. For the Nc wt sample only a slight shift in the resonance position is observed for the α and β (not shown) carbons, indicating a relatively weak perturbation as compared to the interaction with the pure bicelles.

The observed changes (summarized in Table 4) overall indicate that Novicidin and its acylated variants mainly interact with the surface of bicelles composed of zwitterionic and anionic lipids, while more pronounced interactions are observed for the pure zwitterionic

Table 4
Summary of peptide induced-perturbation of CH_n groups in the headgroup (C_α), central (C_3), and tail (C_{14}) regions of zwitterionic (DMPC) and mixed zwitterionic and anionic (DMPC:DMPG) bicelles.[a]

	Peptide	DMPC	DMPC:DMPG (4:1)
Headgroup (C_α)	Nc	++	+
	Nc-C8	+++	++
	Nc-C16	+++	++
Central (C_3)	Nc	++	−
	Nc-C8	++	+
	Nc-C16	++	++
Tail (C_{14})	Nc	−	−
	Nc-C8	−	−
	Nc-C16	+++	+

[a] See labelling of lipid functional groups in Fig. 9B.

lipids. In the latter case is seems that addition of acyl chains accelerates the interaction with perturbation of the inner parts of the membrane for the Nc-C16 acylation. We note that the ^{1}H–^{13}C PISEMA experiments do not provide information on whether this transmembrane perturbation is caused by the formation of ion channels (barrel stave) or static/transient incorporation of monomer/oligomers of acylated peptides. We note that, in full consistency with the NMR observations, the biophysical measurements report the strongest membrane perturbation for the DOPC vesicles, with the requirement of less peptide to penetrate/perturb the vesicles relative to the 80DOPC:20DOPG vesicles — although this appears to occur with very little induction of secondary structure.

4. Discussion

4.1. Acylation promotes higher-order assemblies and α-helical structure

The CD spectra of Nc and the acylated derivatives in buffered solution clearly show that the C12 and C16 acyl chains changed the peptide structure. Nc-C12 is random coil at 40 μM but α-helical at 200 μM, whereas Nc-C16 was α-helical at all measured concentrations (10–100 μM). For Nc-C12, this can be explained by the peptides arranging in a surfactant like fashion (aided by the acyl chain's desire to avoid an aqueous environment) with a critical micelle concentration (CMC) between 40 and 200 μM. Micelle formation results in an α-helical structure, as described by Makovitzki et al. [20]. For Nc-C16, the CMC is either below the peptide concentration tested in this study (i.e. <10 μM) or the structure is stabilized in a different fashion, possibly existing only as a monomer. Solution-state NMR experiments on pure samples of Nc-C12 and Nc-C16 in the absence of lipids showed that both derivatives at ~1 mM in aqueous buffer formed aggregates that did not yield any useful NMR signals (M. F. and R. W., unpublished data). However, when dispersed in DPC, Nc-C16 yielded well-defined NMR spectra. In addition, Dufour et al. [45] have studied linearized versions of the lipopeptide surfactin and found that C10, C14, and C18 surfactin had CMC values of 1113, 301, and 8 μM respectively. These values are consistent with our own observations and also support the Nc-C16 micellization. In principle, the acyl chain could also pack against the peptide at the monomer level provided a suitably hydrophobic binding surface was available as suggested by Makovitzki et al. [20]. A helix projection of Nc (Fig. 1) highlights a perfectly amphipathic helix with a sharp distinction between a hydrophobic face (only interrupted by Gly10) and a cationic face, where the acyl chain is attached to first residue placed in the middle of the cationic face. Nevertheless, Nc-C16's apparent micellization suggests that the C16 chain engages in inter- rather than intramolecular packing. It is likely that the precise site of attachment of the acyl chain will dictate whether it is more favorable for the chain to dock against the peptide, engage with other acyl chains in an intermolecular micellar arrangement, or even combine the two types to form small micelles that also incorporate the peptide, as suggested for the lipopeptides elegantly developed by Privé et al. [46].

It is worth considering how these aggregative tendencies may influence subsequent vesicle interactions: We have a system with two defined states, one monomeric where the peptide has a random conformation, the other most likely multimeric where the peptide has an α-helical structure. Let us assume that the peptide initially inserts as a monomer into the lipid bilayer (even if it binds as a multimer it is likely to rearrange its higher-order arrangement in the bilayer, and possibly monomerize, due to the change in environment). In that case binding will need to be preceded by micelle dissociation above the CMC of the lipopeptide micelle (which is <10 μM for Nc-C16 and between 40 and 200 μM for Nc-C12). Detergent micellar dynamics typically involve two relaxation processes, namely the dissociation of monomer from micelles (on the μs scale) and micelle break-up (on the minute scale depending on the biophysical properties of the

detergent) [47]. Thus, we do not consider it likely that monomer dissociation from micelles is rate-limiting for the kinetics of binding of acylated Nc to membranes.

Furthermore, we do not expect the acylated peptides' aggregation tendencies to play significant roles in their membrane permeabilizing and antimicrobial properties for three reasons: Firstly, these activities are measured at very low concentrations where aggregation in solution is very insignificant for Nc-C8 and Nc-C12 and likely also very low for Nc-C16. Secondly, there is no difference between Nc-C12 and Nc-C16's permeabilizing and antimicrobial activities despite significant differences in aggregation potential. Thirdly, Nc-C8 can be considered a non-aggregating peptide under all our measured conditions and its permeabilizing and antimicrobial activities lie neatly between the unacylated Nc wt and the Nc-C12 and Nc-C16 peptides.

Any changes in membrane disruption kinetics are therefore most likely to reflect changes in the binding to the membrane and/or structural rearrangements in this environment. Let us address these issues.

4.2. Changes in secondary structure caused by the addition of lipids

Nc folding in vesicles is strongly dependent on the lipid headgroup. Nc remains largely random coil in DOPC, but 80DOPC:20DOPG vesicles induce α-helical structure. However, the increase in secondary structure does not in itself favor permeabilization but makes it less efficient. These data can be interpreted in two ways: either Nc binds to a smaller extent to DOPC than to 80DOPC:20DOPG vesicles but the peptide molecules that do bind are much more efficient at permeabilizing DOPC than 80DOPC:20DOPG. Alternatively, Nc binds to DOPC vesicles but in a disordered conformation. We favor the latter interpretation, since we know from three independent techniques (calcein release, fluorescence anisotropy and DSC) that Nc binds at least as well to DOPC vesicles as to 80DOPC:20DOPG vesicles. The differences in structure may reflect different arrangements on the vesicle surface and/or membrane traversion, as suggested also by the different DSC profiles towards zwitterionic versus partially anionic vesicles. One scenario could be that Nc is loosely attached to DOPC vesicles, allowing it to remain relatively unstructured and thus cover a larger surface on the vesicle, while in 80DOPC:20DOPG vesicles Nc is buried at the headgroup-acyl chain interface, favoring an amphipathic α-helix structure. This is consistent with our stopped-flow experiments with Dansyl-Nc where we observe a higher degree of interaction with 80DOPC:20DOPG vesicles both prior to and after vesicle disruption. Our solid-state NMR observations also show that Nc mainly interacts with the lipid headgroups. Previously we observed that the closely related peptide Novispirin was able to bind to the positively charged surfactant LTAC to a more superficial extent than to the complementary SDS micelles, highlighting different levels of interaction [31]. Other studies also indicate that binding and permeabilization can be separate processes, and that binding alone is not sufficient for membrane permeabilization. For example, the amyloid-β peptide can bind to both crystalline and liquid disordered phases but only permeabilize the liquid disordered state [48].

Acylated peptides are α-helical in the presence of zwitterionic vesicles, suggesting that the acyl chain causes the peptides to adsorb to the vesicles in a manner that facilitates the formation of α-helix. One could imagine that the acyl chains work as "anchors" that pull the peptides into the headgroup-acyl chain interface where it then folds into an α-helix, supported by our PRE-data which indicate deeper penetration into micelles by Nc-C16 than Nc wt (Fig. 8B). This anchoring effect may also explain our solid-state NMR observation where we not only observe perturbation of the lipid head groups but also effects in the central and tail parts of the lipids — where α-helical secondary structure would support membrane penetration (static or transient). Graham and Phillips [49] reported that adsorption of rigid

molecules to lipid membranes caused a slower increase in surface pressure compared to flexible molecules. Thus increased peptide rigidity induced by α-helix formation (in combination with "plugging" effects mentioned below) could explain the decreased tendency to disrupt vesicles. In addition, the increased submersion into the lipid bilayer will make the acylated peptides less sensitive to the nature of the headgroup and will thus decrease the preference for zwitterionic lipids shown by Nc.

### 4.3. Changes in lipid specificity caused by acylation

In the steady-state fluorescence measurements of vesicle disruption, we observe that Nc causes calcein release from DOPC vesicles at 7-fold lower concentration than those needed for disruption of 80DOPC:20DOPG vesicles. Solid-state NMR data also reveal a stronger interaction between the peptide and the DMPC membranes than the DMPC:DMPG membranes. Peptide acylation increases the concentrations needed for vesicle disruption, and leads to a decreased preference for zwitterionic vesicles compared to partially anionic vesicles (Fig. 3D). However, this decreased functional efficiency does not reflect a lower degree of overall binding to vesicles, as we need less lipid to induce changes in secondary structure for both Nc-C8 and Nc-C12 compared to Nc. To explain this apparent discrepancy, we speculate that the peptide's N-terminal acyl chain to some degree is able to counteract membrane disruption. The observed faster release rates for acylated peptides could then could then be explained by the higher surface concentration of peptide that has been able to

accumulate up to this level without disrupting the membrane because of the "plugging" effects of the acyl chain which help retain membrane integrity (see model in Fig. 10). The "plugging" effect could very well be what we observe in the solid-state NMR spectra. It is clear that Nc-C16 interacts with central parts of the lipid bilayer as seen in Fig. 9E and H. We note that from the present NMR data, we cannot distinguish whether it is the peptide itself or it is its acyl chains that interact with the central parts of the lipids. Data which could be interpreted in the same light have been observed for the lipopeptide surfactin where an increase in acyl chain length lowers the surface pressure of vesicles [50]. In vivo these effects would presumably lead to a decrease in the haemolytic activity of the peptide as the outer leaflet of red blood cell is primarily composed of the zwitterionic phosphatidylcholine and phosphatidylethanolamine [51].

The decreased preference of acylated Nc for zwitterionic lipids differs significantly from the work of Dathe et al. [52] and Wieprecht et al. [53], who report an increased affinity towards zwitterionic vesicles as a result of increased hydrophobicity. However, in their studies they have made point mutations in order to increase the hydrophobicity, rather than acylating the peptide. As with the acylated variants, this emphasizes the separation of folding and function.

4.4. Vesicle aggregation

The overshoot observed in our calcein release assay is presumably a scattering effect caused by vesicle aggregation. Apparently the
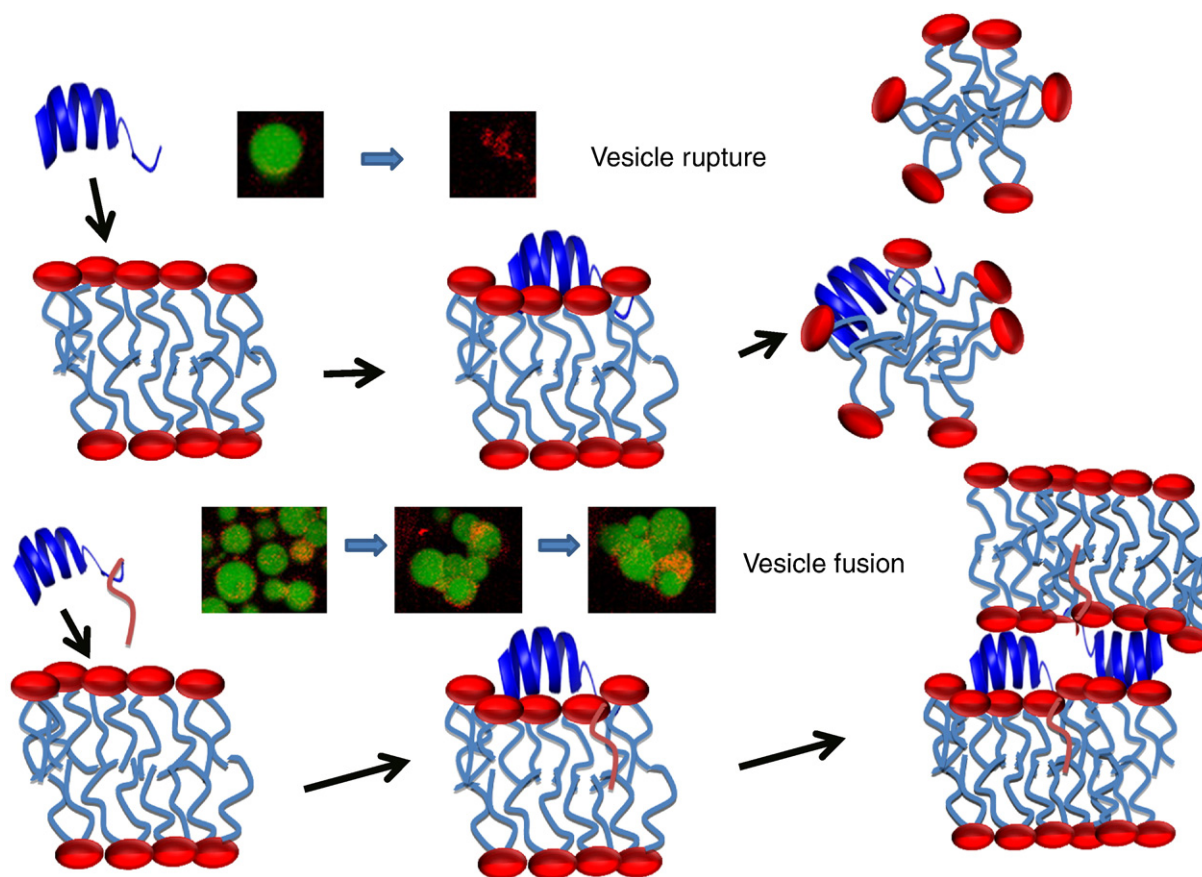
Fig. 10. A schematic model to illustrate why much less Nc wt is required compared to the acylated versions to cause the same degree of vesicle permeabilization. Nc wt (blue) attaches peripherally to DOPC vesicles since there is no significant change in the secondary structure upon binding although we still observe vesicle disruption. In the presence of DOPG, Nc is submerged more extensively in the bilayer, most likely at the acyl chain headgroup interface, leading to increased α-helix structure and an increase in the fluorescence of the dansyl-labelled Nc prior to vesicle disruption. The acylation of Nc (acyl chain in pink) pulls the peptide deeper into the DOPC vesicles as we have formation of α-helix. Nevertheless the insertion is different from that in 80DOPC:20DOPG vesicles, since there are still clear differences in the vesicle disruption kinetics and concentrations needed for the two types of vesicles. The acyl chain helps to counteract the vesicle destabilizing effect of the peptide, leading to the need for higher concentrations of peptides to disrupt the vesicles, irrespective of the lipids used.

vesicle aggregates are subsequently dissolved as we observe the overshoot to decrease over time. This is confirmed in our CLSM experiments where we in some cases clearly observe vesicle aggregation followed by vesicle disruption. Peptide induced aggregation of vesicles has been reported previously for antimicrobial peptides such as Cryptidin-4 and polylysine, measured by FRET and dynamic light scattering [54–56]. The aggregation is believed to be driven primarily by preferential electrostatic interactions, bilayer deformation, and lipid head group dehydration [56,57]. We do observe a link between the aggregation and the acylation, since increasing chain lengths increase the aggregation (though Nc-C8 has reduced aggregation capability compared to non-acylated Nc). One explanation could be that the previously suggested plugging effect, in combination with exposure of cationic side-chains on the surface which can attract neighbouring anionic vesicles, gives the peptide–lipid complexes time to interact and subsequently aggregate. Our working model for the effect of Novicidin on membranes is summarized in Fig. 10.

4.5. In a mixed population of vesicles charge interactions are the governing forces of peptide–lipid interactions

Confocal laser scanning microscopy experiments on the mixed populations of purely zwitterionic and zwitterionic-anionic vesicles (Supplementary material) reveal that peptides show a marked preference towards the (partially) negatively charged DOPC:DOPG vesicles over the zwitterionic DOPC vesicles. This preference differs from our calcein release measurements but does not contradict them. Rather, they simply reveal that long-range interactions in solution, mediated by electrostatics, can be sufficient to trap peptides on or close to a membrane surface for subsequent folding and membrane interactions. Although the visualization of vesicle contents release by peptides and small molecules has been reported previously [58–61], to our knowledge this is the first example of the microscope-based analysis of mixed vesicle populations. This allows us to compare the affinity of wildtype and modified peptides for a specific lipid composition in the presence of competing lipids, and thus ultimately model complex *in vivo* systems, such as the human digestive tract, where the antimicrobial peptides are exposed to a diverse range of possible targets [62,63].

Acknowledgements

Appendix A. Supplementary data

Supplementary data associated with this article can be found, in the online version, at doi:10.1016/j.bbapap.2009.12.006.

References

[1] J.D. Hale, R.E. Hancock, Alternative mechanisms of action of cationic antimicrobial peptides on bacteria, Expert Rev. Anti Infect. Ther. 5 (2007) 951–959.
[2] K. Lohner, S.E. Blondelle, Molecular mechanisms of membrane perturbation by antimicrobial peptides and the use of biophysical studies in the design of novel peptide antibiotics, Comb. Chem. High Throughput Screen. 8 (2005) 241–256.
[3] M. Zasloff, Antimicrobial peptides of multicellular organisms, Nature 415 (2002) 389–395.
[4] K.A. Brogden, Antimicrobial peptides: pore formers or metabolic inhibitors in bacteria? Nat. Rev. 3 (2005) 238–250.
[5] Y.J. Gordon, E.G. Romanowski, A.M. McDermott, A review of antimicrobial peptides and their therapeutic potential as anti-infective drugs, Curr. Eye Res. 30 (2005) 505–515.
[6] J. Andra, J. Howe, P. Garidel, M. Rossle, W. Richter, J. Leiva-Leon, I. Moriyon, R. Bartels, T. Gutsmann, K. Brandenburg, Mechanism of interaction of optimized Limulus-derived cyclic peptides with endotoxins: thermodynamic, biophysical and microbiological analysis, Biochem. J. 406 (2007) 297–307.
[7] O. Taboureau, O.H. Olsen, J.D. Nielsen, D. Raventos, P.H. Mygind, H.H. Kristensen, Design of novispirin antimicrobial peptides by quantitative structure–activity relationship, Chem. Biol. Drug Des. 68 (2006) 48–57.
[8] S. Pistolesi, R. Pogni, J.B. Feix, Membrane insertion and bilayer perturbation by antimicrobial peptide CM15, Biophys. J. 93 (2007) 1651–1660.
[9] M.A. Fazio, L. Jouvensal, F. Vovelle, P. Bulet, M.T. Miranda, S. Daffre, A. Miranda, Biological and structural characterization of new linear gomesin analogues with improved therapeutic indices, Biopolymers 88 (2007) 386–400.
[10] C. Landon, F. Barbault, M. Legrain, L. Menin, M. Guenneugues, V. Schott, F. Vovelle, J.L. Dimarcq, Lead optimization of antifungal peptides with 3D NMR structures analysis, Protein Sci. 13 (2004) 703–713.
[11] O. Taboureau, O.H. Olsen, J.D. Nielsen, D. Raventós, P.H. Mygind, H.-H. Kristensen, Design of Novispirin antimicrobial peptides by quantitative structure–activity relationship, Chem. Biol. Drug Des. 68 (2006) 48–57.
[12] H.E. Hasper, N.E. Kramer, J.L. Smith, J.D. Hillman, C. Zachariah, O.P. Kuipers, B. De Kruijff, E. Breukink, An alternative bactericidal mechanism of action for lantibiotic peptides that target lipid II, Science 313 (2006) 1636–1637.
[13] M.E. Quiñones-Mateu, M.M. Ledermann, Z. Feng, B. Chakraborty, J. Weber, H.R. Rangel, M.L. Marotta, M. Mirza, B.L. Jiang, P. Kiser, K. Medvik, S.F. Sieg, A. Weinberg, Human epithelial beta-defensins 2 and 3 inhibit HIV-1 replication, AIDS 17 (2003) F39–F48.
[14] Y. Shai, Z. Oren, From "carpet" mechanism to de-novo designed diastereomeric cell-selective antimicrobial peptides, Peptides 22 (2001) 1629–1641.
[15] G. Ehrenstein, H. Lecar, Electrically-gated ionic channels in lipid bilayers, Rev. Biophys. 10 (1977) 595–623.
[16] Y. Pouny, D. Rapaport, A. Mor, P. Nicolas, Y. Shai, Interaction of antimicrobial dermaseptin and its fluorescently labeled analogues with phospholipid membranes, Biochemistry 31 (1992) 12416–12423.
[17] E. Gazit, A. Boman, H.G. Boman, Y. Shai, Interaction of the mammalian antibacterial peptide cecropin P1 with phospholipid vesicles, Biochemistry 34 (1995) 11479–11488.
[18] Y. Pouny, Y. Shai, Interaction of D-amino acid incorporated analogues of pardaxin with membranes, Biochemistry 31 (1992) 9482–9490.
[19] Y. Shai, Molecular recognition between membrane-spanning polypeptides, Trends Biochem. Sci. 20 (1995) 460–464.
[20] A. Makovitzki, D. Avrahami, Y. Shai, Ultrashort antibacterial and antifungal lipopeptides, Proc. Natl. Acad. Sci. USA 103 (2006) 15997–16002.
[21] D. Avrahami, Y. Shai, Conjugation of a magainin analogue with lipophilic acids controls hydrophobicity, solution assembly, and cell selectivity, Biochemistry 41 (2007) 2254–2263.
[22] F. Separovic, S. Barker, M. Delahunty, R. Smith, NMR structure of C-terminally tagged gramicidin channels, Biochim. Biophys. Acta 1416 (1999) 48–56.
[23] T.C. Vogt, J.A. Killian, B. De Kruijff, The influence of acylation on the lipid structure modulating properties of the transmembrane polypeptide gramicidin, Biochim. Biophys. Acta 1193 (1994) 55–61.
[24] S.H. White, W.C. Wimley, Membrane protein folding and stability: physical principles, Ann. Rev. Biophys. Biomol. Struct. 28 (1999) 319–365.
[25] M.A. Schmitt, B. Weisblum, S.H. Gellman, Unexpected relationships between structure and function in alpha, beta-peptides: antimicrobial foldamers with heterogeneous backbones, J. Am. Chem. Soc. 126 (2004) 6848–6849.
[26] T.L. Raguse, E.A. Porter, B. Weisblum, S.H. Gellman, Structure–activity studies of 14-helical antimicrobial beta-peptides: probing the relationship between conformational stability and antimicrobial potency, J. Am. Chem. Soc. 124 (2002) 12774–12785.
[27] H. Khandelia, Y.N. Kaznessis, Molecular dynamics simulations of helical antimicrobial peptides in SDS micelles: what do point mutations achieve? Peptides 26 (2005) 2037–2049.
[28] M.V. Sawai, A.J. Waring, W.R. Kearney, P.B.J. McCray, W.R. Forsyth, R.I. Lehrer, B.F. Tack, Impact of single-residue mutations on the structure and function of ovispirin/novispirin antimicrobial peptides, Prot. Eng. 15 (2002) 225–232.
[29] F. Jacobsen, A. Mohammadi-Tabrisi, T. Hirsch, D. Mittler, P.H. Mygind, C.P. Sonksen, D. Raventos, H.H. Kristensen, S. Gatermann, M. Lehnhardt, A. Daigeler, H.U. Steinau, L. Steinstraesser, Antimicrobial activity of the recombinant designer host defence peptide P-novispirin G10 in infected full-thickness wounds of porcine skin, J. Antimicrob. Chemother. 59 (2007) 493–498.
[30] H. Khandelia, Y.N. Kaznessis, Molecular dynamics investigation of the influence of anionic and zwitterionic interfaces on antimicrobial peptides' structure: implications for peptide toxicity and activity, Peptides 27 (2006) 1192–1200.
[31] R. Wimmer, K. Andersen, B. Vad, M. Davidsen, S. Mølgaard, L.W. Nesgaard, H.-H. Kristensen, D.E. Otzen, Versatile interactions of the antimicrobial peptide Novispirin with detergents and lipids, Biochemistry 45 (2006) 481–497.
[32] M.I. Angelova, D.S. Dimitrov, Liposome electroformation, Faraday Discuss. Chem. Soc 81 (1986) 301–311.
[33] B. Vad, K. Bertelsen, C.H. Johansen, J.M. Pedersen, T.S. Skrydstrup, N.C. Nielsen, D.E. Otzen, Pardaxin permeabilizes vesicles more efficiently by pore formation than by disruption, Biophys. J. 98 (4) (2010) 576–585.
[34] S.B. Nicholas, K.D. Philipson, Cardiac expression of the Na(+)/Ca(2+) exchanger NCX1 is GATA factor dependent, Am. J. Physiol. 277 (1999) H324–H330.
[35] C.M. Kusuma, J.F. Kokai-Kun, Comparison of four methods for determining lysostaphin susceptibility of various strains of Staphylococcus aureus, Antimicrob. Agents Chemother. 49 (2005) 3256–3263.

[36] M. Respondek, T. Madl, C. Gobl, R. Golser, K. Zangger, Mapping the orientation of helices in micelle-bound peptides by paramagnetic relaxation waves, J. Am. Chem. Soc. 129 (2007) 5228–5234.
[37] M.V. Sawai, A.J. Waring, W.R. Kearney, P.B. McCray Jr., W.R. Forsyth, R.I. Lehrer, B.F. Tack, Impact of single-residue mutations on the structure and function of ovispirin/novispirin antimicrobial peptides, Protein Eng. 15 (2002) 225–232.
[38] R. Wimmer, K.K. Andersen, B. Vad, M. Davidsen, S. Molgaard, L.W. Nesgaard, H.H. Kristensen, D.E. Otzen, Versatile interactions of the antimicrobial peptide novispirin with detergents and lipids, Biochemistry 45 (2006) 481–497.
[39] V.C. Kalfa, H.P. Jia, R.A. Kunkle, P.B. McCray Jr., B.F. Tack, K.A. Brogden, Congeners of SMAP29 kill ovine pathogens and induce ultrastructural damage in bacterial cells, Antimicrob. Agents Chemother. 45 (2001) 3256–3261.
[40] G. Pintacuda, M.A. Keniry, T. Huber, A.Y. Park, N.E. Dixon, G. Otting, Fast structure-based assignment of 15N HSQC spectra of selectively 15N-labeled paramagnetic proteins, J. Am. Chem. Soc. 126 (2004) 2963–2970.
[41] C.H. Wu, A. Ramamoorthy, S.J. Opella, High-resolution heteronuclear dipolar solid-state NMR spectroscopy, J. Magn. Reson. 109 (1994) 270–272.
[42] A.A. De Angelis, S.J. Opella, Bicelle samples for solid-state NMR of membrane proteins, Nat. Protoc. 2 (2007) 2332–2338.
[43] S. Dvinskikh, U. Dürr, K. Yamamoto, A. Ramamoorthy, A high-resolution solid-state NMR approach for the structural studies of bicelles, J. Am. Chem. Soc. 128 (2006) 6326–6327.
[44] S. Dvinskikh, U. Dürr, K. Yamamoto, A. Ramamoorthy, High-resolution 2D NMR spectroscopy of bicelles to measure the membrane interaction of ligands, J. Am. Chem. Soc. 129 (2007) 794–802.
[45] S. Dufour, M. Deleu, K. Nott, B. Wathelet, P. Thonart, M. Paquot, Hemolytic activity of new linear surfactin analogs in relation to their physico-chemical properties, Biochim. Biophys. Acta 1726 (2005) 87–95.
[46] C.-L. McGregor, L. Chen, N.C. Pomroy, P. Hwang, S. Go, A. Chakrabartty, G.G. Privé, Lipopeptide detergents designed for the structural study of membrane proteins, Nat. Biotechnol. 21 (2003) 171–176.
[47] A. Patist, J.R. Kanicky, P.K. Shukla, D.O. Shah, Importance of micellar kinetics in relation to technological processes, J. Colloid Interface Sci. 245 (2002) 1–15.
[48] P.T. Wong, J.A. Schauerte, K.C. Wisser, H. Ding, E.L. Lee, D.G. Steel, A. Gafni, Amyloid-b membrane binding and permeabilization are distinct processes influenced separately by membrane charge and fluidity, J. Mol. Biol. 386 (2009) 81–96.
[49] D.E.G.a.M.C. Phillips, Proteins at liquid interfaces: I. Kinetics of adsorption and surface denaturation, J. Colloid Interface Sci. 7 (1979) 403–414.
[50] M. Eeman, A. Berquand, Y.F. Dufrene, M. Paquot, S. Dufour, M. Deleu, Penetration of surfactin into phospholipid monolayers: nanoscale interfacial organization, Langmuir 22 (2006) 11337–11345.
[51] A.J. Verkleij, R.F. Zwaal, B. Roelofsen, P. Comfurius, D. Kastelijn, L.L. van Deenen, The asymmetric distribution of phospholipids in the human red cell membrane. A combined study using phospholipases and freeze-etch electron microscopy, Biochim. Biophys. Acta 323 (1973) 178–193.
[52] M. Dathe, T. Wieprecht, H. Nikolenko, L. Handel, W.L. Maloy, D.L. MacDonald, M. Beyermann, M. Bienert, Hydrophobicity, hydrophobic moment and angle subtended by charged residues modulate antibacterial and haemolytic activity of amphipathic helical peptides, FEBS Lett. 403 (1997) 208–212.
[53] T. Wieprecht, M. Dathe, M. Beyermann, E. Krause, W.L. Maloy, D.L. MacDonald, M. Bienert, Peptide hydrophobicity controls the activity and selectivity of magainin 2 amide in interaction with membranes, Biochemistry 36 (1997) 6124–6132.
[54] K. Matsuzaki, M. Fukui, N. Fujii, K. Miyajima, Permeabilization and morphological changes in phosphatidylglycerol bilayers induced by an antimicrobial peptide, tachyplesin I, Colloid Polym. Sci. 271 (1993) 901–908.
[55] G. Fujii, S. Horvath, S. Woodward, F. Eiserling, D. Eisenberg, A molecular model for membrane fusion based on solution studies of an amphiphilic peptide from HIV gp41, Protein Sci. 1 (1992) 1454–1464.
[56] J.E. Cummingsa, T.K. Vanderlick, Aggregation and hemi-fusion of anionic vesicles induced by the antimicrobial peptide cryptidin-4, Biochim. Biophys. Acta 1768 (2007) 1796–1804.
[57] T. Stegmann, R.W. Doms, A. Helenius, Protein-mediated membrane fusion, Annu. Rev. Biophys. Biophys. Chem. 18 (1989) 187–211.
[58] S.T. Henriques, A. Quintas, L.A. Bagatolli, F. Homble, M.A. Castanho, Energy-independent translocation of cell-penetrating peptides occurs without forma-tion of pores. A biophysical study with pep-1, Mol. Membr. Biol. 24 (2007) 282–293.
[59] E.E. Ambroggio, F. Separovic, J.H. Bowie, G.D. Fidelio, L.A. Bagatolli, Direct visuali-zation of membrane leakage induced by the antibiotic peptides: maculatin, citropin, and aurein, Biophys. J. 89 (2005) 1874–1881.
[60] Y. Tamba, M. Yamazaki, Single giant unilamellar vesicle method reveals effect of antimicrobial peptide magainin 2 on membrane permeability, Biochemistry 44 (2005) 15823–15833.
[61] Y. Tamba, S. Ohba, M. Kubota, H. Yoshioka, H. Yoshioka, M. Yamazaki, Single GUV method reveals interaction of tea catechin (−)-epigallocatechin gallate with lipid membranes, Biophys. J. 92 (2007) 3178–3194.
[62] L.R. Montes, A. Alonso, F.M. Goni, L.A. Bagatolli, Giant unilamellar vesicles electroformed from native membranes and organic lipid mixtures under physiological conditions, Biophys. J. 93 (2007) 3548–3554.
[63] L. Dethlefsen, M. McFall-Ngai, D.A. Relman, An ecological and evolutionary perspective on human-microbe mutualism and disease, Nature 449 (2007) 811–818.

Paper III

Co-author statement for Paper III

Magnus Franzmann, Kirstine Lykke Christensen, Daniel Otzen, Reinhard Wimmer: **Structural studies of amphibian antimicrobial peptides in micelle and bicelle phospholipid environments.**

Work in progress

- Magnus Franzmann performed the purification of some of the unlabeled citropin and maculatin, the purification of partly ^{15}N-labeled variants of the peptides, all structure and dynamics measurements in bicelles, dynamics measurements in micelles, all titration experiments in bicelles and wrote the article.
- Kirstine Lykke Christensen performed the purification of some of the unlabeled citropin and maculatin, assigned the NMR signals and calculated the structures in micelles, titrated the micelles with Gd(DTPA-BMA) and did the subsequent PRE calculation. The work was done as part of her master thesis under the supervision of Magnus Franzmann and Reinhard Wimmer.
- Daniel Otzen co-supervised the experiments
- Reinhard Wimmer supervised overall design and execution of the experiments, contributed extensively to the writing of the article.

Kirstine Lykke Christensen _____

Daniel Otzen _____

Reinhard Wimmer _____

Structural Studies of Amphibian Antimicrobial Peptides in Micelle and Bicelle Phospholipid Environments

Magnus Franzmann[a], Kirstine Lykke Christensen[a], Daniel Otzen[b] and Reinhard Wimmer *[a]

In this study, we describe the insertion depth and orientation of two antimicrobial peptides Maculatin 1.1 and Citropin 1.1 from Australian tree frogs in different membrane mimicking environments. Soluble paramagnetic species were used to induce paramagnetic relaxation enhancements (PREs) from which the orientation and insertion depth in micelles and bicelles were determined. Our data suggest that Citropin 1.1 is positioned parallel to the surface of the membrane whereas the interaction of Maculatin 1.1 with the membranes dependents on the charge of the lipid/detergent head groups.

Introduction

Secretion of small peptides with antibiotic properties has been shown to be a vital part of the innate immune system of many organisms. They are typically secreted in tissues that are continuously exposed to the environment like epithelia cells where they act as a first line of defense against microbes. Antimicrobial peptides (AMPs) have attracted considerable amounts of interest for treatment of a rapidly increasing number of microbes with multiresistance phenotypes to traditional antibiotics and they are considered promising candidates as alternative antibiotic agents.[1] Since the characterization of Bombinis by Csordas and Michl in 1969[2, 3] the skin of amphibians like toads and frogs have become one of the riches sources of AMPs with several hundred natural peptides isolated.[4] These peptides are typically cationic peptides consisting of less than 50 amino acids and most of them are unstructured in solution but adopt an α-helical structure in the presence of lipids or other amphipathic molecules.[5] Two overall methods of action for peptides with these characteristic can be described using the Shai-Matsuzaki-Huang model.[6] This postulates that small cationic peptides can either disrupt the cell membrane of the target organisms by forming pores (toroidal or barrel-stave model) or by binding to the surfaces of the microbes in a detergent like manner, leading to displacement of a part of the membrane (carpet model).

The work presented here describes the study of two model peptides that presumably act upon the microbial membranes by either the pore model or the carpet model. The protein groups Citropins and Maculatins consist of amphiphatic α-helix peptides found in the skin secretions of members of the Australian tree frog family.[7] Maculatin 1.1 (hereafter only referred to as maculatin) is a cationic 21 amino acid peptide which has been extracted from the dorsal glands of the frog *Litoria genimacula* and has been shown to have an AMP effect mainly on Gram negative bacteria.[8, 9] It is unstructured in solution but adapts an α-helical structure in TFE/water mixtures or in the presence of membrane mimicking detergents or lipids.[9] The structural studies

in 50% TFE and DPC micelles reveal a slight kink at Pro15 in an approximately 30 Å α-helix which has the length to span the widthof bacterial membranes and to form pores.[9] Citropin 1.1 (hereafter only referred to as citropin) is a 16 amino acid cationic AMP secreted found in the skin secretions of the frog *Litoria citropa*. It shares N-terminal sequential homology with maculatin (see table 1) and is also a peptide that adopts an α-helical structure in membrane mimicking environments.[10] The solution structure of citropin determined in 50% TFE by NMR shows a straight α-helix but the length of this is as opposed to maculatin not sufficiently long to span the bacterial membranes which could indicate a carpet model mode of action.

Direct visualization of leakage of different sized fluorophores from zwitterionic giant unilamellar vesicles (GUVs) upon addition of maculatin or citropin points towards different membrane permeabilizing mechanisms for the two peptides.[11] As maculatin allows passage of small but not large fluorophores these studies suggests that maculatin forms pores in the vesicles. In contrast is the overall structure of membranes exposed to citropin completely destroyed when a critical peptide concentration is reached whereas both small and large fluorophores are retained below this threshold concentration.[11] This indicates that citropin disrupts the membrane through the carpet model. Based upon interpretations of line broadening effect in ^{2}H and ^{31}P solid state NMR spectra it has been suggested that that maculatin inserts

[a] M. Franzmann, K.L. Christensen, Associate Prof. Dr. R. Wimmer
     Department of Biotechnology, Chemistry and Environmenal Engineering,
     Aalborg University
     Sohngaardsholmsvej 49, DK-9000 Aalborg, Denmark
     Fax: (+45)98141808
     E-mail: rw@bio.aau.dk
[b] Prof. Dr. D.E. Otzen
     Interdisciplinary Nanoscience Center (iNANO), Department of Molecular Biology
     Aarhus University
     Gustav Wieds Vej 10 C, DK-8000 Aarhus C, Denmark

deep into the core of anionic bilayers as opposed to zwitterionic bilayers where the peptide binding mostly affects the surface atoms.[12, 13] In contrast does citropins placement near the phosphate head groups appear to be independent of the lipid charge. These finding are supported by surface plasmon resonance (SPR) and Langmuir-monolayer technique studies that like the solid state NMR studies suggest different modes of action for maculatin dependent of the membrane charge.[14] Additional studies by differential scanning calorimetry (DSC) and fourier transform infrared spectroscopy (FTIR) shows a preferred interaction between both maculatin and citropin and bilayers containing 1,2-dimyristoyl-*sn*-glycero-3-phospho-(1'-rac-glycerol)(sodium salt)(DMPG) compared to bilayers with only zwitterionic lipids like 1,2-dimyristoyl-*sn*-glycero-3-phosphatidylcholine (DMPC) or 1,2-ditetradecanoyl-sn-glycero-3-phosphoethanolamine (DMPE).[3, 15] Somehow ambiguous to these combined results are the solid state NMR study of maculatins impact of the phospholipid membranes of live *E. coli* cells. The appearance of isotropic peaks upon addition of maculatin indicates a formation of small micelle structures originating from the disintegration of the cell membrane which corresponds to a carpet model mode of action.[3] Likewise is a considerable disruption of the overall structure of the bacteria *S. aureus* observed by electron microscopy when maculatin are added to the cells.[16] Although these later two examples could be caused by extreme amount of toroidal pores it is apparent that further studies are needed to fully elucidate the membrane disrupting mechanisms of citropin and especially maculatin.

Previous NMR studies have in order to analyze the membrane interaction of maculatin and citropin relied on line broadening effects and chemical shift changes observed on the lipid resonance signals.[12, 13, 17] Although this provides valuable information whether the peptide is surface bound or inserted into the membrane it is due to spectral overlap not possible to unambiguously identify all atoms in the lipid acyl chains hence determining the insertion depth with even low levels of precision. The accuracy is further worsened by the mobility of the lipids where especially the tail regions of the lipids are highly mobile.[18]

Here we present an atomic resolution solution study of citropin and maculatin inserted into detergent micelles and both anionic and zwitterionic phospholipid bicelles. Besides a widespread use in alignment media bicelles are also used as membrane mimicking systems because they presumably provides a more native like lipid environment compared to micelles due to the more planar shape of the bilayers.[19] However, because micelles are considerable smaller and easier to handle than disc shaped bicelles, micelles are more frequently used to study membrane associated proteins and peptides. Questions regarding the biological relevance when studying protein and peptides in detergent micelles have been raised and we therefore compare data from both micelle and bicelles solutions to seen whether the orientation and the immersion depth differs in the two membrane mimicking systems.[19] From distance restrains obtained from NOESY and dihedral angles obtained from HSQC spectra we were able to determine high resolution structures of the peptides incorporated into the membrane mimicking systems. From titrating lipid or detergent bound maculatin and citropin with the water soluble paramagnetic agents Gd(DTPA-BMA) and a polylysine dendrimeric form of 24 Gd(DOTA) complexes (24Gd(DOTA)) we have determined PREs from peptide atoms of interest. The PRE values provided distance information between the free floating paramagnetic centers and the peptide protons.

Because the peptide atoms to different degrees were embedded into the lipids/detergent and thereby inaccessible by the water soluble Gd complexes we have combined the calculated structures with the PRE data to obtain information concerning the orientation and immersion depth of the peptides. To gain a deeper insight into the membrane disrupting mechanisms of the two peptides we have compared the PRE values obtained by the relative small Gd(DTPA-BMA) which presumably are capable of entering any transmembrane pores and the much larger 24Gd(DOTA) polymer which on the other hand is very unlikely to do so.

Table 1	
Peptide	Sequence
Maculatin 1.1	GLFGVLAKVAAHVVPAIAEHF-NH$_2$
Citropin 1.1	GLFDVIKKVASVIGGL-NH$_2$

Results and Discussion

Structure calculations.

The proton signals of the two peptides citopin and maculatin in the presents of DPC detergent micelles were assigned with the aid of sets of homonuclear DQF-COSY, TOCSY and NOESY spectra and the carbon signals were assigned with the aid of ^{1}H,^{13}C-HSQC spectra recorded at natural abundance. For each peptide 80 structures were calculated based on distance restraints derived from NOE integrals and dihedral angle restraints obtained from the chemical shift values using the software program TALOS.[20] The 20 structures with the lowest residual target function were collected for both citropin and
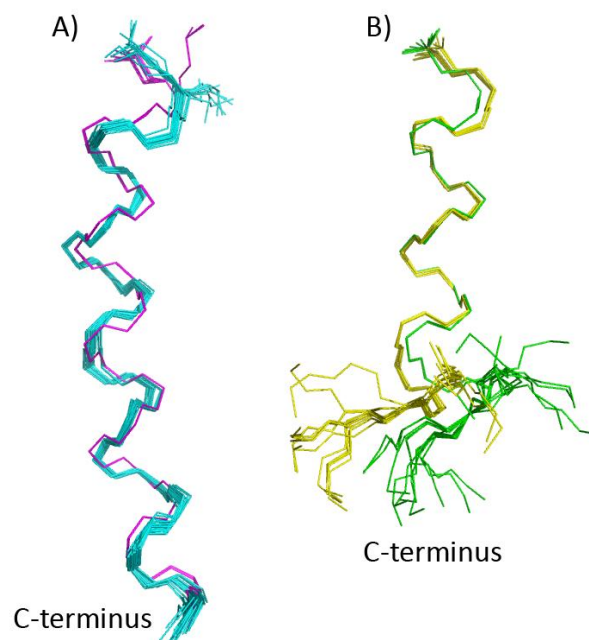
Figure 1 A) Overlay of maculatin structures in the presence of DPC micelles (magenta) or DMPC/DHPC bicelles (cyan). B) Overlay of citropin structures in the presence of DPC micelles (green) and DMPC/DHPC bicelles (yellow). All bundles show the 20 structures with the lowest residual target functions, with N, C' and C$^\alpha$ from residues 2-20 and 2-12 aligned for maculatin and citropin respectively.

2

Table 2. Quality Criteria for the Calculated Structures				
	Maculatin (DPC)	Citropin (DPC)	Maculatin (DMPC/DHPC)	Citropin (DMPG/DMPC/DHPC)
number of distance constraints	200	153	112	152
- of which intraresidual	119	97	60	83
- of which sequential	48	30	39	52
- of which medium-range ($2 \leq \Delta_{res} \leq 4$)	33	26	13	17
number of angle constraints[a]	22	20	22	20
- of which φ	11	10	11	10
- of which ψ	11	10	11	10
CYANA residual target function	0.21 ± 0.02 Å^2	0.097 ± 0.002 Å^2	0.16 ± 0.028 Å^2	0.54 ± 0.036 Å^2
distance restraints violated by more than 0.2Å	0	0	0	0
angle restraints violated more than 5°[b]	0	0	0	0
rmsd residues 2-20 (mac) or 2-15 (cit)[c]	0.04 ± 0.03 Å	0.21 ± 0.01 Å	0.30 ± 0.11 Å^2	0.74 ± 0.19 Å^2
% of residues in Ramachandran plot [d]				
- in most favored regions	98.2	100	96.5	91.7
- less favored regions	1.8	0	3.2	8.3
- generously allowed regions	0	0	0.3	0
- disallowed regions	0	0	0	0

(a) Only those derived from TALOS, (b) Per molecule, (c) For backbone atoms C', C$^\alpha$ and N, as calculated by CYANA from the pair wise rmsd values of each of the 20 structures against a mean structure, (d) as calculated by PROCHECK_NMR

maculatin and least squared fits are shown in figure 1. Key values of the structure calculations are listed in table 2. Neither the reported structure of citropin[10] nor maculatin[9] have been submitted to the Biological Magnetic Resonance Data Bank (www.bmrb.wisc.edu/) and it is therefore not possible to compare them in details to our structure. However, roughly based on the published figures our calculated structures appear to be highly similar to both citropin dissolved in 50% TFE[10] and maculatin dissolved in 50% TFE and DPC[9]. Maculatin forms a slightly curved and clearly amphiphatic α-helix with the hydrophilic residues Gly1, Gly4, Lys8, Ala11, His12, Gly15, Ala16, Glu19, His20 located on one side of the helix. Citropin is likewise an amphipathic α-helix with the hydrophilic Gly1, Asp4, Lys7, Lys8, Gly14, Gly15 located on one side of the helix, however, the α-helical axis of citropin is more straight compared to maculatin.

Bicelles solutions with lipid concentrations of 15% (w/v) and a long chained lipid to short chain lipid ratio of 0.5 e.g. ([DMPG]+[DMPC])/[DHPC]=0.5 have been shown to be highly suitable for NMR studies of membrane associated proteins and peptides.[19, 21] They form approximately discoid lipid bilayers with a diameter of 80-100 Å and a thickness of ~50 Å consisting of long chained lipids which are rimmed by short chained lipids thus shielding the hydrophobic tails of the lipids from the surrounding water and thereby stabilizing the overall structure.[19, 21, 22] The relaxation properties of proton coherences are very fast in bicelles which makes it very difficult to observe any J coupling hence any signals in COSY, TOCSY or HSQC type spectra.[23] However, dipole-dipole interactions observed in NOESY type spectra were clearly observable although due to the size of the DMPC/DHPC bicelles the line width of the maculatin and citropin

signals were considerable broadened when studied in bicelles compared to the in the much smaller DPC micelles. DMPC and DMPG are to our knowledge not commercially available in fully deuterated forms but merely as partly deuterated where only the hydrogens of the lipid tails are replaced by deuterium. By using these partly deuterated lipids and applying a selective pulse and transverse signal cancellation using pulsed field gradient we were able to suppress most of the very strong and disturbing lipid signals. Only minor chemical shift differences were observed between citropin and maculatin dissolved in DPC and bicelle solutions. The assignments of the NOESY peaks from the peptides in DPC solutions were therefore used as basis for the assignment of citropin and maculatin in bicelle solutions, although due to broader peptide signals in bicelles solutions a lower amount of signals were observed. Similar to the structure determination of citropin and maculatin in DPC solutions the reduced numbers of distance restraints in bicelles solutions obtained from NOEs and dihedral angle constrains obtained from chemical shifts (although merely from proton chemical shifts) were used as input for the structure calculation program. From 80 calculated structures the 20 with the lowest residual target function were collected (see figure 1). The RMSD between maculatin dissolved in DPC and DMPC/DHPC solutions is 1.36 Å and between citropin in DPC and DMPG/DMPC/DHPC solutions it is 0.86 Å. Key values of the structure calculations are listed in table 2.

Paramagnetic relaxation enhancements

PRE values of the H$^\alpha$ atoms of citropin and maculatin in DPC micelles have been obtained by titrating the samples with
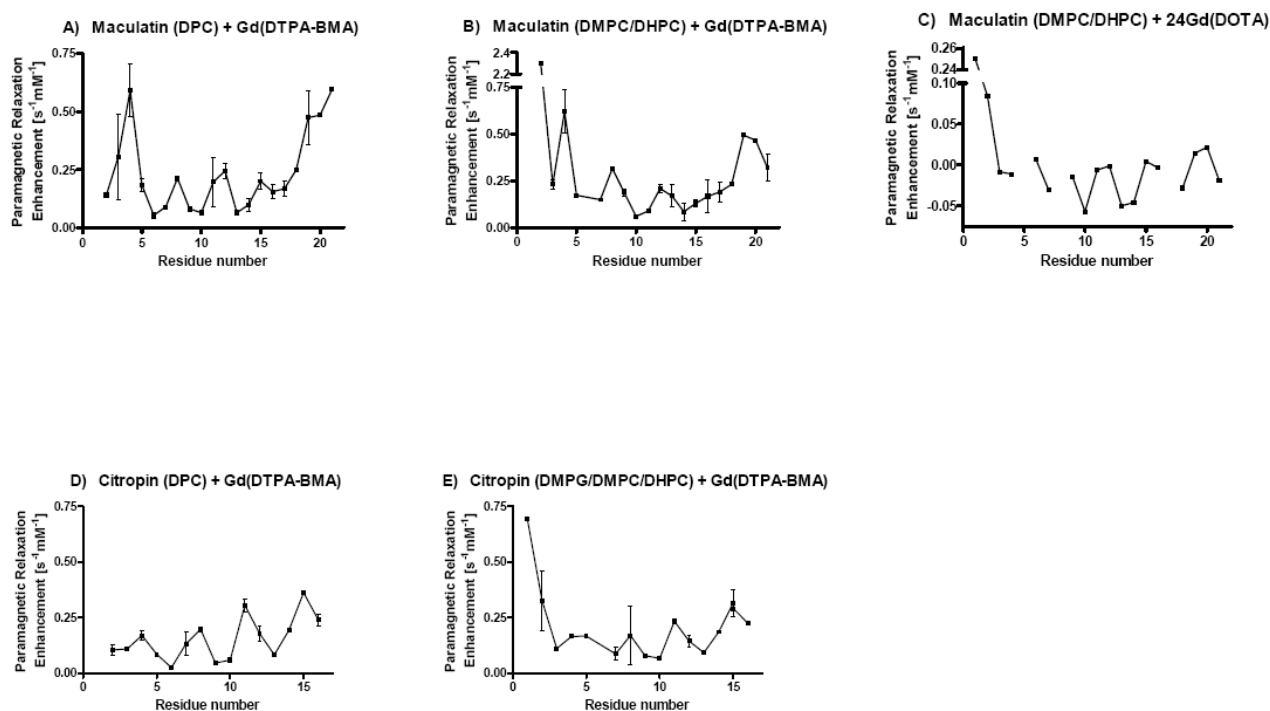
Figure 2 PRE values for Hα nuclei of (A) maculatin in DPC titrated with Gd(DTPA-BMA), (B) maculatin in DMPC/DHPC titrated with Gd(DTPA-BMA), (C) maculatin in DMPC/DHPC titrated with 24Gd(DOTA), (D) citropin in DPC titrated with Gd(DTPA-BMA) and (E) citropin in DMPC/DHPC titrated with Gd(DTPA-BMA). Error bars indicate variations in PRE values obtained from fitting several peaks.

Table 3							
Citropin		Val5	Ala10	Gly14	Gly15	Leu16	
Citropin (DPC)	T_1 (s^{-1})	0.60 ± 0.011	0.55 ± 0.005	0.60 ± 0.010	0.71 ± 0.037	0.70 ± 0.025	
	T_2(s^{-1})	0.12 ± 0.006	0.17 ± 0.012	0.15 ± 0.009	0.16 ± 0.012	0.13 ± 0.007	
Maculatin		Leu2	Val9	Ala11	Val13	Gly15	Phe21
Maculatin (DPC)	T_1 (s^{-1})		1.08 ± 0.34	8.18 ± 0.094	1.27 ± 0.54	0.97 ± 0.26	1.43 ± 0.60
	T_2(s^{-1})		0.095 ± 0.0047	0.097 ± 0.012	0.096 ± 0.0048	0.095 ± 0.0030	0.13 ± 0.0063
Maculatin (DMPG/DMPC/DHPC)	T_1 (s^{-1})	0.94 ± 0.007	0.79 ± 0.172	0.86 ± 0.016	0.86 ± 0.014	0.95 ± 0.024	0.84 ± 0.011
	T_2(s^{-1})	0.036 ± 0.0013	0.053 ± 0.013	0.035 ± 0.0012	0.035 ± 0.0012	0.044 ± 0.0011	0.034 ± 0.0004

Gd(DTPA-BMA) and the values plotted as a function of the residue numbers (see figure 2). For both peptides a wavelike pattern with a wavelength between 3-4 residues are observed spanning the entire length of the peptides which is characteristic for α-helices lying parallel to the surface of micelles as previously described.[24, 25] The PRE maxima of maculatin are observed for Gly4, Lys8, His12, Gly15, Glu19, His20 and Phe21 which corresponds to the hydrophilic side of the structure with exception of the C-terminal phenylalanine. The PRE values of protons depend on the inverse of the third power of the distance between the measured nuclei and the paramagnetic center when using a free-floating noninvasive paramagnetic agent like Gd(DTPA-BMA).[24, 25, 26] It can therefore be assumed that when comparing PRE values relative to each other, the ones with the highest PRE values must be located nearer towards the paramagnetic agent and hence towards the solution. It is therefore clear that the hydrophilic side of the peptide is facing the outside of the micelles as would be expected. The PRE values with the highest values observed for citropin are Asp4, Lys8, Ser11 and Gly15 which like maculatin is located on the hydrophilic side of the peptide.

PRE values and hence the calculated distances between the peptide atoms and micelles center are dependent of the dynamical properties of the molecules as can be seen from eq. 3 and 4.[27] Therefore, it is not straightforward to calibrate PRE values on one system with known distances and then to apply this calibration on a different molecular system with potentially different dynamic behavior. There, we have investigated the dynamic properties of DPC, maculatin and citropin in micelles and maculatin in bicelles. Residue specific T_1 and T_2 relaxation times were obtained for selected ^{15}N labeled amino acids in the

4

two peptides dissolved in DPC micelles or maculatin in DMPG/DMPC/DHPC bicelles and the values are listed in table 3.[28] From the average values of T_1/T_2 we have calculated the correlation times (τ_r) of the peptides as described previously by Clore et al. to $1.01 * 10^{-8}$ s, $1.55 * 10^{-8}$ s, and $5.9 * 10^{-9}$ s for maculatin in micelles, maculatin in bicelles and citropin in micelles, respectively.[29] For DPC we have calculated a correlation time based on correlation times obtained from Beswick et al.[30] They measure τ_L (correlation time characterizing the internal motion) to ~80 ps at 285 K and ~50 ps at 298 K from which we have extrapolated τ_L to be 33.8 ps at 310 K. The overall correlation time for the micelle was calculated from the equations[31]:

$$\tau_m = \frac{4\pi\eta r^3}{3kT} \text{ and } D = \frac{kT}{6\pi\eta r} \quad (1)$$

where η is the viscosity, r is the radius of the micelle, k the Boltzmann constant, T the temperature and D is the diffusion constant. We have measured the diffusion constant for a DPC micelle to $1 * 10^{-10}$ m^2/s at 310 K and by assuming a micelle radius of 22.5 Å we have calculated τ_m to $1.13 * 10^{-8}$ s. The effective correlation time is given by:

$$\tau_R = \frac{1}{S^2/\tau_m + \left(\dfrac{S^2-1}{\tau_L}\right)} \quad (2)$$

where S^2 is the order parameter, τ_m is the correlation time of overall ensemble motion and τ_L is the correlation time of the internal motions. By inserting the order parameters, the extrapolated τ_L from Beswick et al.[30] and the calculated τ_m we have calculate the effective correlation time for micelle bound DPC to $4.22 * 10^{-11}$ s.

To be able to compare the obtained τ_R values impact on R_1 relaxation (PREs) we have plotted the proton relaxation rates as a function of the correlation time as calculated from eq. 3 and 4 (see figure 3):

$$PRE = \frac{2}{15}\left(\frac{\mu_0}{4\pi}\right)^2 \frac{\gamma_I^2\ g_J\mu_B^2\ J\ J+1}{r^6}\left(\frac{3\tau_c}{1+\omega_H^2\tau_c^2}+\frac{7\tau_c}{1+\omega_S^2\tau_c^2}\right) \quad (3)$$

$$\frac{1}{\tau_c} = \frac{1}{T_{1e}}\frac{1}{\tau_M}\frac{1}{\tau_R} \quad (4)$$

where J is the electronic spin, r the distance between the electron and ^{1}H spin, μ_0 is the magnetic susceptibility in vacuum, γ_H the ^{1}H gyromagnetic ratio, g_J the Landé factor, μ_B the Bohr magneton
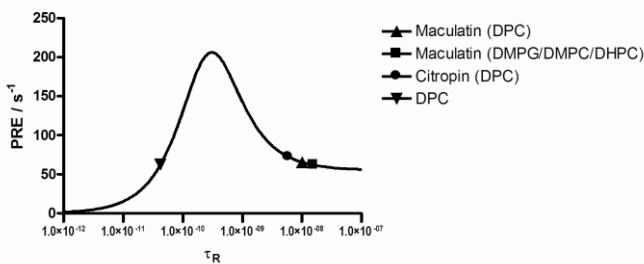
Figure 3 PRE plotted as a function of τ_R. Correlation times for DPC(▼), maculatin in DPC micelles (▲), maculatin in DMPG/DMPC/DHPC bicelles (■) and citropin in DPC micelles(●)

and ω_H and ω_S the Larmor frequencies of the ^{1}H and electron spin, respectively, τ_M is the lifetime of the intermolecular adducts (estimated to 2.4 ns based on τ_c and τ_R values from[25, 27]), τ_r the correlation time of the molecules in question and T_{1e} the electron relaxation time ($1 * 10^{-8}$).[27, 32]

Eq. 3 and 4 are only valid when both the paramagnetic species and the nuclear spin whose PRE is observed, are attached to the same rigid molecular framework. If the paramagnetic species floats freely, the PRE only depends on the inverse 3rd power of r[24, 25]:

$$PRE = \frac{2}{15}\left(\frac{\mu_0}{4\pi}\right)^2 \frac{\gamma_I^2\ g_J\mu_B^2\ J\ J+1}{r^3}\left(\frac{3\tau_c}{1+\omega_H^2\tau_c^2}+\frac{7\tau_c}{\omega_S^2\tau_c^2}\right) \quad (5)$$

The effective correlation time of DPC give a PRE value of 63 s^{-1} compared to 62, 66 and 73 s^{-1} for maculatin in bicelles, maculatin in micelles and citropin in micelles, respectively (the values are plotted in figure 3). It therefore turns out that, despite large differences in correlation times between DPC and peptide atoms, the correlation time dependent term of eq. 3 and 4 are most fortunately very similar for DPC and for citropin and maculatin. It is therefore possible to calibrate the distance dependence of PREs on DPC and use the calibration on PREs measured for the peptides embedded in the micelles.[24] Taken into consideration that the calculated distances are dependent on the inverse third power of the PREs (eq. 5) an error in PRE calibration due to differences in correlation times translates to a mere cubic root of this error in determined distance. For citropin in micelles, which is the value with the largest τ_c difference from DPC, the error in distance is approximately 5%.

H^α PRE values of citropin and maculatin have been converted into distances to their respective micelle centers. The distances are plotted in figure 4. These distances have then been converted to distance restraints and used as input for the structure calculation program alongside the distance restraints derived from NOEs and chemical shifts as described previously.[24] From is seen that both citropin and maculatin are positioned near the surface of the micelles and that the hydrophilic side chains together with the N and C termini of both citropin and maculatin are located in the DPC/solution interface.

PRE values of H^α atoms of maculatin in DMPC/DHPC bicelles have been obtained by titrating the bicelles with Gd(DTPA-BMA) and the values have been plotted as a function of the residue
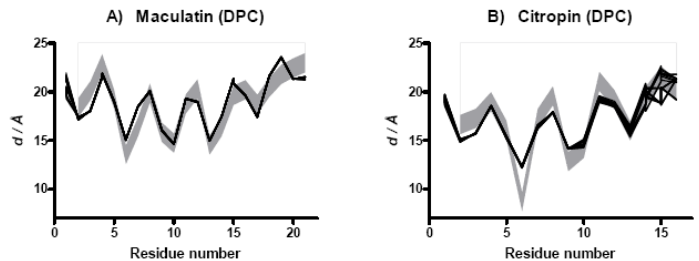
Figure 4 Black lines show the calculated distances between H^α atoms of the 20 structures with the lowest residual target function and the center of the micelle. The gray area defines the range between the upper and lower distance restraints, based on the PRE values of the H^α atoms. Restraints are obtained from the average PRE values of maculatin (A) and citropin (B) ± 1 Å. d corresponds to the distance to the micelle center.
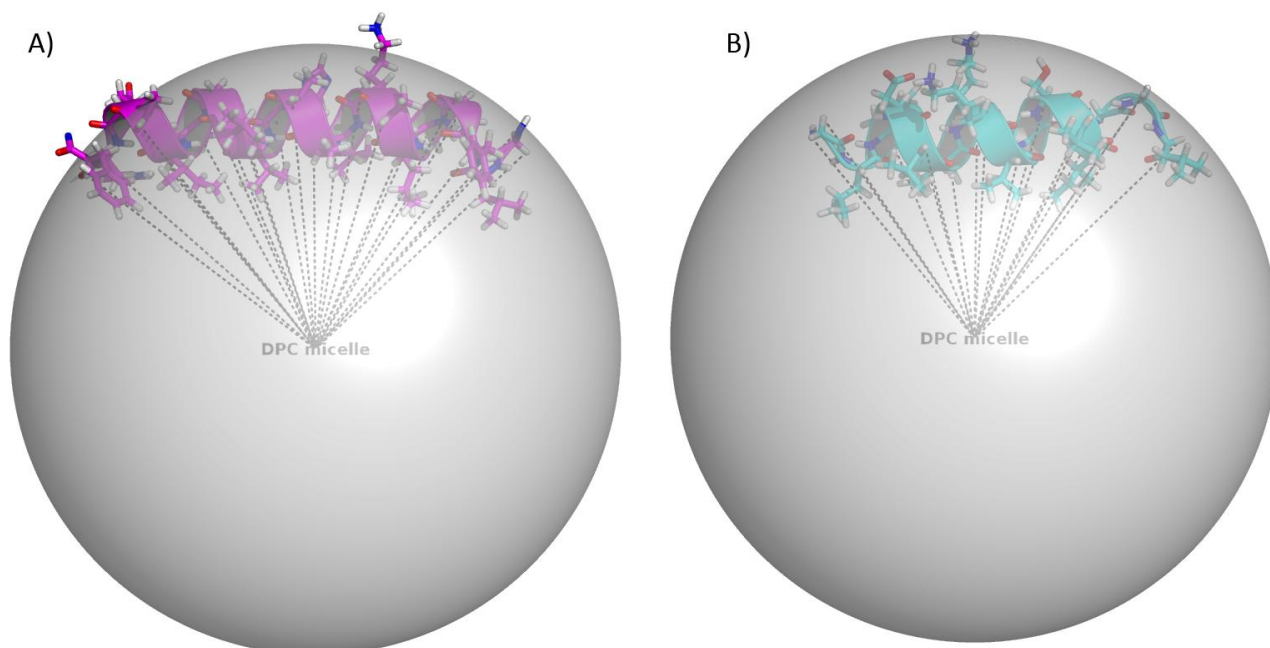
Figure 5 The structures of maculatin (A) and citropin (B) with the calculated distances to the micelles centers depicted as dotted lines. Spheres of 45.2 Å diameters are shown to illustrate the approximate size of DPC micelles.

numbers (see figure 2). Despite difficulties obtaining high quality data due to increased signal line width, it is possible to observe tendencies in the PRE curves. The PRE maxima of the maculatin H^α atoms titrated with Gd(DTPA-BMA) are observed for Leu2, Gly4, Lys8, His12 and Glu19 which is identical with the PRE maxima of maculatin in DPC micelles except from Leu2, the absence of Gly15 and lower values of the C-terminal residues His20 and Phe21. These data clearly points to maculatin as positioned at the surface of the zwitterionic bicelles. However, if maculatin were forming toroidal pores with a internal diameter large enough for the passage of Gd(DTPA-BMA) molecules with a diameter of 7 Å[27] the hydrophilic residues would still be facing the solution hence the paramagnetic agent and a wavelike pattern would still be observed. We therefore titrated DMPC/DHPC bicelles with 24Gd(DOTA) which is very unlikely to travel through pores due to the much larger size.[11] The resulting PRE values gave somehow ambiguous data (see figure 2). Although it is difficult to determine the maximum values of the PRE curve due to missing data the residues Gly1, His12, Gly15 and His20 appear to be peak values. This would correspond well to the maxima of maculatin in DPC micelles which also had maximum values at His12, Gly15, His20 in addition to Gly4, Lys8, Glu19 and Phe21. More worrying is the fact that some of the PREs have negative values which should not be possible. One should obviously be careful drawing conclusions based on these data however there are indications that maculatin remains to be positioned near the head groups of the bicelles lipids like it is seen in DPC micelles.

Despite great interest (and efforts) we have not been successful in acquiring useful PRE values for maculatin in anionic DMPG/DMPC/DHPC bicelles. As has been observed by Marcotte et al.[13] the bicelles are disrupted by insertion of amphibian AMPs over the relative long acquisition time (> 1 day) for the NMR experiments. The disruption causes a visible milky precipitate in the NMR tube and the signals are consequently broadened beyond detection due to the size of the aggregates. Interestingly

does maculatin cause precipitation in the anionic bicelles much faster (<1 day) compared to in zwitterionic bicelles where the solution stays clear for well over a week. As has been observed by several other groups this is a clear indication that maculatins affinity and likely also its mode of action is different in anionic lipids compared to in zwitterionic lipids.[12, 13]

Citropin in DMPG/DMPC/DHPC bicelles did not precipitate over time as observed for the maculatin sample and we were therefore able obtain PRE values by titrating the sample with Gd(DTPA-BMA). The values have been plotted as a function of the residue numbers (see figure 2), and the PRE maxima of the citropin H^α atoms are observed for Gly1, Asp4/Val5, Lys8, Ser11, Gly15 which is identical to the PRE maxima observed in micelles except that a data point for Gly1 H^α can be obtained, because Leu2 H^N is observable in the bicelles sample. Combined with knowledge of citropin's mode of action from previously published studies[11] this clearly indicates that citropin acts by the carpet model due to its apparent position at the solution/lipid interface of the bicelles.

Conclusion

We have used PRE values of H^α atoms in both a qualitative and quantitative manner to obtain information concerning the orientation and immersion depth into membrane mimicking environments of the two model AMPs citropin and maculatin. Compared to previously published studies of citropin's and maculatin's interaction with lipids and detergents at low resolutions[3, 11, 12, 13, 14, 15, 17], our data provides results at atomic resolution in micelles and bicelles from where conclusions can be drawn to their antimicrobial mode of action. In agreement with these previously studies our data shows that both citropin and maculatin forms amphipathic α-helical structure in the presents of detergent or lipids, and that both peptides are located in at the water/detergent interface near the head groups of the zwitterionic

DPC micelles. Furthermore does our data suggest that citropin and maculatin are likewise positioned at the surface of DMPG/DMPC/DHPC and DMPC/DHPC bicelles, respectively, which is also in agreement with previous publications.[12, 13] As the data obtained in micelles are highly similar to the data obtained in bicelles (and therefore also likely at bacterial membranes), our data suggests that simple micelle systems are well suited to determine the structure and position of membrane associated peptides and at least AMPs positioned parallel to the surface of the membrane. Because we were unable to measure PRE values of maculatin in anionic bicelles due to significantly reduced stability of the samples we have been unable to measure whether maculatin forms transmembrane pores under these lipid conditions. However, the altered bicelles stability properties induced by the addition of maculatin clearly indicated that the peptide interacts differently with the anionic lipids however it is not possible based on these observations to conclude if there is any changes in its mode of action. Further studies of maculatin are clearly needed in order to fully elucidate the membrane penetrating mechanism of the peptide.

Experimental Section

Materials. DPC, DHPC, DMPC and DMPG were purchased from Avanti Polar Lipids (USA) and DPC-d$_{38}$, DMPC-d$_{54}$, DMPG-d$_{54}$ and DHPC-d$_{22}$ as well as ^{15}N labeled FMOC Leu, Val, Ala, Phe and Gly were purchased from Cambridge Isotope Laboratories Inc. (USA). Gadomer17 (24Gd(DOTA)) were purchased from InvivoContrast (Germany) and Omniscan (Gd(DTPA-BMA)) was generously provided by Aalborg Hospital. Wang resins and Rink-Amide MBHA resin were obtained from Iris Biotech GmbH (Germany) and Fmoc-L-amino acids from Advanced ChemTech (USA).

Solid Phase Synthesis. Both partially ^{15}N labeled and unlabeled maculatin and citropin were synthesized by solid phase peptide synthesis on an Activo-P11 Automated Peptide Synthesizer (Activotec, Cambridge, UK). Wang resins were preloaded with Rink-Amide MBHA resin. 25% piperidine in dimethyldformamide (DMF) was used for FMOC deprotection of all resins and amino acids, and 0.5 M HOBt/HBTU in DMF were used for activation of the amino acids. The amino acid couplings were performed using 1 M diisopropylethylamine (DIPEA) in DMF under nitrogen atmosphere with coupling times of 60 min. Dichloromethane (DCM) was used for final washing and the peptides were cleaved from the resin using 2 mL 95:2.5:2.5 (v/v/v) mixture of trifluoroacetic acid/triisopropylsilane/H$_2$O with a cleaving time of 60 min. The peptides were precipitated with 10 mL cold diethyl ether and centrifuged at 300 g for 10 min (4 ^{o}C). The supernatant was removed and the pellet containing the peptide was washed twice with cold diethyl ether before lyophilizing.

Reverse phase HPLC purification of the peptides were performed on a UltiMate 3000 LC system (Dionex, USA) with a C18 semi-preparative column (Luna 5u C18(2), Phenomenex). The solid phase synthesis product were dissolved in a small amount of DMSO and subsequently diluted with 0.1% TFE in H$_2$O and applied to the column. Purification was achieved using a linear gradient from 20 to 100 % of eluant A acetonitrile. 0.1% TFA was always present. The flow rate of 5 mL/min over 30 min. Fractions of interest were collected and pooled before dilution with H$_2$O and lyophilizing.

MALDI-TOF Mass spectrometry was used for verification of the synthesis product. Peptides were dissolved in 5% (v/v) formic acid in H$_2$O and mixed 1:1, 1:2 and 1:3 with saturated sinapinic acid (SA) followed by sonication and centrifugation. 1 μL of the solutions was dried on a MALDI-TOF target plate and data were recorded using a Bruker Reflex III spectrometer (Bruker-Daltronics, Germany).

NMR samples. Both 2 mM maculatin and 2 mM citropin were dissolved in 90 mM DPC-d$_{38}$, 10 mM phosphate buffer, 0.05% (w/v) NaN$_3$, 5% (v/v) D$_2$O, pH 6 to final volumes of 500 μL. Furthermore were either 2 mM maculatin or 2 mM citropin mixed with 1,2-dimyristoyl(d54)-sn-glycero-3-phosphatidylcholine (DMPC) and if stated 1,2-dimyristoyl(d54)-sn-glycero-3-phospho-(1'-rac-glycerol)(sodium salt) (DMPG) both dissolved in 10 mM phosphate buffer, 0.05% (w/v) NaN$_3$, 5% (v/v) D$_2$O, pH 6. The solutions were subjected to a series of heat/cold/vortex cycles before mixing with 1,2-dihexanoyl(d22)-sn-glycero-3-phosphocholine in 10 mM phosphate buffer, 0.05% (w/v) NaN$_3$, 5% (v/v) D$_2$O, pH 6 to give final volumes of 300 μL and lipid concentrations of 15 % (w/v) with a long/short lipid ratio (q) of 0.5. Peptide samples with selectively ^{15}N labeled amino acids (Leu2, Val9, Ala11, Val13, Gly15, Phe21 in maculatin and Leu2, Val5, Ala10, Gly14, Gly15, Leu16 in citropin) were prepared in DPC-d$_{38}$ solutions as described above. Selectively labeled maculatin was furthermore prepared in a [2]H-DMPG/DMPC/DHPC solution as described above.

NMR recording. All NMR spectra were recorded at 310 K on a BRUKER DRX600 spectrometer operating at a field strength of 14.1 T, equipped with a TXI(H/C/N) probe with triple-axis gradients. NOESY, TOCSY, DQF-COSY and ^{1}H,^{13}C-HSQC spectra were recorded for maculatin and citropin samples dissolved in DPC as described previously.[24] NOESY spectra were recorded for maculatin and citropin dissolved in lipid mixtures. Assignment of all NMR spectra was performed using the program CARA version 1.5.5.[33] NOE cross peaks were subsequently integrated using the NEASY subroutine of CARA[34]. Backbone torsion angle restraints were obtained from chemical shift values using the program TALOS[20] and the CALIBA[35] subroutine in CYANA was used to convert integrated cross-peak intensities from the NOESY spectra into distance constraints. These combined constraints provided the input for the structure calculation using the torsion angle dynamics program CYANA[36]. Structure calculations were started from 80 conformers with random torsion angle values and the 20 structures with the lowest CYANA target function were collected and analyzed using Pymol.[37]

For the PRE measurement, the samples were titrated with either Gd(DTPA-BMA) to final concentrations of 2, 5 and 10 mM or with 24Gd(DOTA) to final concentrations of 0.1 and 0.2 mM. For the two samples containing either maculatin or citropin in the presence of DPC eight inversion recovery NOESY spectra with recovery delay times of 1, 50, 150, 400, 700, 1200, 2600 and 4000 ms were recorded on the samples without paramagnetic agents and for each titration point in order to obtain the T$_1$ relaxation time. For the two samples containing maculatin and citropin in the presence of lipid mixtures six inversion recovery NOESY spectra with recovery delay times of 1, 150, 400, 700, 1200 and 2600 ms were recorded on the samples without paramagnetic agents and for each titration point in order to obtain the T$_1$ relaxation time. T$_1$ and T$_2$ relaxation times of the NH groups at the selectively labeled amino acids of maculatin and citropin were obtained using pulse sequences described by Kay et al.[28] For T$_1$ experiments relaxation delays of 1, 200, 400, 800, 1600, 5000 ms were used and for T$_2$ experiments relaxation delays of 0, 16, 31, 63, 130, 250 ms were used. All spectra were processed using Topspin version 1.3. Assignment of all NMR spectra were performed using the program CARA version 1.5.5[33] and cross peaks were subsequently integrated using the NEASY subroutine of CARA.[34]

[1]   M. Zasloff, *Nature* **2002**, *415*(6870), 389-395.

[2]   A. Csordás, H. Michl, *Toxicon* **1969**, *7*(2), 103-108.

[3]   C. S. Chia, J. Torres, M. A. Cooper, I. T. Arkin, J. H. Bowie, *FEBS Lett* **2002**, *512*(1-3), 47-51.

[4]   M. A. Apponyi, T. L. Pukala, C. S. Brinkworth, V. M. Maselli, J. H. Bowie, M. J. Tyler, G. W. Booker, J. C. Wallace, J. A. Carver, F. Separovic, J. Doyle, L. E. Llewellyn, *Peptides* **2004**, *25*(6), 1035-1054.

[5]   M. Simmaco, G. Mignogna, D. Barra, *Biopolymers* **1998**, *47*(6), 435-450.

[6]   K. Matsuzaki, *Biochim Biophys Acta* **1999**, *1462*(1-2), 1-10; L. Yang, T. M. Weiss, R. I. Lehrer, H. W. Huang, *Biophys J* **2000**, *79*(4), 2002-2009; Y. Shai, *Biochim Biophys Acta* **1999**, *1462*(1-2), 55-70.

[7]   D. I. Fernandez, J. D. Gehman, F. Separovic, *Biochim Biophys Acta* **2009**, *1788*(8), 1630-1638.

[8]   T. Rozek, R. J. Waugh, S. T. Steinborner, J. H. Bowie, M. J. Tyler, J. C. Wallace, *J Pept Sci* **1998**, *4*(2), 111-115.

[9]   B. C. Chia, J. A. Carver, T. D. Mulhern, J. H. Bowie, *Eur J Biochem* **2000**, *267*(7), 1894-1908.

[10]   K. L. Wegener, P. A. Wabnitz, J. A. Carver, J. H. Bowie, B. C. Chia, J. C. Wallace, M. J. Tyler, *Eur J Biochem* **1999**, *265*(2), 627-637.

[11]   E. E. Ambroggio, F. Separovic, J. H. Bowie, G. D. Fidelio, L. A. Bagatolli, *Biophys J* **2005**, *89*(3), 1874-1881.

[12]   J. D. Gehman, F. Luc, K. Hall, T. H. Lee, M. P. Boland, T. L. Pukala, J. H. Bowie, M. I. Aguilar, F. Separovic, *Biochemistry* **2008**, *47*(33), 8557-8565.

[13]   I. Marcotte, K. L. Wegener, Y. H. Lam, B. C. Chia, M. R. de Planque, J. H. Bowie, M. Auger, F. Separovic, *Chem Phys Lipids* **2003**, *122*(1-2), 107-120.

[14]   E. E. Ambroggio, F. Separovic, J. Bowie, G. D. Fidelio, *Biochimica et Biophysica Acta (BBA) - Biomembranes* **2004**, *1664*(1), 31-37.

[15]   G. W. Seto, S. Marwaha, D. M. Kobewka, R. N. Lewis, F. Separovic, R. N. McElhaney, *Biochim Biophys Acta* **2007**, *1768*(11), 2787-2800.

[16]   T. L. Pukala, J. H. Bowie, V. M. Maselli, I. F. Musgrave, M. J. Tyler, *Nat Prod Rep* **2006**, *23*(3), 368-393.

[17]   M. S. Balla, J. H. Bowie, F. Separovic, *Eur Biophys J* **2004**, *33*(2), 109-116.

[18]   F. Aussenac, M. Laguerre, J.-M. Schmitter, E. J. Dufourc, *Langmuir* **2003**, *19*(25), 10468-10479.

[19]   R. R. Vold, R. S. Prosser, A. J. Deese, *J Biomol NMR* **1997**, *9*(3), 329-335.

[20]   G. Cornilescu, F. Delaglio, A. Bax, *J Biomol NMR* **1999**, *13*(3), 289-302.

[21]   D. Lee, K. F. Walter, A. K. Bruckner, S. Hilty, C. Becker, C. Griesinger, *J Am Chem Soc* **2008**, *130*(42), 13822-13823.

[22]   K. J. Glover, J. A. Whiles, G. Wu, N. Yu, R. Deems, J. O. Struppe, R. E. Stark, E. A. Komives, R. R. Vold, *Biophys J* **2001**, *81*(4), 2163-2171.

[23]   J. Dittmer, L. Thogersen, J. Underhaug, K. Bertelsen, T. Vosegaard, J. M. Pedersen, B. Schiott, E. Tajkhorshid, T. Skrydstrup, N. C. Nielsen, *J Phys Chem B.* **2009**, *113*(19), 6928-6937.

[24]   M. Franzmann, D. Otzen, R. Wimmer, *Chembiochem* **2009**, *10*(14), 2339-2347.

[25]   M. Respondek, T. Madl, C. Gobl, R. Golser, K. Zangger, *J Am Chem Soc* **2007**, *129*(16), 5228-5234.

[26]   Z. Luz, S. Meiboom, *J Chem Phys* **1964**, *40*, 2686-2692; Z. Luz, S. Meiboom, *J Chem Phys* **1964**, *40*(4), 1058-1066.

[27]   G. Pintacuda, G. Otting, *J Am Chem Soc* **2002**, *124*(3), 372-373.

[28]   L. E. Kay, D. A. Torchia, A. Bax, *Biochemistry* **1989**, *28*(23), 8972-8979.

[29]   G. M. Clore, P. C. Driscoll, P. T. Wingfield, A. M. Gronenborn, *Biochemistry* **1990**, *29*(32), 7387-7401.

[30]   V. Beswick, R. Guerois, F. Cordier-Ochsenbein, Y. M. Coic, H. D. Tam, J. Tostain, J. P. Noel, A. Sanson, J. M. Neumann, *Eur Biophys J* **1999**, *28*(1), 48-58.

[31]   M. R. Wand Aj Fau - Ehrhardt, P. F. Ehrhardt Mr Fau - Flynn, P. F. Flynn, (0027-8424 (Print)).

[32]   D. H. Powell, O. M. N. Dhubhghaill, D. Pubanz, L. Helm, Y. S. Lebedev, W. Schlaepfer, A. E. Merbach, *Journal of the American Chemical Society* **1996**, *118*(39), 9333-9346.

[33]   R. Keller, 'OPTIMIZING THE PROCESS OF NUCLEAR MAGNETIC RESONANCE SPECTRUM ANALYSIS AND COMPUTER AIDED RESONANCE ASSIGNMENT' obtained from the website www.nmr.ch.

[34]   C. Bartels, T. Xia, M. Billeter, P. Güntert, K. Wüthrich, *J. Biomol NMR* **1995**, *6*(1), 1-10.

[35]   P. Guntert, W. Braun, K. Wuthrich, *J Mol Biol* **1991**, *217*(3), 517-530.

[36]   P. Guntert, C. Mumenthaler, K. Wuthrich, *J Mol Biol* **1997**, *273*(1), 283-298.

[37]   W. L. DeLano, *The PyMOL Molecular Graphics System*, www.pymol.org **2002**.

Paper IV

Co-author statement for Paper IV

Magnus Franzmann, Daniel Otzen, Reinhard Wimmer: **Stereospecific assignment of protein NMR resonances using paramagnetic environment relaxation enhancements**

Submitted to J Biomol NMR

- Magnus Franzmann performed all experiments and wrote the article
- Daniel Otzen co-supervised the experiments
- Reinhard Wimmer supervised overall design and execution of the experiments, contributed extensively to the writing of the article.

Daniel Otzen   _____

Reinhard Wimmer   _____

Magnus Franzmann, Daniel Otzen, Reinhard Wimmer

Stereospecific assignment of protein NMR resonances using paramagnetic environment relaxation enhancements

M. Franzmann, Dr. R. Wimmer
Department of Biotechnology, Chemistry and Environmenal Engineering,
Aalborg University
Sohngaardsholmsvej 49, DK-9000 Aalborg, Denmark

Dr. D.E. Otzen
Interdisciplinary Nanoscience Center (iNANO), Department of Molecular Biology
Aarhus University
Gustav Wieds Vej 10 C, DK-8000 Aarhus C, Denmark

(+45)99408518
(+45)98141808
 rw@bio.aau.dk

NMR spectroscopy, protein structures, paramagnetic relaxation enhancement, antimicrobial agents, Plectasin

We report a new NMR method for determining the stereospecific assignment of prochiral protons in proteins based on the structures of the peptide in simulated water environments and differences in paramagnetic relaxation enhancement exerted by a non-perturbing water soluble paramagnetic agent. Paramagnetic relaxation enhancements of peptide atoms provide information concerning the relative orientation of prochiral protons towards the solvent. Together with a preliminary structure, this information can be used to stereospecifically assign prochiral protons. This information can then be used to improve the structure calculation.

Introduction

NMR structure determination of proteins and peptides is mainly based on NOESY spectra, where cross peak intensities are used to derive upper distance constraints(Wuthrich 2003). This requires knowledge of which two atoms, nearly exclusively hydrogen atoms (in NMR often referred to as "protons"), are responsible for the cross peak. Such knowledge is typically referred to as the NOE assignment. It is usually not possible to stereospecifically assign resonances from chemically nonequivalent, diastereotopic, protons, e.g. the diastereotopic protons in CH_2 groups or the two non-equivalent methyl groups in isopropyl moieties. However, NOEs to these groups are a vital source of structural information, and discarding them would significantly reduce the quality of the obtained structures. In an attempt to retain the use of NOEs involving protons whose stereospecific assignment is not known, pseudoatoms were introduced.(Guntert 1998) Pseudoatoms are artificial atoms fixed to the molecular framework at a location at the center of mass of a group of protons. NOEs observed to any member of this group are then in the structure calculation treated as NOEs to these pseudoatoms. However, the actual distance of an atom outside the group to the pseudoatom is only rarely the same as the distance to the single members of the group. This is accounted for by introducing a pseudoatom correction, where the upper distance limit between the affected atoms is increased by the distance between the pseudoatom and the members of the group, which is the maximum possible error introduced. While this ensures that no additional constraint violations are introduced by the introduction of the pseudoatoms, it constitutes a loss of information, as the introduced error in most cases is much lower than the pseudoatom correction accounts for. This loss of information leads to more loosely defined structures. To avoid this problem and to improve the quality of the calculated structures, various methods have been developed to stereospecifically assign diastereotopic groups in proteins, thus eliminating the need for introduction of pseudoatoms. Nonrandom, fractional labeling of proteins with [13]C(Neri and others 1989; Senn and others 1989) or [2]H(Curley and others 1994; Ostler and others 1993) valine, leucine and glycine can be used to stereospecifically assign diastereotopic groups using scalar couplings. Chemical shift calculations can reveal stereospecific assignments, if the chemical shift differences are more than 0.3 ppm(Williamson and Asakura 1992). $^3J_{\alpha\beta}$ couplings in combination with H^α-

H$^\beta$ distances obtained from NOEs can be used for assignments of β-methylene protons (Hyberts and others 1987; Xu and others 1992; Zuiderweg and others 1985) which also has been combined with grid searches in X-ray structure databases.(Nilges and others 1990) Furthermore, C,H and H,H dipolar couplings can be used for determining the stereospecificity of CH_2 groups provided that additional structural information is known.(Carlomagno and others 2000)

The extensively used software program HABAS (Guntert and others 1989) calculates proton stereospecific assignments based on scalar couplings and the intraresidual and sequential NOEs. The program GLOMSA (Guntert and others 1991) provides additional assignments of diastereotopic substituents based on distance restraints and calculated structures.

Here we use paramagnetic relaxation enhancements (PREs) for stereospecific assignment. PREs have previously been used to map protein surfaces (Pintacuda and Otting 2002), refine protein NMR structures (Madl and others 2009; Madl and others 2006) and determine the position and orientation of peptides in micelles (Franzmann and others 2009; Respondek and others 2007; Zangger and others 2009). We calculate the structure of a peptide by standard methods and determine the PREs for a maximum possible number of diastereotopic protons. Subsequently, we compare the obtained PREs with the distances of individual atoms from the solution in our first structure. If there is a consistent correlation between the observed PREs and distances, we define a stereospecific assignment. Finally, we repeat the structure calculation with the stereospecific assignments.

We used Omniscan (Gd(DTPA-BMA)) as a paramagnetic relaxation enhancement agent, as it has been shown not to interact specifically with proteins (Pintacuda and Otting 2002).

As model system we used the 40 residue peptide Plectasin, an antimicrobial peptide from a fungus with known structure.(Mygind and others 2005)

Materials and methods

Materials: Plectasin was generously provided by Novozymes A/S and Omniscan (Gd(DTPA-BMA)) was generously provided by Aalborg Hospital.

NMR recording: All NMR spectra were recorded at 300 K on a BRUKER DRX 600 spectrometer operating at a field strength of 14.1 T, fitted with a TXI (H/C/N) probe with triple-axis gradients. A NMR sample containing 1 mM Plectasin, 30

mM acetic acid, 5% D2O, 0.05% azide at pH 3.8 was prepared. A 2D NOESY spectrum with 50 ms mixing time was recorded with a WATERGATE water suppression.(Piotto and others 1992) [^{1}H, ^{1}H]-TOCSY spectra with 50 ms mixing time were recorded using a clean-TOCSY pulse sequence with a 15 kHz spin-lock and excitation sculpting water suppression.(Griesinger and others 1988; Hwang and Shaka 1995) 2QF-COSY and [^{1}H-^{13}C]-HSQC spectra were recorded using standard pulse sequences taken from the Bruker Topspin pulse sequence library. All spectra were processed using Topspin version 1.3. Assignment of all NMR spectra were based on previously published resonance frequencies by Mygind et al.(Mygind and others 2005) and performed using the program CARA version 1.5.5(Keller). NOE cross peaks were integrated using the NEASY subroutine of CARA(Bartels and others 1995), and the CALIBA(Guntert and others 1991) subroutine in CYANA was used to convert integrated cross-peak intensities from the NOESY spectra into distance constraints. These combined constraints provided the input for the structure calculation using the torsion angle dynamics program CYANA(Guntert and others 1997). Structure calculations were started from 80 conformers with random torsion angle values and the 20 structures with the lowest CYANA target function were collected and analyzed using Pymol(DeLano 2002).

For proton PRE measurements of Plectasin the sample was titrated to 2, 5 and 10 mM final concentration of Gd(DTPA-BMA). 8 inversion recovery [^{1}H-^{13}C]-HSQC spectra with recovery delay times of 1, 50, 120, 250, 700, 1000, 2000, 3000 ms were recorded with 0 mM Gd(DTPA-BMA) present and for each titration point in order to obtain the T_1 relaxation time. Relaxation rates ($1/T_1$) were plotted against the concentration of the Gd-complex, a linear regression yielded the PRE values as the slope of the regression line.

Water simulation: calculated peptide structures were placed in simulation boxes, extending 1.5 nm from the peptide along all three axes. The boxes were filled with TIP3P water and sodium ions were iteratively placed at the coordinates with the lowest electrostatic potential. Simulations were started with a steepest descent minimization (until atom speed <2200 m/s) and followed by 500 steps of simulated annealing using the YASARA 8.9.11 MD protocol.(Krieger and others

2004) Water atoms were removed from the PDB files using the program pymol(DeLano 2002)

Results and discussion

The proton signals were assigned using a standard set of homonuclear 2D-spectra, and the carbon shifts of the residues were assigned using a ^{1}H-^{13}C-HSQC spectrum. From an inversion recovery [^{1}H-^{13}C]-HSQC spectrum we identified 24 prochiral proton pairs for which we could determine the PRE values by measuring the T_1 relaxation times at increasing concentrations of relaxation agent. Due to a higher spectral overlap in the lower ^{1}H-ppm range, the identified protons pairs were mainly bound to C^α (5) and C^β (15) carbons of their respective amino acids while only a few pairs were bound to C^δ (1) or C^γ (3) carbons. The PRE values of protons depend on the inverse of the third power of the distance between the measured nuclei and the paramagnetic center when using a free-floating noninvasive paramagnetic agent like Gd(DTPA-BMA).(Franzmann and others 2009; Luz and Meiboom 1964a; Luz and Meiboom 1964b; Respondek and others 2007) It can therefore be assumed that when comparing the PRE values of two atoms relative to each other, the one with the highest PRE value must be located nearest towards the paramagnetic agent and hence towards the solution. The PRE values of the 24 measured prochiral proton pairs are listed in table 1.

A set of 80 structures was calculated and the 20 structures with the lowest residual target functions were collected. The HABAS program was used in the structure calculation and yielded 14 stereospecifically assigned pairs out of 50 possible. The structure contains an α-helix and two antiparallel β-strands in an αβ-defensin motif and is cross-linked by three disulfide bridges. Key values of the structure calculations are listed in table 2. The structure of Plectasin has previously been published(Mygind and others 2005) (pdb code 1zfu) and our structure is, as expected, practically identical with the previously published structure (see figure 1a) with a backbone RMSD of 0.795 Å between the two structures. To obtain information concerning the relative orientation of the Plectasin proton pairs towards the surrounding water, the distances between the peptide and water atoms were measured for all atoms in each of the 20 calculated peptide structures in water simulated boxes. Distances below 5.9 Å were discarded as it is not possible

for the paramagnetic center to come closer to the peptide surfaces than this due to the 3.5 Å radius of the chelate(Pintacuda and Otting 2002) plus two hydrogen van der Waals radii. Minimum distances between peptide atoms and water were collected for the 24 prochiral proton pairs with measurable PRE values. If the same proton (of the two protons in the group) was situated closer to the surface in ≥90% of the structures, we assumed it to be safe to assign this proton to the NMR resonance showing the higher PRE. This was the case in 15 out of the 24 proton pairs with measurable PREs. As this is synonymous with being closer to the paramagnetic atoms we can for the 15 stereo pairs combine this information with the PRE values and thereby stereospecifically assign the proton resonances.

15 stereo specific proton pair assignments obtained from the interpretation of PRE data were introduced into the structure calculation protocol and the structure was recalculated. The HABAS protocol yielded further stereospecific assignments for 12 proton pairs. The convergence of the 20 structures with the lowest CYANA residual target function was significantly improved from 0.64 ± 0.2 Å to 0.37 ± 0.09 Å (see figure 1b and 1c respectively). The introduction of the restraints only gave rise to two distance violations in the new structure calculation. These violations were at the residue 14 $H^{\beta2}$/ $H^{\beta3}$ stereo pair. We cannot explain these violations and excluded this particular stereospecific assignment from the structure calculation.

We have been using inversion recovery edited [^{1}H-^{13}C]-HSQC spectra for the measurement of T_1 but, any type of experiment that measures T_1 relaxation can be used. The method presented here is limited to protons not too distant from the protein surface, which shows measurably different PREs. However, this will not likely be a practical limitation: of the protons from which we have obtained PRE values usable for stereospecific assignment, Cys 15 $H^{\beta2}$/$H^{\beta3}$ have the largest distance to the protein surface, 7.2 and 6.5 Å, respectively. Although paramagnetic effects of chelated Gd^{3+} have been observed at distances up to 30 Å(Vlasie and others 2007) let us assume that our method in principle only can assign diastereotopic protons that are no more than 7Å away from the protein surface. Globular protein molecules of 20-25 kDa usually have a radius of 10-13 Å on the shortest axis. Approximating the protein as a perfect sphere with a radius of 13Å, $(13^3-(13-7)^3)/13^3 = 90\%$ of the volume of the protein and hence the amino

acid residues will be within 7 Å from the surface and thus accessible for the proposed method for stereospecific assignment.

The improvement in RMSD observed here is in agreement with several previous publications which have reported that the precision of NMR structures is improved when using stereospecific assignments of side chain atoms compared to structures calculated without them.(Driscoll and others 1989; Guntert and others 1989; Nilges and others 1990) In contrast to many of the previously published methods, our method does not require any expensive labeling schemes and it is easy to implement in preexisting structure determination routines. At the same time, it yields a higher number of stereospecific assignments than the widely employed, purely computational HABAS method.

Bartels C, Xia T, Billeter M, Güntert P, Wüthrich K. 1995. The program XEASY for computer-supported NMR spectral analysis of biological macromolecules. J. Biomol NMR 6(1):1-10.

Carlomagno T, Peti W, Griesinger C. 2000. A new method for the simultaneous measurement of magnitude and sign of 1DCH and 1DHH dipolar couplings in methylene groups. J Biomol NMR 17(2):99-109.

Curley RW, Jr., Panigot MJ, Hansen AP, Fesik SW. 1994. Stereospecific assignments of glycine in proteins by stereospecific deuteration and 15N labeling. J Biomol NMR 4(3):335-40.

DeLano WL. 2002. The PyMOL Molecular Graphics System, www.pymol.org.

Driscoll PC, Gronenborn AM, Clore GM. 1989. The influence of stereospecific assignments on the determination of three-dimensional structures of proteins by nuclear magnetic resonance spectroscopy. Application to the sea anemone protein BDS-I. FEBS Lett 243(2):223-33.

Franzmann M, Otzen D, Wimmer R. 2009. Quantitative use of paramagnetic relaxation enhancements for determining orientations and insertion depths of peptides in micelles. Chembiochem 10(14):2339-47.

Griesinger C, Otting G, Wuethrich K, Ernst R. 1988. Clean TOCSY for proton spin system identification in macromolecules. J Am Chem Soc 110(23):7870 - 7872.

Guntert P. 1998. Structure calculation of biological macromolecules from NMR data. Q Rev Biophys 31(2):145-237.

Guntert P, Braun W, Billeter M, Wuthrich K. 1989. Automated Stereospecific 1H NMR Assignments and Their Impact on the Precision of Protein Structure Determination sin Solution. J Am Chem Soc 111:3997 - 4004.

Guntert P, Braun W, Wuthrich K. 1991. Efficient computation of three-dimensional protein structures in solution from nuclear magnetic resonance data using the program DIANA and the supporting programs CALIBA, HABAS and GLOMSA. J Mol Biol 217(3):517-30.

Guntert P, Mumenthaler C, Wuthrich K. 1997. Torsion angle dynamics for NMR structure calculation with the new program DYANA. J Mol Biol 273(1):283-98.

Hwang TL, Shaka AJ. 1995. Water Suppression That Works. Excitation Sculpting Using Arbitrary Waveforms and Pulsed Field Gradients. J Magn Reson 112:275 - 279.

Hyberts SG, Marki W, Wagner G. 1987. Stereospecific assignments of side-chain protons and characterization of torsion angles in Eglin c. Eur J Biochem 164(3):625-35.

Keller R.'OPTIMIZING THE PROCESS OF NUCLEAR MAGNETIC RESONANCE SPECTRUM ANALYSIS AND COMPUTER AIDED RESONANCE ASSIGNMENT' obtained from the website www.nmr.ch.

Krieger E, Darden T, Nabuurs SB, Finkelstein A, Vriend G. 2004. Making optimal use of empirical energy functions: force-field parameterization in crystal space. Proteins 57(4):678-83.

Luz Z, Meiboom S. 1964a. Nuclear Magnetic Resonance Study of the Solvation of Co^{++} in Methanol and Methanol-Water Mixtures. J Chem Phys 40(4):1058-1066.

Luz Z, Meiboom S. 1964b. Proton Relaxation in Dilute Solutions of Cobalt(II) and Nickel(II) Ions in Methanol and the Rate of Methanol Exchange of the Solvation Sphere. J Chem Phys 40:2686-2692.

Madl T, Bermel W, Zangger K. 2009. Use of relaxation enhancements in a paramagnetic environment for the structure determination of proteins using NMR spectroscopy. Angew Chem Int Ed Engl 48(44):8259-62.

Madl T, Van Melderen L, Mine N, Respondek M, Oberer M, Keller W, Khatai L, Zangger K. 2006. Structural basis for nucleic acid and toxin recognition of the bacterial antitoxin CcdA. J Mol Biol 364(2):170-85.

Mygind PH, Fischer RL, Schnorr KM, Hansen MT, Sonksen CP, Ludvigsen S, Raventos D, Buskov S, Christensen B, De Maria L and others. 2005. Plectasin is a peptide antibiotic with therapeutic potential from a saprophytic fungus. Nature 437(7061):975-80.

Neri D, Szyperski T, Otting G, Senn H, Wuthrich K. 1989. Stereospecific nuclear magnetic resonance assignments of the methyl groups of valine and leucine in the DNA-binding domain of the 434 repressor by biosynthetically directed fractional 13C labeling. Biochemistry 28(19):7510-6.

Nilges M, Clore GM, Gronenborn AM. 1990. 1H-NMR stereospecific assignments by conformational data-base searches. Biopolymers 29(4-5):813-22.

Ostler G, Soteriou A, Moody CM, Khan JA, Birdsall B, Carr MD, Young DW, Feeney J. 1993. Stereospecific assignments of the leucine methyl resonances in the 1H NMR spectrum of Lactobacillus casei dihydrofolate reductase. FEBS Lett 318(2):177-80.

Pintacuda G, Otting G. 2002. Identification of protein surfaces by NMR measurements with a pramagnetic Gd(III) chelate. J Am Chem Soc 124(3):372-3.

Piotto M, Saudek V, Sklenár V. 1992. Gradient-tailored excitation for single-quantum NMR spectroscopy of aqueous solutions. J Biomol NMR 2(6):661-665.

Respondek M, Madl T, Gobl C, Golser R, Zangger K. 2007. Mapping the orientation of helices in micelle-bound peptides by paramagnetic relaxation waves. J Am Chem Soc 129(16):5228-34.

Senn H, Werner B, Messerle BA, Weber C, Traber R, Wüthrich K. 1989. Stereospecific assignment of the methyl 1H NMR lines of valine and leucine in polypeptides by nonrandom 13C labelling. FEBS Letters 249(1):113-118.

Vlasie MD, Comuzzi C, van den Nieuwendijk AM, Prudencio M, Overhand M, Ubbink M. 2007. Long-range-distance NMR effects in a protein labeled with a lanthanide-DOTA chelate. Chemistry 13(6):1715-23.

Williamson MP, Asakura T. 1992. The application of 1H NMR chemical shift calculations to diastereotopic groups in proteins. FEBS Lett 302(2):185-8.

Wuthrich K. 2003. NMR studies of structure and function of biological macromolecules. Biosci Rep. 23(4):119-68.

Xu RX, Olejniczak ET, Fesik SW. 1992. Stereospecific assignments and chi 1 rotamers for FKBP when bound to ascomycin from 3JH alpha,H beta and 3HN,H beta coupling constants. FEBS Lett 305(2):137-43.

Zangger K, Respondek M, Gobl C, Hohlweg W, Rasmussen K, Grampp G, Madl T. 2009. Positioning of micelle-bound peptides by paramagnetic relaxation enhancements. J Phys Chem B 113(13):4400-6.

Zuiderweg ERP, Boelens R, Kaptein R. 1985. Stereospecific assignments of 1H-nmr methyl lines and conformation of valyl residues in the lac repressor headpiece. Biopolymers 24(4):601-611.

Figure legends

Fig 1 a) Comparison of the previously published Plectasin structure (red) with the structure calculated by us without PRE based stereo specific assignments (blue). b) The bundle of 20 Plectasin structures with the lowest residual target function calculated without PRE based stereo specific assignments. c) As "b" but calculated with PRE based stereo specific restraints. Table 2 gives the quality criteria for the two structures shown in b) and c)

Table 1. Pairs of prochiral protons in Plectasin for which it was possible to measure the PRE values. Protons with the relative highest PRE values are marked in gray.

Table 2. Quality criteria for the calculated Plectasin structures. (a) Distance restraint obtained from NOE's without including distance restraints from disulfide bonds. (b) Per molecule, (c) For backbone atoms C', C^{α} and N, as calculated by CYANA from the pairwise rmsd values of each of the 20 structures against a mean structure (d) As calculated by PROCHECK_NMR

a) b) c)
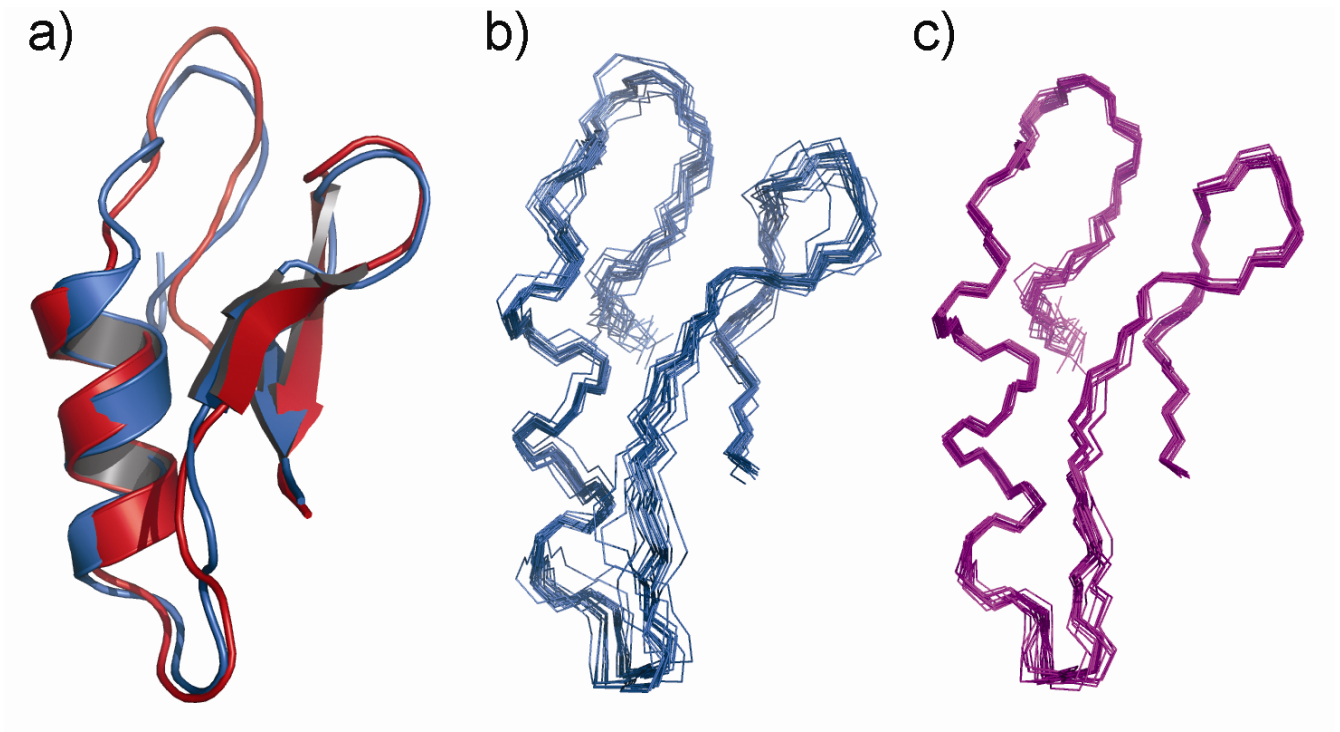
Fig 1

Residue	Atom type	PRE
G3	HA2	1.75± 0.255
G3	HA3	0.70 ± 0.077
C4	HB2	0.39 ± 0.034
C4	HB3	0.40 ± 0.029
G6	HA2	0.92 ± 0.023
G6	HA3	1. 03 ± 0.065
P7	HD2	1.40 ± 0.024
P7	HD3	1.12 ± 0.037
P7	HG2	2.02 ± 0.067
P7	HG3	1.11 ± 0.318
D9	HB2	1.29 ± 0.306
D9	HB3	1.97 ± 0.352
E10	HB2	0.89 ± 0.167
E10	HB3	0.98 ± 0.164
Q14	HB2	0.49 ± 0.210
Q14	HB3	1.18 ± 0.222
Q14	HG2	1.96 ± 0.108
Q14	HG3	1.28 ± 0.097
C15	HB2	0.42 ± 0.080
C15	HB3	0.29 ± 0.020
H16	HB2	0.75 ± 0.015
H16	HB3	1.22 ± 0.186
H18	HB2	0.58 ± 0.023
H18	HB3	0.48 ± 0.009
S21	HB2	2.04 ± 0.126
S21	HB3	1.24 ± 0.176
I22	HG12	1.67 ± 0.073
I22	HG13	1.09 ± 0.037
K23	HB2	2.11 ± 0.084
K23	HB3	2.68 ± 0.097
Y25	HB2	0.74 ± 0.015
Y25	HB3	0.97 ± 0.162
K26	HB2	1.71 ± 0.127
K26	HB3	1.21 ± 0.267
G28	HA2	0.54 ± 0.039
G28	HA3	1.54 ± 0.293
C30	HB2	0.39 ± 0.064
C30	HB3	0.75 ± 0.112
G33	HA2	4.34 ± 0.163
G33	HA3	2.67 ± 0.066
G34	HA2	0.71± 0.110
G34	HA3	0.89 ± 0.087
C37	HB2	0.57 ± 0.055
C37	HB3	0.49 ± 0.024
K38	HB2	0.88 ± 0.088
K38	HB3	1.12 ± 0.066
C39	HB2	1.65 ± 0.308
C39	HB3	0.56 ± 0.019

Table 1

	without stereospecific assignment	with stereospecific assignment
number of distance constraints [a]	356	360
- of which intraresidual	172	172
- of which sequential	105	107
- of which medium-range ($2 \leq \Delta res \leq 4$)	35	37
-of which long-range (>4)	44	44
CYANA residual target function	$0.59 \pm 0.08 \ \text{Å}^2$	$0.70 \pm 0.11 \ \text{Å}^2$
distance restraints violated by more than 0.2Å	0	0
angle restraints violated more than 5° [b]	0	0
rmsd residues 2-39 [c]	$0.63 \pm 0.2 \ \text{Å}$	$0.37 \pm 0.09 \ \text{Å}$
% of residues in Ramachandran plot [d]		
- in most favored regions	80.7	81.3
- less favored regions	19	18.7
- generously allowed regions	0.3	0
- disallowed regions	0	0
% of diastereotopic groups stereospecifically assigned	28	52

Table 2